

University of Windsor

Scholarship at UWindor

Electronic Theses and Dissertations

Theses, Dissertations, and Major Papers

9-26-2019

Inclusion of Aerodynamic Effects in Multibody Vehicle Dynamics

Mingyu Sun

University of Windsor

Follow this and additional works at: <https://scholar.uwindsor.ca/etd>

Recommended Citation

Sun, Mingyu, "Inclusion of Aerodynamic Effects in Multibody Vehicle Dynamics" (2019). *Electronic Theses and Dissertations*. 7847.

<https://scholar.uwindsor.ca/etd/7847>

This online database contains the full-text of PhD dissertations and Masters' theses of University of Windsor students from 1954 forward. These documents are made available for personal study and research purposes only, in accordance with the Canadian Copyright Act and the Creative Commons license—CC BY-NC-ND (Attribution, Non-Commercial, No Derivative Works). Under this license, works must always be attributed to the copyright holder (original author), cannot be used for any commercial purposes, and may not be altered. Any other use would require the permission of the copyright holder. Students may inquire about withdrawing their dissertation and/or thesis from this database. For additional inquiries, please contact the repository administrator via email (scholarship@uwindsor.ca) or by telephone at 519-253-3000ext. 3208.

Inclusion of Aerodynamic Effects in Multibody Vehicle Dynamics

By

Tony SUN Mingyu

A Thesis

Submitted to the Faculty of Graduates Studies

Through the Department of Mechanical, Automotive, & Materials Engineering

in Partial Fulfillment of the Requirements for

the Degree of the Degree of Master of Applied Science

at the University of Windsor

Windsor, Ontario, Canada

2019

©2019 Tony SUN Mingyu

Inclusion of Aerodynamic Effects in Multibody Vehicle Dynamics

by

Mingyu Sun

APPROVED BY

R. Rieveley
Ford Motor Company

S. Cheng
Department of Civil & Environmental Engineering

V. Roussinova
Department of Mechanical, Automotive, & Materials Engineering

B. Minaker, Advisor
Department of Mechanical, Automotive, & Materials Engineering

September 26, 2019

Declaration of Originality

I hereby certify that I am the sole author of this thesis and that no part of this thesis has been published or submitted for publication.

I certify that, to the best of my knowledge, my thesis does not infringe upon anyone's copyright nor violate any proprietary rights and that any ideas, techniques, quotations, or any other material from the work of other people included in my thesis, published or otherwise, are fully acknowledged in accordance with the standard referencing practices. Furthermore, to the extent that I have included copyrighted material that surpasses the bounds of fair dealing within the meaning of the Canada Copyright Act, I certify that I have obtained a written permission from the copyright owner(s) to include such material(s) in my thesis and have included copies of such copyright clearances to my appendix.

I declare that this is a true copy of my thesis, including any final revisions, as approved by my thesis committee and the Graduate Studies office, and that this thesis has not been submitted for a higher degree to any other University or Institution.

Abstract

In vehicle motion analysis, it is often of interest to predict the aerodynamic load and moment acting on the vehicle body, typically with the intention of maximizing tire grip through downward force generated by wings and other aerodynamic devices. This project is not focused on maximizing downward force generated but rather recognizes that an attached wing itself may change the dynamic properties of the vehicle, similarly to the way in which the variation of the wing configuration can lead to changes in the eigenvalues, natural frequencies, and the dynamic modes of an aircraft.

To explore this idea further, a multibody method incorporating aerodynamics effects has been developed. An attached wing system is applied on the multibody mechanical system, which generate forces and moments on the various individual bodies. The force and moment coefficient of the wing is a 6×6 matrix, which is perfectly suitable for incorporation into the equation of motion for multibody dynamics as an additional damping term.

A vehicle model with variable wing geometry has been proposed, and a number of numerical tests have been conducted to explore its behaviour. Wing orientation and a wing sensitivity are explored during tests, making sure the system is operating within an effective but stable range. Effects from unsprung mass distribution and varying velocity are evaluated.

To my parents, for their love and support.

Acknowledgements

I would like to take this opportunity to express my gratitude and special appreciation to my master's degree advisor, Prof. Bruce Minaker, for his encouragement and patient guidance throughout my graduate study. Your advice on my career path has been absolutely invaluable. You are not just my supervisor, you're my mentor and life role model. Without your constant enthusiasm and support it would not be possible for me to pursue my graduate study.

I would also like to thank my thesis committee members for their ideas, discussions, and feedback. Their generous help has been motivating my research study moving forward. The assistance from my colleagues Zhe Ma, Zheng Yao, and Changdong Liu are greatly appreciated; thank you for your inspirations and support.

This amazing journey would not have been possible without the love and support from my beloved parents. I am grateful for their emotional and financial support throughout my education. Thank you for always believing in me, and helping me to better myself. Both of you have given me infinite amounts of time, energy, and love, and your companionship through the ups and downs of my life. Thank you for always being there for me, for better or for worse. Words cannot describe how grateful I am for all of the sacrifices that you've made on my behalf. Thank you for being the foundation for who I am today and who I want to become going forward in my life. You should be proud of the impact you've had, not only on me but the people around you. I love you both dearly.

Contents

Declaration of Originality	iii
Abstract	iv
Dedication	v
Acknowledgements	vi
List of Figures	x
List of Tables	xii
1 Introduction	1
1.1 Background	1
1.1.1 Racing vehicles	2
1.1.2 Truck and trailer	3
1.2 Motivation	4
1.3 Literature Review	5
1.4 Research Objectives	8
1.5 Thesis Structure	8
2 Multibody Dynamics	10
2.1 Generating the equation of motion	10
2.1.1 Definition of coordinates	11
2.1.2 Kinematic differential equations	11
2.1.3 Newton Euler equations	13
2.1.4 Constraint equations	14
2.2 Software tools	15
2.3 Examples	17
2.3.1 Shimmy model	17
2.3.2 Quarter car model	18
Frequency response	19
2.3.3 The yaw plane model	20
2.3.4 Bounce pitch model	22

Summary	24
3 Aerodynamics	25
3.1 Equations of motion of a moving wing	25
3.2 Aerodynamic forces and moments	27
3.2.1 General nonlinear form	27
3.2.2 Integration into the linearized equation of motion	28
3.2.3 Property estimation	31
3.3 Example	32
4 Vehicle Model	35
4.1 Model properties	35
4.2 Model geometry	36
4.3 Random road	38
4.3.1 Wheelbase filter	40
5 Simulation Results	42
5.1 Wing orientation	42
5.1.1 Bounce and pitch response	43
5.2 Wing sensitivity	45
5.2.1 Bounce pitch response	47
5.2.2 Frequency response	51
5.2.3 Wing performance	51
5.3 Unsprung mass effects	54
5.3.1 Bounce pitch response	56
5.4 Velocity effects	56
5.4.1 Bounce pitch response	56
5.4.2 Frequency Response	65
6 Conclusions and Recommendations	67
6.1 Conclusions	67
6.2 Recommendations	68
6.2.1 Improved quantification of ride quality	68
6.2.2 Optimum control	69
6.2.3 Wing design	69
6.2.4 Future experiments or simulations	69
6.3 Summary of contributions	70
References	73
A Model Details	74

A.1	Equations of motion	74
A.2	Code	75
A.2.1	Input file for half car model with wing	75
A.2.2	Run file	82
A.2.3	Random road	90
B	Eigenvalue Results	92
B.1	Eigenvalue tables	92
B.1.1	Eigenvalue and eigenvalue analysis table(baseline)	92
B.1.2	Eigenvalue and eigenvalue analysis table (premium)	93
	Vita Auctoris	94

List of Figures

1.1	Race car with aerodynamic elements	2
1.2	Truck and trailer with aerodynamic elements	3
2.1	Swivel wheel, a single rigid body constrained as a xy planar motion with a constant forward speed. The tire is non slip tire.	18
2.2	Quarter car model.	19
2.3	Frequency response: z_g	20
2.4	Yaw plane model(Bicycle model)	21
2.5	Bounce pitch model	22
3.1	Spring mass wing model.	25
3.2	Swivel wheel with wing element	33
3.3	Fast eigenvalue for shimmy example	34
3.4	Slow eigenvalue for shimmy example	34
4.1	Bounce pitch model	36
4.2	The bounce pitch model	37
4.3	Sample random roads	40
5.1	Half car model with wing effect	43
5.2	Half car model with wing effect (reverse)	43
5.3	Bounce response of the half car model on random road with varying wing configurations	44
5.4	Pitch response of the half car model on random road with varying wing configurations	45
5.5	Front wing system geometry	46
5.6	Rear wing system geometry	46
5.7	Test point map	47
5.8	Map showing stable region	47
5.9	Bounce response for varying wing sensitivity for Configurations C and D	48
5.10	Bounce response for varying wing sensitivity for Configurations E and F	48
5.11	Pitch response for varying wing sensitivity for Configurations C and D	50
5.12	Pitch response for varying wing sensitivity for Configurations E and F	50

5.13	Frequency response: Wheel bump. System with wings has a lower transfer function means lower output to input ratio. The natural frequencies of the system become lower.	52
5.14	Front wing tilt angle	52
5.15	Rear wing tilt angle	53
5.16	Front wing angle while operating on the road level 3. The range of the tilting angle become narrow within $\pm 7^\circ$ while the road disturbance decreases.	54
5.17	Rear wing angle at road level 3. The range of the tilting angle become narrow within $\pm 5^\circ$ while the road disturbance decreases.	55
5.18	Road bounce response for different unsprung mass distribution	55
5.19	Road pitch response for different unsprung mass distribution	57
5.20	Road bouncing response with a forward speed of 30 m/s.	57
5.21	Road pitch response with a forward speed of 30 m/s.	58
5.22	Road bouncing response with a forward speed of 40 m/s.	58
5.23	Road pitch response with a forward speed of 40 m/s.	59
5.24	Road bouncing response with a forward speed of 50 m/s.	59
5.25	Road pitch response with a forward speed of 50 m/s.	60
5.26	Road bouncing response with a forward speed of 50 m/s at road level 3.	60
5.27	Road pitch response with a forward speed of 50 m/s at road level 3.	61
5.28	Road bouncing response with a forward speed of 10 m/s.	61
5.29	Road pitch response with a forward speed of 10 m/s.	62
5.30	Road bouncing response with a forward speed of 51 m/s.	63
5.31	Road pitch response with a forward speed of 51 m/s.	63
5.32	Frequency response: Wheel bump at 10 m/s forward speed	65
5.33	Frequency response: Wheel bump at 30 m/s forward speed.	66
5.34	Frequency response: Wheel bump at 40 m/s forward speed.	66

List of Tables

2.1	Types of items in EoM	16
3.1	Partial derivative of aerodynamic forces and moments, from[21]	30
4.1	Parameters in half car model	37
4.2	ISO 8608 values of $G_d(n_0)$ and $G_d(\Omega_0)$ [22]	38
4.3	ISO road roughness classification	39
5.1	Wing system parameters	49
5.2	Different unsprung mass distribution	56
5.3	Eigenvalues at forward speed 51 m/s	64
B.1	Eigenvalues for baseline model	92
B.2	Eigenvalue Analysis for baseline model	92
B.3	Eigenvalues for premium model	93
B.4	Eigenvalue Analysis for premium model	93

Chapter 1

Introduction

1.1 Background

Centuries ago, when the automobile supplanted carriage horses, aerodynamics was not taken into account at all in the design. The intention of the vehicle body shell was to simply protect passengers from raw weather events, enhancing the passenger's privacy and enjoyment of traveling[1]. The idea of utilizing aerodynamics in the automobile industry occurred much later. As the road vehicle industry made recognizable progress developing new technologies, the similarity between aircraft and automobiles raised a new perspective on the application of aerodynamics in the automobile industry. For instance, streamlined shapes were employed to reduce the drag effects in vehicles design to allow them to travel faster and further.

While automotive aerodynamics adopt similar design principles to aircraft aerodynamics, they still differ in several ways. For example, the road vehicle is working with respect to the ground, which is much different from the aircraft operating in free air. Secondly, the normal speeds of ground vehicles are much lower than those of aircraft, and the lift and drag forces, which vary with the square of speed, are disparate. Thirdly, a road vehicle generally has fewer degrees of freedom when compared to an aircraft, (or at least the range of motion is more constrained). For the reasons listed, the overall motion of a road vehicle will be less affected by the aerodynamic forces than an aircraft. However, in top-class auto racing competition, racing vehicles commonly apply aerodynamic elements to generate negative lift, which is well known as aerodynamic downforce. The vehicle stability and handling are substantially improved by this generated force. So despite these differences, there are still opportunities for the application of aerodynamic devices to road vehicles. This is applied to many different vehicle models such as a racing cars, long haul trucks and trailers, and others.

In this thesis, a wing system is applied to a road vehicle to create lift and downforce that is dependent on different conditions, to allow the vehicle to travel faster with more comfortable ride quality.



FIGURE 1.1: Race car with aerodynamic elements. Image reproduced from www.wikipedia.org.

1.1.1 Racing vehicles

Auto racing competition has always been pushing the automobile industry forward. Katz[2] indicates movement of air can affect all components and the overall vehicle performance. The research on aerodynamic forces can be extended to multiple design components of the car. In point of fact, the tire adhesion can be enhanced using vehicle aerodynamics forces, hence improving the overall vehicle performance. The design of racing cars using aerodynamics are not only focusing on reducing drag, but have also branched out to explore the potential to improve the vehicle travelling speed. For instance, under high-speed conditions, tire-to-road adhesion can be improved by the application of aerodynamic downforce without increasing the vehicle mass. The improvements in cornering and braking are significant, along with refinement of vehicle stability. Predominantly, the study is targeting improvement of the overall efficiency of the downforce with low drag cost. The proposition of reducing drag focuses on extending laminar boundary layers and minimizing the flow separation. The related information is established in aircraft-type configurations.

The implementation of aerodynamic elements can have not only positive but also negative effects on vehicle performance. In Gullberg et al[3], a simulation model was conducted to explore the aerodynamic effects on the famous Le Mans car crash accident of 1955. Several testing results were examined to explore the relationship between aerodynamics and the accident. There was a positive correlation found between the aerodynamic lifting forces and pitch angles. On account of the increasing rotating moment generated by the aerodynamic lifting forces, the pitch angle of the vehicle tends to increase significantly, often growing without limit. The drag coefficient has a tendency to decrease when the vehicle leaves the ground. Results suggest that the raising the air brake increases both the drag and pitch coefficients, subsequently complicating the handling. The

effects that the pitch angle has on the aerodynamic drag, lift, as well as rotating moment is very noticeable. In brief, the results demonstrated the important effects of aerodynamics on vehicles with air brakes in operation. Despite the advances in the understanding of aerodynamics over the years, another very noteworthy accident occurred, again at Le Mans, in 1999. Driver Peter Dumbreck's Mercedes went airborne several meters and crashed heavily, with only aerodynamic instability as the cause of the accident.

1.1.2 Truck and trailer

More recently, the truck and trailer combination has been considered as an important vehicle model when analyzing vehicle motions, in as much as the stability is substantially affected by the many different operating conditions. For example, the design of the large frontal area causes significant drag, and cross winds will generate lateral forces, so that the vehicle dynamic properties will be affected, such as yaw, pitch and roll moments. Various modifications are often applied to the modern long haul truck to reduce drag in order to reduce fuel consumption and improve the vehicle stability.

To maximize the load volume with the limitation of the size of the truck, a rectangular configuration with a large frontal area is frequently chosen. The total frontal area of the truck and trailer model includes both the tractors' frontal area, and the trailer's frontal area that is exposed above the tractor. Usually, the truck and trailer has a large separation left in between, in order to have a larger maximum turning angle while operating on the road. However, this gap in between the truck and trailer results in poor aerodynamic characteristics and will cause a substantial wind drag, and high fuel consumption while at high speed operation.



FIGURE 1.2: Truck and trailer with aerodynamic elements. Image reproduced from www.shell.com.

Many modifications and optimizations in design have been developed over time, to arrange the air stream passing around the truck and trailer. For example, a roof mounted on the top of the tractor redirects the airflow directly to the top surface of the trailer, eliminating the large drag generated by the exposed front bluff surface of the trailer. Also, a downward force is applied on the truck itself, improving its stability. In addition, a special design called a resilient semi-flexible side panel is developed by Witten[4] to provide a better air flow quality while the truck and trailer are turning. The panels work the same way as the articulation joints between train sections. By adding a modified connecting section between the truck and the trailer, the panel is adequate to support itself rigidly on the vehicle, and simultaneously provide enough flexibility to bend during a turning maneuver, since the panel can slide in and out from the pocket structure attached on both sides of the trailer.

1.2 Motivation

For many years, the study of vehicle dynamics has produced vehicle models of increasing complexity and fidelity. Early research used relatively simple single or two body models such the yaw plane or quarter car models, e.g., Olley[5]. However, with the advent of low cost high speed computing, most modern studies in vehicle dynamics utilize a computer based multibody dynamics approach. There are several multibody software tools that are widely used in the automotive industry, e.g., ADAMS, DADS, MotionView, CarSim, etc. Blundell[6] has discussed this in detail in his 2004 text *Multi-Body Systems Approach to Vehicle Dynamics*.

At the same time, it also well known that vehicle motion is affected significantly by aerodynamics when the vehicle is moving with high velocity[7]. Yet, aerodynamic effects are frequently ignored in most road vehicle motion analyses. Arguably, most drivers operate their vehicle at speeds where aerodynamic effects are less important, perhaps justifying their omission. In any case, there is a lack of widely available software tools that combine multibody dynamics with aerodynamic effects. This research explores effects from including aerodynamic surfaces on the motion of multibody systems, in particular, vehicle motion.

This thesis is based on the Equations of Motion (EoM) software, developed by the University of Windsor Vehicle Dynamics and Control Research Group, which can be used to automatically generate linear or linearized equations of motion for mechanical systems, and is particularly well suited to vehicle dynamics.

This work details the relevant theory and equations for both multibody dynamics and vehicle aerodynamics, which get combined in the models. The half car model is tested with and without wings attached. A random road input is applied, and bounce and pitch time history and frequency response plots will show how the aerodynamics affect the entire system.

It is important to note that this research is *not* concerned with maximizing the downward force generated by the wing. In fact, the wing itself may change the dynamic properties of the vehicle,

similarly to the way in which the variation of the wing configuration can lead to change in the natural dynamic modes of an aircraft, such as the phugoid mode, spiral mode, or dutch-roll mode[8]. This work focuses on exploring to what extent an attached wing could influence the stability of bounce, pitch, yaw, or roll motions of a road vehicle, or change their natural frequencies, or their sensitivity to external input.

1.3 Literature Review

As mentioned there is very little software available for the analysis of multibody dynamics including aerodynamic effects. It is perhaps then not surprising that the literature on the topic is quite sparse. Nevertheless, there are some advantages in vehicle motion characteristics that can be obtained through careful application of aerodynamics, so there are some examples in which the authors develop vehicle models that include those effects, but most are small or simple enough that the equations of motion can be generated by hand.

In the paper previously mentioned, A.R. Sackoor and C.T. Chou [9] are applying aerodynamic effects onto the yaw plane model, which is referred to as the bicycle model. In order to minimize the body sideslip angle and the delay in responses of lateral acceleration and yaw rate respect to steering input, this paper applied aerodynamic actuators to generate a yaw moment M_z and a roll moment M_x , such that both angles are trying to remain zero at all time. And the closed loop vehicle response with dual actuators shows superior and more stable performance than the passive vehicle response.

The work of Doniselli et al.[10] explores the high-speed vehicle performance under various road conditions including a study of aerodynamic effects, targeting an enhancement of the overall ride quality. The relationship between the surrounding air motion and the vehicle vibration has been detailed in the article. Both measured testing and theoretical data were obtained through experiments and simulations to explore the possible modifications that can be made to the vehicle design to improve the comfort level of the ride when vehicle is operating at a high speed. This paper included additional attention on the study of the effects of aerodynamics when the vehicle encounters different road profiles. A suggestion to combine proper suspension system and streamline shaped vehicle body has been proposed. Taking into account of the non-uniform road surface pattern and the air motion effects, it brought a new prescriptive on the study of reducing vertical vibrations. The authors assume that downward force generated by the wing is based on the general equations of lift and drag, without including the effect of the specific wing geometry (i.e., the particular choice of airfoil). Three aerodynamic coefficients are used to represent both forces acting on the front and rear axles, and the drag coefficient. All of the coefficients are functions of the vertical displacements of vehicle's front and rear suspension.

The development of advanced engineering technologies has always been pushing the motor vehicle industrial forward. The application of engineering technologies improves the safety and

performance of the vehicle by modifying the forces affecting vehicle longitudinal dynamics and stability. Diba et al.[11] explored the efficiency of an actively controlled aerodynamic system applied to enhance the controllability and safety performance of small-size race car in lane changing movements on wet roads. In order to achieve the goal of stabilizing the race car under high acceleration and top speed conditions, an approach which required increasing the longitudinal forces acting on the vehicle was proposed. Their study indicates the capacity of active forces on the tires relates to the friction coefficient between the road surface and tires, and the effect of tire normal force. An application of an active inverted wing has been introduced to the comprehensive non-linear vehicle model analysis, to explore the potential ways of improving the vehicle stability and controllability. The main results of this article from is the study of the racing car lane change maneuver on both wet and dry surface road. Results from the computer simulations show the increasing sensitivity of the steering system with the application of the controller system; the vehicles have a tendency to perform safely with a higher speed. However, most of the airfoils have a stalling angle of attack around 15° – 20° and after the angle is reached, the lifting force will reduce. The angle of attack in the paper is increasing up to even 60° , which is not reasonable, and the testing vehicle mass is about 227 kg, which is very light when compared with a normal passenger car. A controller system is used to control the active aerodynamic system and apply it on the vehicle system.

Another interesting example of vehicle and aerodynamic interaction is described in ‘Modelling and handling dynamics of a wind-driven vehicle’[12], referring to a wind driven land yacht with a total mass of approximately 100 kg, and a vertical wing (using a NACA0012 profile) attached in front of the centre of mass.

In the paper by Corno[13], the main focus is on semi-active and active suspension technologies to ameliorate the vehicle’s road holding ability, without incurring costs in ride quality. A design of a closed-loop controller is proposed to decrease the dynamic tire deflection, which has a direct impact on the vehicle road holding capability. Simulation has been performed on a quarter-car vehicle model to verify the importance of road roughness, vehicle speed, and airfoil design on the vehicle. The discussion of improving the overall ride quality has been expanded based on three main categories: comfort, handling, and road holding. In this paper, the authors are mainly working on examination of the application of vehicle aerodynamics on the road holding ability by adding a controller suspension system to the model. The semi-active implementation is referred to as ‘ground-hook’, which imitates an imaginary damper between the tire and the road surface. It genuinely improves the vehicle road holding ability, but often the penalty of losing ride comfort comes along with such improvements. This study is aiming at minimizing this trade-off through the application of aerodynamics; maintaining the ride quality while improving the vehicle road holding ability.

The primary goal of Kajiwara [14] is to apply a rear wing design to improve the vehicle handling and performance during a cornering maneuver. The air resistance has a positive correlation with the angle of attack of the designed rear wing when a vehicle performs at a high speed, which generates a larger drag force, consequently, the fuel efficiency will decrease under these circumstances. In order to alleviate this effect, they propose to modify the wing geometry when cornering at high speed. A passive-type variable rear wing has been introduced to the design, and both numerical computer simulation and laboratory wind tunnel test have been performed. The final results suggest the possibility of a passive type variable rear wing design to generate a relatively large downforce to accommodate the existing situation, which has the similar responses as a fixed-type rear wing under low speed condition, and decreasing drag under high-speed conditions.

Differing from previous research articles that have been reviewed, in the paper by Meijaard et al [15], a design featuring a combination of suspension actuators and body mounted aerodynamic actuators was proposed to investigate the potential improvement of ride quality and road holding ability of the vehicle. A design of a control system to stabilize the vehicle and to keep the dynamic wheel load uniformly distributed was proposed. Nevertheless, this controller system design is not applicable, as it requires an infinite bandwidth, along with accurate knowledge of the design parameters. The article also introduced an alternative design similar to the proposed controller system design, which is more practical in real life design applications. Overall, the study was focused on the ability to conduct a proper design of the combined controller system that can enhance the overall ride quality without imposing a penalty on the dynamic load acting on the wheel.

A yaw stability and control analysis is found in Ahangarnejad and Melzi[16]. One of the most significant parameters affecting vehicle performance is the normal force distribution on the tires. By utilizing the normal loads on the tires, vehicle controllability can be increased. An actively controlled aerodynamic system can be applied to exploit the angle of attack of the spoilers, which can modify the normal loads, and the distribution on both front and rear axles of the vehicle during a high lateral acceleration. Numerical simulation is performed based on a nonlinear 4 DOF car model, to explore the effects of control logic on both oversteer and understeer responses. Active Aerodynamics Control (AAC) changes the normal load distribution under the effects of aerodynamic downforce. The algorithm governing the inclination of the spoilers can be modified for different aerodynamic responses.

In conclusion, many researchers are interested in the potential improvements that aerodynamic effects can have on the vehicle motion. In most research, an attached wing system is applied on the model to generate significant downforce, in order to improve the normal force acting on the tire, improving the vehicle handling. Most of the models are built based on the assumption that certain types of control system are able to supply the required wing forces and moments by actively orienting the wing, rather than actually simulating a real wing. This is significant, since the coefficient of lift is not linear, and the stalling angle of most airfoils are around 20° at which

point, the wing may not be able to generate the forces requested. A major portion of the papers listed focus on discussing vehicle handling and stability during cornering maneuver. A similar type of investigation will be carried out in this thesis, with particular consideration of the ride quality of the half car model with an attached wing system.

1.4 Research Objectives

There are three primary goals established in the beginning of this project.

The first goal is to verify the assumption that attached wings could make significant differences within the dynamic properties of a multibody mechanical system. A simple model is tested first, the shimmy problem, a simple single body model that has been widely explored in the literature. Preliminary results suggest that an attached wing could allow improvements in vehicle stability, shown by both eigenvalues and frequency response.

The second goal is to extend this analysis onto the half car model. The half car model is a three body, four degree of freedom model, extended from the simpler bounce pitch model with the addition of unsprung mass effects for both the front and rear suspensions.

In the proposed model, both front and rear wings are attached at different varying orientations, where mechanical linkage systems are used to drive the angle of the wing. The wing is tilting in response to displacement from the suspension systems, to make the wing angle of attack a variable, amplifying the aerodynamic effect. It is proposed to generate the equations of motion of this model using a multibody-dynamics tool rather than by hand, to exploit the potential improvement of more complex systems.

The third goal is to compare and analyze the model both with and without wings, with different factors, to optimize the performance of the wing system, e.g, to ensure the wing is working in the most beneficial manner while the vehicle is moving, to determine a fit size of the wing configuration, and test how the various factors are affecting the system.

1.5 Thesis Structure

In this section, the remaining chapters will be briefly described, to establish the structure of the thesis.

Chapter 2 will introduce the theory of multibody dynamics and describe how the equations of motion are generated. This chapter will also discuss the software tools utilized in the thesis, and explain how the results demonstrate the system dynamic properties. Some well known example systems from the literature and their equations of motion will be included in this chapter.

Chapter 3 is a presentation on aerodynamic theory. Aero forces and moments are described using the concept of lift and drag coefficients, which are expanded and developed into an 'effective

damping' matrix that can be included in the multibody formulation. An example is shown in the chapter to explain how the equation of motion of a sample wing is generated and how aerodamping effects are captured in the EoM software.

In Chapter 4, the vehicle model will be described. General information regarding the system is given, e.g., inertial properties, detailed geometry, etc. Also, the concept of the random road is included to introduce how this multibody model is tested, and explain how the time history response is generated.

Chapter 5 will list the simulation results, including eigenvalues, frequency response, and time history response for the random road. Comparisons will be made for the model with and without wings. This chapter also includes a study on the effect from different wing system configurations, different unsprung mass distributions, and speeds. A detailed discussion of the results is included in this chapter.

The thesis will end with Chapter 6, including the conclusions, recommendations, and summary of contributions.

Chapter 2

Multibody Dynamics

In this chapter, the generation of the equations of motion, including methods and theories used during the process will be described. This is the method used by the EoM software, which is developed by the University of Windsor Vehicle Dynamics and Control Research Group, and restricts the analysis to linear systems.

After building the equations of motion, the next step is to compute the solution. Note that treating the system as nonlinear may offer more precision, but restrict the solution to time history only, where linear systems also offer the possibility of eigen analysis and frequency domain studies.

Many well known sample models including the shimmy model, the quarter car model, the yaw plane model, and the bounce pitch model are described. Note that these models are simple enough to generate by hand, but are also easily modelled in EoM.

2.1 Generating the equation of motion

It is more challenging to generate the equations of motion of a vehicle (or any mechanical system) as the complexity of the model grows. Instead of generating the equations of motion by hand, an automatic equation generation tool can be used. In practice, for some very complex models, automatic generation is effectively a requirement. A vehicle can be treated as a regular mechanical system, with several rigid bodies connected by different kinds of mechanical joints. Generation and solution of the equations of motion of such mechanical systems are introduced as ‘multibody dynamics’.

In the most general cases, the equations of motion of a constrained mechanical system are a set of coupled nonlinear differential algebraic equations (DAEs). The three necessary parts to complete the format:

- The *kinematic differential equations* are used to relate velocities and angular velocities to the rate of change of positions and orientations. This is not always a direct equivalence when different coordinate systems are involved.

- The *Newton Euler equations* introduce the relationship between forces and moments and rate of change of velocities and angular velocities.
- The *constraint equations* describe the restrictions on the motions, and are used to solve for the constraint forces acting on the hinges and other connectors installed between individual rigid bodies.

2.1.1 Definition of coordinates

Generation of the equations will begin with defining a set of coordinates to describe the motion of the system. Generally, six coordinates will be assigned to the centre of mass of each body, which is the reference point. Three of the coordinates are for position and three are for orientation.

One issue in three dimensional motion that requires attention is that rotation is not a vector quantity like translation. When a sequence of translations is applied on a body, the order of translations does not make any difference to the final position. In contrast, the final orientation will be affected by the order in which the individual rotations are applied. As a result, in the general case, there is some complexity in defining angular motion coordinates, but since the linearization process restricts the motion to small angles, they can be considered as independent rotations around the x , y , and z axes.

The position and orientation coordinates are written in a $6n \times 1$ combined vector as \mathbf{p} :

$$\mathbf{p} = \left[x'_1 \quad \theta'_1 \quad x'_2 \quad \theta'_2 \quad \cdots \quad x'_n \quad \theta'_n \right]' \quad (2.1)$$

where n represents the number of rigid bodies in the system. Positions and orientations for each body are defined in a fixed global reference frame, and they are all zero while the system is in the reference configuration. Velocities and angular velocities for each body are defined in a body fixed reference frame, which is noticed as frame attached to each individual rigid body. The velocities and angular velocities are also written as a combined vector term, represented by \mathbf{w} .

2.1.2 Kinematic differential equations

The kinematic differential equations relate rate of change in position coordinates to the velocity coordinates. In some cases, if position and velocity coordinates are defined in the same reference frame, the velocity would be simply the time derivative of position. This relationship will become more complex when different reference frames are used.

In order to align different reference frames, a three by three transformation matrix \mathbf{R} is used, also called a rotation matrix. The rotation matrix is generally used to describe the relative misalignment of two reference frames. The formation of the rotation matrix depends on the two orientations defined and it is a function of the rotation angles.

The analysis here will start with considering translations. The relationship between the rate of change in position and velocity will be:

$$\dot{\mathbf{x}} = \mathbf{R}(\boldsymbol{\theta})\mathbf{v} \quad (2.2)$$

where:

$$\mathbf{R} = \mathbf{I} + \sin \theta \tilde{\mathbf{u}} + (1 - \cos \theta) \tilde{\mathbf{u}}\tilde{\mathbf{u}} \quad (2.3)$$

the orientation is function of the rotation of angle θ around the unit vector \mathbf{u} . For small rotation angles, it could be linearized as:

$$\mathbf{R} \approx \mathbf{I} + \tilde{\boldsymbol{\theta}} = \begin{bmatrix} 1 & -\psi & \theta \\ \psi & 1 & -\phi \\ -\theta & \phi & 1 \end{bmatrix} \quad (2.4)$$

In the equation, $\boldsymbol{\theta} = \theta\mathbf{u}$, and $\tilde{\boldsymbol{\theta}}$ represents the skew symmetric matrix of the three small angles used to define the orientation of the frame. The same relationship is applied to relate the angular motions.

$$\mathbf{S} = \mathbf{I} + \frac{\theta}{2} \tilde{\mathbf{u}} + \left(1 - \frac{\theta \sin \theta}{2(1 - \cos \theta)}\right) \tilde{\mathbf{u}}\tilde{\mathbf{u}} \quad (2.5)$$

For small rotation angles, the expression simplifies.

$$\mathbf{S} \approx \mathbf{I} + \frac{1}{2} \tilde{\boldsymbol{\theta}} \quad (2.6)$$

A 6×6 matrix \mathbf{P} used in the kinematic differential equations is defined in terms of \mathbf{R} and \mathbf{S} .

$$\mathbf{P} = \begin{bmatrix} \mathbf{R} & \mathbf{0} \\ \mathbf{0} & \mathbf{S} \end{bmatrix} \quad (2.7)$$

The kinematic differential equations become:

$$\begin{Bmatrix} \dot{\mathbf{x}} \\ \dot{\boldsymbol{\theta}} \end{Bmatrix} = \begin{bmatrix} \mathbf{R} & \mathbf{0} \\ \mathbf{0} & \mathbf{S} \end{bmatrix} \begin{Bmatrix} \mathbf{v} \\ \boldsymbol{\omega} \end{Bmatrix} \quad (2.8)$$

or:

$$\dot{\mathbf{p}} = \mathbf{P}(\mathbf{p})\mathbf{w} \quad (2.9)$$

Taking a variation to linearize gives:

$$\delta \dot{\mathbf{p}} = \delta \mathbf{P} \mathbf{w} + \mathbf{P} \delta \mathbf{w} \quad (2.10)$$

Recognizing that $\mathbf{P} = \mathbf{P}(\mathbf{p})$, and at the point of linearization (where $\mathbf{p} = \mathbf{0}$), that \mathbf{P} evaluates to the identity allows:

$$\begin{bmatrix} \mathbf{I} & \mathbf{0} \end{bmatrix} \begin{Bmatrix} \delta \dot{\mathbf{p}} \\ \delta \dot{\mathbf{w}} \end{Bmatrix} + \begin{bmatrix} \mathbf{V} & -\mathbf{I} \end{bmatrix} \begin{Bmatrix} \delta \mathbf{p} \\ \delta \mathbf{w} \end{Bmatrix} = \mathbf{0} \quad (2.11)$$

where the \mathbf{V} matrix depends only on the velocities \mathbf{w} at the point around which the kinematic differential equations are linearized.

2.1.3 Newton Euler equations

The next step in generating the equations of motion is to write the Newton Euler equations of motion of each body based on the equation that the rate of change in velocities times the mass equals to the sum of the forces. Those forces are functions of the velocity and position of the bodies. In this case, terms are grouped in order to get a better sense while reading, i.e., the mass term will include both mass and moment of inertia, linear and angular velocity will be both included in the velocity term, and forces represents for forces and moments.

$$\mathbf{M} \dot{\mathbf{w}} = \sum \mathbf{f}(\mathbf{p}, \mathbf{w}, t) \quad (2.12)$$

The mass matrix is filled diagonally by mass for each body and the moment of inertia in the system.

$$\mathbf{M} = \begin{bmatrix} m_1 & 0 & 0 & 0 & 0 & 0 \\ 0 & m_1 & 0 & 0 & 0 & 0 \\ 0 & 0 & m_1 & 0 & 0 & 0 \\ 0 & 0 & 0 & I_{xx_1} & -I_{xy_1} & -I_{xz_1} & \dots \\ 0 & 0 & 0 & -I_{xy_1} & I_{yy_1} & -I_{yz_1} \\ 0 & 0 & 0 & -I_{xz_1} & -I_{yz_1} & I_{zz_1} \\ \vdots & & & & & & \ddots \end{bmatrix} \quad (2.13)$$

The force could be sorted into different types, such as inertia force f_i , elastic force f_e , constraint force f_c , and applied force f_a . Therefore the equation of motion can be expressed as:

$$\mathbf{M} \dot{\mathbf{w}} = \sum \mathbf{f}_i + \sum \mathbf{f}_e + \sum \mathbf{f}_c + \sum \mathbf{f}_a \quad (2.14)$$

When the Newton Euler equations are linearized, the elastic forces result in the stiffness (\mathbf{K}) and damping (\mathbf{L}) matrices, and the inertial forces also contribute to terms in the \mathbf{L} matrix.

$$\begin{bmatrix} \mathbf{0} & \mathbf{M} \end{bmatrix} \begin{Bmatrix} \delta \dot{\mathbf{p}} \\ \delta \dot{\mathbf{w}} \end{Bmatrix} + \begin{bmatrix} \mathbf{K} & \mathbf{L} \end{bmatrix} \begin{Bmatrix} \delta \mathbf{p} \\ \delta \mathbf{w} \end{Bmatrix} = \delta f_c + \delta f_a \quad (2.15)$$

2.1.4 Constraint equations

After formation of the Newton Euler equations and kinematic differential equations, the final step will be exclusion of the constraint forces. In multibody systems, mechanical joints and connectors are used to connect rigid bodies in order to limit the degrees of freedom of the system. These joints and connectors will not deform elastically. The degrees of freedom of the mechanism will affect number of independent motions that the system can have. Normally, a unconstrained body will have six degrees of freedom, three are translation on x , y , z axes and the remaining three would be rotational motion around the axes. For example, if n is the number of bodies and m represents number of constraints, then the number of degrees of freedom will be $6n - m$. Every mechanical connector will add constraints onto the system, and remove degrees of freedom.

The constraint Jacobian \mathbf{J} is used to minimize the size of the matrix for equation of motions, since the constrained motion is not able to occur. The equation is written including both holonomic and nonholonomic constraints, which are represented by \mathbf{J}_h and \mathbf{J}_{nh} matrices, respectively. (Holonomic constraints are those that form relationships between the positions of the various bodies, where the nonholonomic constraints depend on relationships between the velocities that cannot be expressed as functions of position.)

$$\begin{bmatrix} \mathbf{J}_h & \mathbf{0} \\ \mathbf{J}_h \mathbf{V} & \mathbf{J}_h \\ \mathbf{0} & \mathbf{J}_{nh} \end{bmatrix} \begin{bmatrix} \delta \dot{\mathbf{p}} & \delta \mathbf{p} \\ \delta \dot{\mathbf{w}} & \delta \mathbf{w} \end{bmatrix} = \begin{bmatrix} \mathbf{0} & \mathbf{0} \\ \mathbf{0} & \mathbf{0} \\ \mathbf{0} & \mathbf{0} \end{bmatrix} \quad (2.16)$$

An orthogonal complement of the constraint Jacobian is applied in order to minimize the size of the coordinates since the constrained degrees of freedom will no longer shown in the equation of motion. Find a constant matrix \mathbf{T} , which satisfies:

$$\mathbf{JT} = \mathbf{0} \quad (2.17)$$

Then, define new coordinates vector \mathbf{x} , such that

$$\mathbf{T}\mathbf{x} = \begin{Bmatrix} \delta \mathbf{p} \\ \delta \mathbf{w} \end{Bmatrix} \quad (2.18)$$

Therefore:

$$\mathbf{JT}\mathbf{x} = \mathbf{J} \begin{Bmatrix} \delta \mathbf{p} \\ \delta \mathbf{w} \end{Bmatrix} = \mathbf{0} \quad (2.19)$$

Similarly, the matrix \mathbf{U} is defined such that:

$$\mathbf{U} \begin{Bmatrix} \mathbf{0} \\ \mathbf{f}_c \end{Bmatrix} = \mathbf{0} \quad (2.20)$$

While the equations are reduced to minimal coordinates, the result will become a set of first order linear equations.

$$\mathbf{U} \begin{bmatrix} \mathbf{I} & \mathbf{0} \\ \mathbf{0} & \mathbf{M} \end{bmatrix} \mathbf{T} \dot{\mathbf{x}} + \mathbf{U} \begin{bmatrix} \mathbf{V} & -\mathbf{I} \\ \mathbf{K} & \mathbf{L} \end{bmatrix} \mathbf{T} \mathbf{x} = \mathbf{U} \begin{Bmatrix} \mathbf{0} \\ \mathbf{f}_a \end{Bmatrix} \quad (2.21)$$

To simplify,

$$\mathbf{A} = -\mathbf{U} \begin{bmatrix} \mathbf{V} & -\mathbf{I} \\ \mathbf{K} & \mathbf{L} \end{bmatrix} \mathbf{T} \quad (2.22)$$

$$\mathbf{B} \mathbf{u} = \mathbf{U} \begin{Bmatrix} \mathbf{0} \\ \mathbf{f}_a \end{Bmatrix} \quad (2.23)$$

$$\mathbf{E} = \mathbf{U} \begin{bmatrix} \mathbf{I} & \mathbf{0} \\ \mathbf{0} & \mathbf{M} \end{bmatrix} \mathbf{T} \quad (2.24)$$

Once these terms are substituted, the result will be the descriptor state space form of the equations.

$$\begin{bmatrix} \mathbf{E} & \mathbf{0} \\ \mathbf{0} & \mathbf{I} \end{bmatrix} \begin{Bmatrix} \dot{\mathbf{x}} \\ \mathbf{y} \end{Bmatrix} = \begin{bmatrix} \mathbf{A} & \mathbf{B} \\ \mathbf{C} & \mathbf{D} \end{bmatrix} \begin{Bmatrix} \mathbf{x} \\ \mathbf{u} \end{Bmatrix} \quad (2.25)$$

where \mathbf{x} is the state vector, \mathbf{y} represents the output and \mathbf{u} is the input vector. The state vector is generated by the system automatically while output and input vector are chosen by user.

2.2 Software tools

This section discusses the Equation of Motion (EoM) multibody dynamics software developed by University of Windsor Vehicle Dynamics and Control Research Group. The EoM software can generate linear or linearized equation of motion for multibody mechanical systems using the algorithm detailed above. It is completely open source and runs within MATLAB, or it can be operated on a cost free syntax compatible language called Octave. It has also recently been translated into Julia, which is a new open source high performance programming language. The open source code editor/development environment Atom can be used as a framework. It has many extensions available, making it easier to work with the Julia language. EoM is freely available online at the software hosting site www.github.com; Octave, Julia, and Atom are also freely available.

When using EoM, each system has both an input and output file. The input file is a simple function file to build up the system definition with a freely chosen set of parameters. Each component in the system is defined as an ‘item’. There are many different types of item defined, e.g., the basic ‘body’, or rigid and flexible connectors that connect two or more rigid bodies. Table 2.1 lists all the available types of items used in EoM.

TABLE 2.1: Types of items in EoM

Type of item	Definition
body	a rigid body
spring	a two point elastic spring, with linear or torsional stiffness and damping, non-zero free length
link	a two point massless rigid link
rigid_point	a generic point constraint with a variable number of constraint forces and moments
flex_point	a point spring with translational and/or rotational stiffness and damping
nh_point	a non-holonomic constraint to prevent velocity but not displacement
beam	a zero mass beam spring with bi-directional bending and shear stiffness
load	constant forces or moments applied to the system
actuator	applied force or moment, proportional to an input signal
sensor	used to measure displacement, velocity, or acceleration

While analyzing a multibody system, EoM starts by reading information for the input data to fill in the necessary stiffness and constraint information, in order to collect the preload and constraint forces. The stiffness matrices will be updated with tangent stiffness terms after preloads and constraint forces are known.

The most recent version of EoM has expanded the form of the equation of motion to allow systems that depend not only on the value of the input, but also the rate of change of the input, e.g.,

$$m\ddot{x} + c\dot{x} + kx = fu + g\dot{u} \quad (2.26)$$

The equivalent matrix form, in EoM, before reduction to minimal coordinates becomes:

$$\begin{bmatrix} \mathbf{I} & \mathbf{0} & \mathbf{0} \\ \mathbf{0} & \mathbf{M} & -\mathbf{G} \\ \mathbf{0} & \mathbf{0} & \mathbf{0} \end{bmatrix} \begin{Bmatrix} \dot{\mathbf{p}} \\ \dot{\mathbf{w}} \\ \dot{\mathbf{u}} \end{Bmatrix} + \begin{bmatrix} \mathbf{V} & -\mathbf{I} & \mathbf{0} \\ \mathbf{K} & \mathbf{L} & -\mathbf{F} \\ \mathbf{0} & \mathbf{0} & \mathbf{I} \end{bmatrix} \begin{Bmatrix} \mathbf{p} \\ \mathbf{w} \\ \mathbf{u} \end{Bmatrix} = \begin{bmatrix} \mathbf{0} \\ \mathbf{0} \\ \mathbf{I} \end{bmatrix} \begin{Bmatrix} \mathbf{u} \end{Bmatrix} \quad (2.27)$$

The F and G matrices relate applied forces to the input and the rate of change of input, respectively.

The differential equations generated by EoM are solved, and the result is included in the output report. The software finds the eigenvalues and natural frequencies for different types of motion, using the relationship:

$$\det[\mathbf{E}s - \mathbf{A}] = 0 \quad (2.28)$$

The eigenvalues can be expressed with two parts, $s = a \pm ib$. The real part a represents decay of motion, while the imaginary part b of the roots shows the frequency. When the real parts are negative, the motion is stable, and it will decay approaching to zero with time. Otherwise, the motion will grow. The imaginary part shows the frequency of oscillation motion; if the imaginary part is zero, then there will be no oscillation in the unforced motion.

The output file is a system report in a .pdf format, containing the state space form of the equations. Each mode of the system will have corresponding eigenvalues and frequencies, which describes the system behaviour.

2.3 Examples

Over the years, researchers in vehicle dynamics have introduced many important models, e.g., the yaw plane (or bicycle) model, the truck and trailer model, the quarter car model, the bounce pitch model, and the half car model. A few of the more important models relevant to this thesis will be introduced in this section. This thesis is based on a half car model, which is a combination of bounce pitch model and quarter car model. Therefore, the quarter car model and bounce pitch model are included and detailed in this section. The yaw plane model is added to the section; it contains both yaw and lateral motions, which are general vehicle motions.

2.3.1 Shimmy model

In order to prove that the aerodynamic forces and moments have significant effects on control and stability, the shimmy problem has initially been tested. Shimmy, as sometimes occurs on the nose landing gear of aircraft, is a self-excited angular oscillatory motion around the vertical axis. It can cause excessive tire wear and poses a serious safety hazard. The tire will have better grip if the system moves smoothly in the longitudinal direction. Otherwise, as the amplitude of oscillatory motion grows with time, it can cause the tire to lose grip and slip off the track.

This swivel wheel problem was not well understood until it was investigated by Den Hartog[17], and later by Schwab and Meijaard[18]. A model as single rigid body model was built, constrained to xy planar motion, with a constant forward speed as shown in Figure 2.1.

Point C is where the wheel strut is built on the plane. Point B is the connecting point between the spring and landing gear. The spring represents the flexibility in the gear mount to the aircraft. The point G represents the center of gravity of the landing gear. In this model, the landing gear is simplified as a single body and the tire is modelled as a nonholonomic (i.e., its lateral slip speed is zero). The properties of the mechanical system used for this analysis are: $m = 5.0$ kg, $l = 1.0$ m,

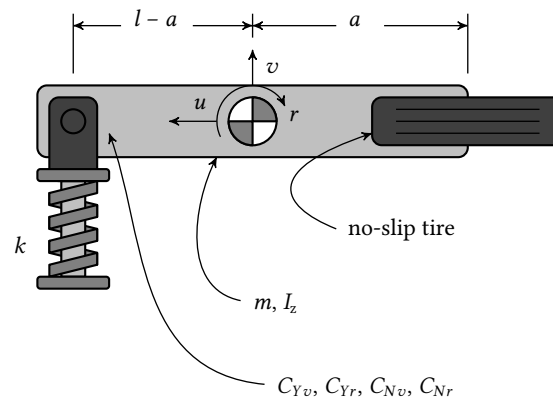


FIGURE 2.1: Swivel wheel, a single rigid body constrained as a xy planar motion with a constant forward speed. The tire is non slip tire.

$I_z = 1.05 \text{ kg m}^2$, $k = 1.5 \text{ N/m}$, and $u = 10.0 \text{ m/s}$. The location of the mass centre is varied from the front to the rear of the model.

The model has two degrees of freedom; these are the lateral and yaw motions. Normally one would expect two second order differential equations as a result, or equivalently a fourth order system, but the nonholonomic constraint reduces the system to third order. (One might think of nonholonomic systems as having half degrees of freedom, as the displacements are independent but the velocities are not.)

The result shows one real root and one set of complex roots. The real root is relatively stable, while the complex roots can become unstable. The results are strongly relying on the location of the mass center; while it is near the middle point between the tire and lateral spring, the motion is stable. Otherwise, the result will predict an unstable system.

The shimmy example will be repeated in Chapter 3 with an aerodynamic surface added to the model.

2.3.2 Quarter car model

The quarter car model is a famous vehicle model that has been used for many year for analyzing ride quality. Two rigid bodies are constrained to vertical translation, giving a simple two degree of freedom system. The sprung mass represents the chassis, powertrain and driver, while the unsprung mass includes the wheel, hub and brake system. Figure 2.2 shows the quarter car model.

The suspension connects the sprung and unsprung mass, and is represented by a linear spring and damper system with coefficients k_s and c_s . The tire is assumed to be a spring connecting the unsprung mass and the ground. Tire damping is typically ignored since practically the damping of the tire is very small. The terms z_s and z_u are the displacement of the sprung and unsprung mass measured from the inertial reference frame, and z_g is the disturbance from the road. Newton's equation of motion for each of the two rigid bodies will be expressed as, for the sprung mass:

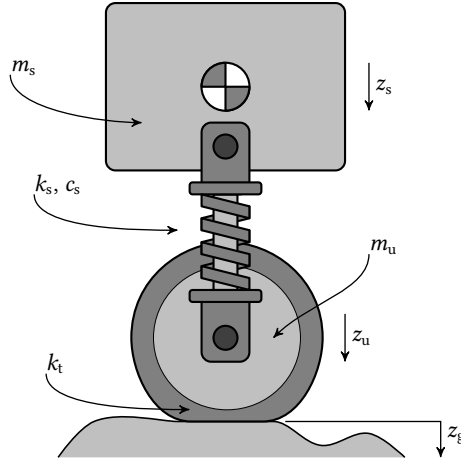


FIGURE 2.2: Quarter car model.

$$m_s \ddot{z}_s + c_s \dot{z}_s - c_s \dot{z}_u + k_s z_s - k_s z_u = 0 \quad (2.29)$$

For unsprung mass will be:

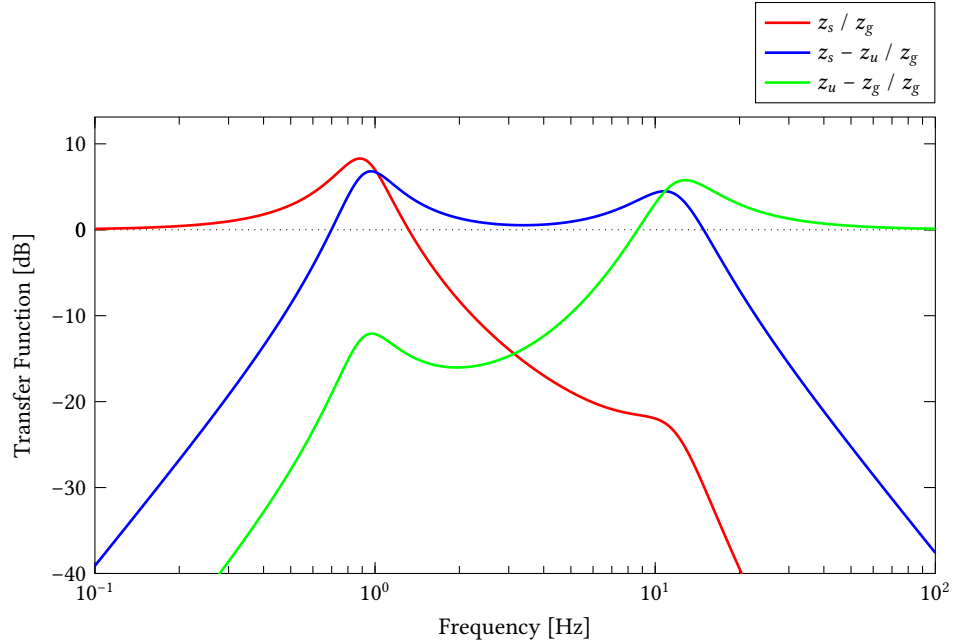
$$m_u \ddot{z}_u + c_s \dot{z}_u - c_s \dot{z}_s + k_s z_u - k_s z_s + k_t z_s = k_t z_g \quad (2.30)$$

These two equations could be combined and written into vector equation and simplified as:

$$\mathbf{M}\ddot{\mathbf{z}} + \mathbf{L}\dot{\mathbf{z}} + \mathbf{K}\mathbf{z} = \mathbf{F}\mathbf{u} \quad (2.31)$$

Frequency response

Using the quarter car model with a smooth random road profile and a very low damping coefficient, as described in the figure 2.3, the frequency responses shown in Figure were obtained. With all three lines, z_s/z_g represents the sprung mass response which is the vehicle body; $z_s - z_u/z_g$ shows the suspension and the tire response is represented by $z_u - z_g/z_g$. As the figure shows, the lower frequency range is associated with the vehicle body motion, which is making sense, that while the vehicle is moving up and down slowly enough, the vehicle body will simply follow the lower frequency road curve. Mid-range frequency responses shows that suspension becomes functional and absorb the disturbance from the road while the frequency is in between 1 Hz and 10 Hz. If the vehicle is moving faster or the wavelength becomes smaller, most of the road disturbance will transferred into the deformation of tires.

FIGURE 2.3: Frequency response: z_g

2.3.3 The yaw plane model

The yaw plane model is also called the bicycle model, because the width of the vehicle is neglected in the development of the model. When the width of the vehicle is neglected, the illustrations look similar to a bicycle. The width of the vehicle will affect the lateral weight transfer, which could in turn change the tire behaviour, but the effect is generally small and ignored in the yaw plane model to preserve linearity. This model has been used extensively to analyze vehicle handling.

There are only two degrees of freedom in this model, the lateral velocity v , and the yaw plane velocity r of the vehicle. The forward speed u is assumed to be constant and it is mostly like a parameter of the model instead of a variable. The vehicle mass m and the moment of inertia around the z axis I_{zz} form up the mass matrix of the equation. The distance from the center of mass to the front and rear axle are represented by a and b . The cornering stiffnesses for the front and rear tires are shown as c_f and c_r in the equation, which is measuring the lateral forces generated by the rolling tire.

The longitudinal equation is not considered in the model; the lateral force equation will be expressed as:

$$\sum Y = Y_f + Y_r = m(\dot{v} + ru) \quad (2.32)$$

Only the z component is considered during the rotation equation; it is also a function of the lateral forces.

$$\sum N = aY_f - bY_r = I_{zz}\dot{r} \quad (2.33)$$

Therefore, the two equations of motion become:

$$\begin{Bmatrix} \sum Y \\ \sum N \end{Bmatrix} = \begin{bmatrix} 1 & 1 \\ a & -b \end{bmatrix} \begin{Bmatrix} Y_f \\ Y_r \end{Bmatrix} = \begin{Bmatrix} m(\dot{v} + ur) \\ I_{zz}\dot{r} \end{Bmatrix} \quad (2.34)$$

Lateral forces generated between the tire and ground are depending on many factors, but the main reason is the misalignment between the direction the tire is pointing and the direction the tire is travelling. The lateral forces are assumed to be proportional to the tire slip angle α , since the a linear tire model is used in the bicycle model. The forces then become:

$$\begin{Bmatrix} Y_f \\ Y_r \end{Bmatrix} = - \begin{bmatrix} c_f & 0 \\ 0 & c_r \end{bmatrix} \begin{Bmatrix} \alpha_f \\ \alpha_r \end{Bmatrix} \quad (2.35)$$

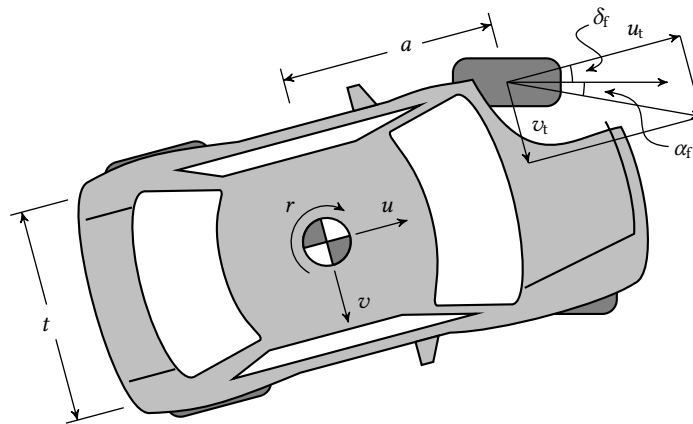


FIGURE 2.4: The tire slip angle shows the difference between direction the tire is travelling to and the direction the tire is pointing. Figure reproduced from Mianaker[19].

From Figure 2.4, the tire lateral speed will be the sum of the lateral speed of the vehicle and the effect from the yaw velocity. And similarly, the tire forward speed equals to the vehicle forward speed plus the effect from the yaw velocity.

$$v_t = v + ra \quad (2.36)$$

$$u_t = u + \frac{rt}{2} \quad (2.37)$$

Therefore, the relationship between the steer angle, slip angle and velocities could be expressed,

$$\tan(\alpha_f + \delta_f) = \frac{v + ra}{u + \frac{rt}{2}} \quad (2.38)$$

Compared to the vehicle forward speed, the effect of yaw velocity will become very small, or in other words, the width of the vehicle could be ignored in the simulation within the calculation of longitudinal speeds. Therefore, the left and right side will have the same result, since both sides have the same slip angle. Linearizing the equations for small slip angles:

$$\begin{Bmatrix} \alpha_f \\ \alpha_r \end{Bmatrix} = \frac{1}{u} \begin{bmatrix} 1 & a \\ 1 & -b \end{bmatrix} \begin{Bmatrix} v \\ r \end{Bmatrix} - \begin{Bmatrix} \delta_f \\ 0 \end{Bmatrix} \quad (2.39)$$

Working with substitution, the equations can be rewritten as:

$$\begin{bmatrix} m & 0 \\ 0 & I_{zz} \end{bmatrix} \begin{Bmatrix} \dot{v} \\ \dot{r} \end{Bmatrix} + \frac{1}{u} \begin{bmatrix} c_f + c_r & ac_f - bc_r + mu^2 \\ ac_f - bc_r & a^2c_f + b^2c_r \end{bmatrix} \begin{Bmatrix} v \\ r \end{Bmatrix} = \begin{bmatrix} c_f \\ ac_f \end{bmatrix} \begin{Bmatrix} \delta_f \end{Bmatrix} \quad (2.40)$$

The final equation of bicycle model is well known and has been used for many years. It ignores some factors during the calculation, but the result is still considered as reasonably accurate.

2.3.4 Bounce pitch model

The bounce pitch model is analyzing both bounce and pitch motion of the vehicle model, without considering the suspension system and unsprung mass effects, since the sprung and unsprung mass tend to have very different natural frequencies. The vehicle is assumed to be a single rigid body and the pitch angle is also assumed to be small enough to ignore the trigonometric functions.

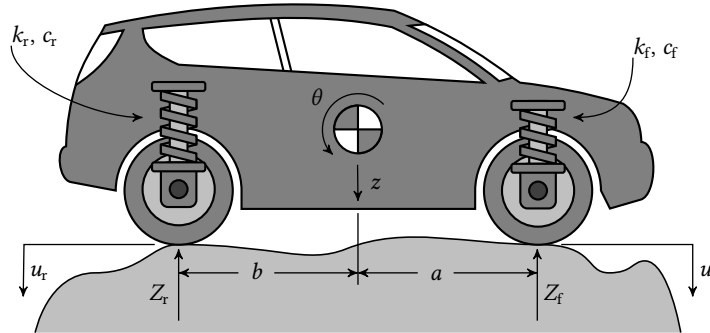


FIGURE 2.5: Bounce pitch model, used to analysis riding quality. Figure reproduced from Minaker[19]

The deflection of front and rear suspension will be function of z , the vertical motion of the center of mass, and the pitch angle θ . The front suspension deflection will be:

$$z_f = z - a\theta - u_f \quad (2.41)$$

and the rear suspension is:

$$z_r = z + b\theta - u_r \quad (2.42)$$

Suspension forces in both front and rear will be linearly expressed with respect to stiffness and damping effects as:

$$Z_f = k_f z_f + c_f \dot{z}_f \quad (2.43)$$

$$Z_r = k_r z_r + c_r \dot{z}_r \quad (2.44)$$

These can be summed to get the equation of motion for vehicle bounce.

$$\sum Z = -Z_f - Z_r = m\dot{w} = m\ddot{z} \quad (2.45)$$

When expanded the bounce equation becomes:

$$m\ddot{z} + c_f(\dot{z} - a\dot{\theta}) + c_r(\dot{z} + b\dot{\theta}) + k_f(z - a\theta) + k_r(z + b\theta) = c_f\dot{u}_f + c_r\dot{u}_r + k_f u_f + k_r u_r \quad (2.46)$$

In this case, c_f and c_r are used to represent damping stiffness. Since there are forces generated on each axle, there is corresponding moment generated at the same time around the vehicle's center of mass. The moments from both axles sum to give the equation of motion for vehicle pitch:

$$\sum M = aZ_f - bZ_r = I_{yy}\ddot{\theta} \quad (2.47)$$

$$I_{yy}\ddot{\theta} - ac_f(\dot{z} - a\dot{\theta}) + bc_r(\dot{z} + b\dot{\theta}) - ak_f(z - a\theta) + bk_r(z + b\theta) = -ac_f\dot{u}_f + bc_r\dot{u}_r - ak_f u_f + bk_r u_r \quad (2.48)$$

Combining bounce and pitch will give the vector equation:

$$\begin{aligned} \begin{bmatrix} m_s & 0 \\ 0 & I_{yy} \end{bmatrix} \begin{Bmatrix} \ddot{z} \\ \ddot{\theta} \end{Bmatrix} + \begin{bmatrix} c_f + c_r & bc_r - ac_f \\ bc_r - ac_f & a^2 c_f + b^2 c_r \end{bmatrix} \begin{Bmatrix} \dot{z} \\ \dot{\theta} \end{Bmatrix} + \begin{bmatrix} k_f + k_r & bk_r - ak_f \\ bk_r - ak_f & a^2 k_f + b^2 k_r \end{bmatrix} \begin{Bmatrix} z \\ \theta \end{Bmatrix} \\ = \begin{bmatrix} k_f & k_r \\ -ak_f & bk_r \end{bmatrix} \begin{Bmatrix} u_f \\ u_r \end{Bmatrix} + \begin{bmatrix} c_f & c_r \\ -ac_f & bc_r \end{bmatrix} \begin{Bmatrix} \dot{u}_f \\ \dot{u}_r \end{Bmatrix} \end{aligned} \quad (2.49)$$

or

$$\mathbf{M}\ddot{\mathbf{x}} + \mathbf{L}\dot{\mathbf{x}} + \mathbf{K}\mathbf{x} = \mathbf{F}\mathbf{u} + \mathbf{G}\dot{\mathbf{u}} \quad (2.50)$$

Summary

This chapter has described a number of vehicle models from the literature. Because they were all relatively small models, they are suitable for symbolic derivation by hand. In this thesis, the half car model is used to reveal aerodynamic effects for vehicle models. It is quite similar to the bounce pitch model, with the difference of additional suspension and unsprung mass effect. It has two wheel hub motions, one vehicle body bounce motion, and body pitch motion; all the motions are constrained to occur in the vertical plane. The half car is effectively the combination of a quarter car model and a bounce pitch model. It has one sprung mass and two unsprung masses. Bounce motion occurs while the two suspension systems are moving in phase, otherwise, pitch motion will participate. The equations for the half car model are not presented here; they can be derived by hand, but the half car model marks a transition where hand based derivation starts to become unwieldy. The model used in this thesis adds additional complexity in the aerodynamic surface control mechanism, such that it is much more attractive to use a multibody dynamics tool to generate the equations.

Chapter 3

Aerodynamics

This chapter will cover the basic theories and equations of flight dynamics; in particular the stability derivatives are demonstrated as aerodynamic effectiveness coefficients matrix. The method by which the aero forces and moments are integrated into the equation of motion is shown. An example is included at the end of the chapter.

3.1 Equations of motion of a moving wing

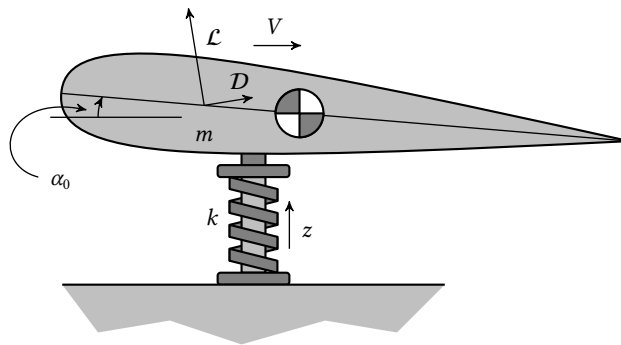


FIGURE 3.1: Spring mass wing model. Note that the lift and drag forces are assumed to remain perpendicular and parallel to the airflow direction, respectively, when measured in a reference frame that moves with the wing. Figure reproduced from Minaker et al[20].

To illustrate the inclusion of the aerodynamic effect and show the generation of the equation of motion, a simple spring mass system with a wing attached, as shown in Figure 3.1, is considered. Generation starts with breaking the net aerodynamic force into lift and drag forces. The lift force \mathcal{L} and drag force D are functions of the dynamic pressure q , and both of them are in proportion to the wing area S . The terms C_L and C_D are the dimensionless lift and drag coefficients.

$$q = \frac{1}{2} \rho V^2 \quad (3.1)$$

$$\mathcal{L} = q S C_L \quad (3.2)$$

$$D = qSC_D \quad (3.3)$$

In this case, an assumption has been made that lift and drag forces remain perpendicular and parallel, respectively, to the direction of the airstream, measured within the reference frame that moves with the wing. While the wing is moving in the vertical direction, the airflow will appear to come from the front and the top. The airflow will have a negative vertical velocity component, quantified by the angle of attack. The angle of attack can be written in terms of vertical speed of the wing while the angle is small.

$$\alpha \approx \alpha_0 - \frac{\dot{z}}{V} \quad (3.4)$$

Taking the vertical component of the aero forces gives:

$$Z = \mathcal{L} \cos(\alpha - \alpha_0) + D \sin(\alpha - \alpha_0) \quad (3.5)$$

Linearizing the equation, the Taylor series is applied.

$$Z \approx Z_0 + \left. \frac{\partial Z}{\partial \alpha} \right|_{\alpha=\alpha_0} (\alpha - \alpha_0) \quad (3.6)$$

Taking partial derivative for both lift and drag coefficients, since they are assumed to be functions of the angle of attack.

$$\frac{\partial Z}{\partial \alpha} = \frac{\partial \mathcal{L}}{\partial \alpha} \cos(\alpha - \alpha_0) - \mathcal{L} \sin(\alpha - \alpha_0) + \frac{\partial D}{\partial \alpha} \sin(\alpha - \alpha_0) + D \cos(\alpha - \alpha_0) \quad (3.7)$$

$$\left. \frac{\partial Z}{\partial \alpha} \right|_{\alpha=\alpha_0} = \left. \frac{\partial \mathcal{L}}{\partial \alpha} + D = qS \left(\frac{\partial C_L}{\partial \alpha} + C_D \right) \right|_{\alpha_0} \quad (3.8)$$

As a result:

$$Z = Z_0 + qS \left(\frac{\partial C_L}{\partial \alpha} + C_D \right) \Big|_{\alpha_0} (\alpha - \alpha_0) \quad (3.9)$$

Using Equation 3.4 gives:

$$Z = Z_0 - \frac{qS}{V} \left(\frac{\partial C_L}{\partial \alpha} + C_D \right) \Big|_{\alpha_0} \dot{z} \quad (3.10)$$

Combining the sum of the aerodynamic and spring forces, and equating to mass times acceleration gives the familiar second order linear differential equation of motion. Note that the deflection z is measured from equilibrium, where any static lift forces Z_0 are offset by the spring preload kz_0 ,

(weight force is neglected, but would have no effect in this example).

$$m\ddot{z} = Z - k(z + z_0) = Z_0 - \frac{1}{V} \frac{\partial Z}{\partial \alpha} \dot{z} - k(z + z_0) \quad (3.11)$$

Simplifying:

$$m\ddot{z} + \frac{qS}{V} (C_{L_\alpha} + C_D)|_{\alpha_0} \dot{z} + kz = 0 \quad (3.12)$$

It is notable that the dynamic pressure q is parabolic in V , so the wing behaves effectively as a damper whose coefficient increases linearly with airspeed. This is noteworthy in a vehicle dynamics context, as it is in contrast to a typical slip-based tire model, where the tire is effectively a damper whose coefficient varies as the inverse of forward speed.

3.2 Aerodynamic forces and moments

Generation of aerodynamic forces and moments are explored in this section and the development of equations are based on the textbooks by Schmidt[21] and Drela[8], with some changes in respect to the vehicle models.

3.2.1 General nonlinear form

Consider a moving body immersed in a stationary fluid. In this situation, the fluid and the body have forces and moments that act between them. In the general case, the forces acting on the body would contain both aerodynamic and propulsive forces. However, in this case, the propulsive forces are assumed to be zero. The aero forces will be expressed in the body fixed frame as :

$$\mathbf{F}_A = X_A \hat{\mathbf{i}}_V + Y_A \hat{\mathbf{j}}_V + Z_A \hat{\mathbf{k}}_V \quad (3.13)$$

When the nonlinear expressions are used, usually the body fixed reference frame will be the fuselage-referenced axes of the aircraft. Three aerodynamic force components are described as lift, drag, and side force, corresponding with x , y , and z axes, and are expressed in as:

$$X_A = C_X qS = -D \cos \alpha \cos \beta - S \cos \alpha \sin \beta + L \sin \alpha \quad (3.14)$$

$$Y_A = C_Y qS = -D \sin \beta - S \cos \beta \quad (3.15)$$

$$Z_A = C_Z qS = -D \sin \alpha \cos \beta - S \sin \alpha \sin \beta + L \cos \alpha \quad (3.16)$$

where α and β are the angle of attack and the sideslip angle in the body fixed reference frame. Here, D , \mathcal{L} and S are the drag, lift and side force respectively. The C terms are nondimensional coefficients. The wing area is S , and q is the dynamic pressure, which is equal to:

$$q = \frac{1}{2}\rho V^2 \quad (3.17)$$

where ρ is the fluid mass density, and V is the speed of the body. Similarly, the aero moments expressed within the body fixed frame, and divided into different components, are:

$$\mathbf{M}_A = L_A \hat{\mathbf{i}}_V + M_A \hat{\mathbf{j}}_V + N_A \hat{\mathbf{k}}_V \quad (3.18)$$

Assuming that the body has a general planform shape, the components could be individually listed as:

$$L_A = C_L q S b \quad (3.19)$$

$$M_A = C_M q S c \quad (3.20)$$

$$N_A = C_N q S b \quad (3.21)$$

Note here that the term C_L does not refer to the coefficient of lift, as is commonly used. The term b represents the wingspan of the planform shape, and c is the average chord length. These three aerodynamic moments are the rolling, pitching and yawing moments, respectively. In the integration of the forces into the linearized equation of motion, all of these six nondimensional coefficients will become factors in a 6×6 ‘damping’ coefficient term. The term damping is used, as the forces and moments are expressed as a linear function of the velocity and angular velocity.

3.2.2 Integration into the linearized equation of motion

It is assumed that forces and moments are depend on the six velocity coordinates:

$$\mathbf{w}' = \begin{bmatrix} u & v & w & p & q & r \end{bmatrix} \quad (3.22)$$

which are the variations in velocities as in the x , y , and z directions, followed by the angular velocities in the same sequence. The forces can equivalently be considered as functions of

$$\mathbf{w}^{*'} = \begin{bmatrix} u & \beta & \alpha & p & q & r \end{bmatrix} \quad (3.23)$$

since while the angles are small enough, they can be linearized as:

$$\alpha \approx \frac{w}{U_0} \quad (3.24)$$

and:

$$\beta \approx \frac{v}{U_0} \quad (3.25)$$

where U_0 is the x component of the velocity vector. If the body is assumed to be symmetric in the $x - z$ plane, and moving along a direction that lies in the plane, the forces could be expressed as:

$$X_A = \left. \frac{\partial X_A}{\partial u} \right|_0 u + \left. \frac{\partial X_A}{\partial \alpha} \right|_0 \alpha + \left. \frac{\partial X_A}{\partial q} \right|_0 q \quad (3.26)$$

$$Y_A = \left. \frac{\partial Y_A}{\partial \beta} \right|_0 \beta + \left. \frac{\partial Y_A}{\partial p} \right|_0 p + \left. \frac{\partial Y_A}{\partial r} \right|_0 r \quad (3.27)$$

$$Z_A = \left. \frac{\partial Z_A}{\partial u} \right|_0 u + \left. \frac{\partial Z_A}{\partial \alpha} \right|_0 \alpha + \left. \frac{\partial Z_A}{\partial q} \right|_0 q \quad (3.28)$$

The remaining coordinates not shown in the equation above usually have negligible effect on the forces. And similarly, the moments become:

$$L_A = \left. \frac{\partial L_A}{\partial \beta} \right|_0 \beta + \left. \frac{\partial L_A}{\partial p} \right|_0 p + \left. \frac{\partial L_A}{\partial r} \right|_0 r \quad (3.29)$$

$$M_A = \left. \frac{\partial M_A}{\partial u} \right|_0 u + \left. \frac{\partial M_A}{\partial \alpha} \right|_0 \alpha + \left. \frac{\partial M_A}{\partial q} \right|_0 q \quad (3.30)$$

$$N_A = \left. \frac{\partial N_A}{\partial \beta} \right|_0 \beta + \left. \frac{\partial N_A}{\partial p} \right|_0 p + \left. \frac{\partial N_A}{\partial r} \right|_0 r \quad (3.31)$$

Substituting back into 3.14, 3.15, 3.16, and working through the details in 3.1, the partial derivatives of the aerodynamic forces and moments could be defined after linearization as listed in Table 3.1. Based on the calculation, the aerodynamic forces and moments could be finally expressed as:

$$X_A = qS(-C_{D_u} + \frac{2}{U_0} C_{D_0})u + (-C_{D_\alpha} + C_{L_0})\alpha - C_{D_q}q \quad (3.32)$$

$$Y_A = qS(C_{S_\beta}\beta + C_{S_p}p + C_{S_r}r) \quad (3.33)$$

$$Z_A = qS(-C_{L_u} + \frac{2}{U_0} C_{L_0})u + (-C_{L_\alpha} + C_{D_0})\alpha - C_{L_q}q \quad (3.34)$$

$$L_A = qSb(C_{L_\beta}\beta + C_{L_p}p + C_{L_r}r) \quad (3.35)$$

$$M_A = qS((C_{M_u} + \frac{2}{U_0} C_{M_0})u + C_{M_\alpha}\alpha + C_{M_q}q) \quad (3.36)$$

$$N_A = qSb(C_{N_\beta}\beta + C_{N_p}p + C_{N_r}r) \quad (3.37)$$

These coefficients will be expressed as:

TABLE 3.1: Partial derivative of aerodynamic forces and moments, from[21]

Case	u	α	q
$\frac{1}{qS} \frac{\partial X_A}{\partial \cdot}$	$-(C_{D_u} + \frac{2}{U_0} C_{D_0})$	$(-C_{D_\alpha} + C_{L_0})$	$-C_{D_q} \approx 0$
$\frac{1}{qS} \frac{\partial Z_A}{\partial \cdot}$	$-(C_{L_u} + \frac{2}{U_0} C_{L_0})$	$(-C_{L_\alpha} - C_{D_0})$	$-C_{L_q}$
$\frac{1}{qSc} \frac{\partial M_A}{\partial \cdot}$	$-(C_{M_u} + \frac{2}{U_0} C_{M_0})$	C_{M_α}	C_{M_q}
Case	β	p	r
$\frac{1}{qS} \frac{\partial Y_A}{\partial \cdot}$	C_{Y_β}	C_{Y_p}	C_{Y_r}
$\frac{1}{qSb} \frac{\partial L_A}{\partial \cdot}$	C_{L_β}	C_{L_p}	C_{L_r}
$\frac{1}{qSb} \frac{\partial N_A}{\partial \cdot}$	C_{N_β}	C_{N_p}	C_{N_r}

In these damping coefficients, C_{D_u} , C_{L_u} and C_{M_u} are considered as changing with respect to the speed change. This is to allow for compressability effects at high speed. However, in this case, the speed of vehicle is very slow compared with the usual velocity of aircraft, which is often measured in Mach number (the fraction of the speed of sound). Even at the speed of very fast road vehicles, these three coefficients can be considered as zero.

The model in Chapter 4 will combine aero effects into the multibody dynamics in the half car model. This model does not consider roll, yaw, or lateral motion, which means many of the coefficients in the general case can be neglected, except C_{X_u} , C_{X_α} , C_{Z_u} , and C_{Z_α} . Only these coefficients will affect bouncing and pitching motion and they are all function of drag and lift coefficients. In this study, all the wing models have the pressure centre and the reference point at the same place, which is located at the quarter chord point. Therefore, there is no internal moment applied on the wing body with respect to the variables on the wing, thus C_{M_α} and C_{M_u} will not be considered as effective factors in the matrix.

Finally, the aerodynamic forces can be expressed using the damping term L as,

$$\begin{Bmatrix} X_A \\ Y_A \\ Z_A \\ L_A \\ M_A \\ N_A \end{Bmatrix} = \mathbf{L} \mathbf{w} \quad (3.38)$$

where:

$$\mathbf{L} = -\frac{qS}{U_0} \begin{bmatrix} C_{X_u} & 0 & C_{X_\alpha} & 0 & \frac{1}{2}cC_{X_q} & 0 \\ 0 & C_{Y_\beta} & 0 & \frac{1}{2}bC_{Y_p} & 0 & \frac{1}{2}bC_{Y_r} \\ C_{Z_u} & 0 & C_{Z_\alpha} & 0 & \frac{1}{2}cC_{Z_q} & 0 \\ 0 & bC_{l_\beta} & 0 & \frac{1}{2}b^2C_{l_p} & 0 & \frac{1}{2}b^2C_{l_r} \\ cC_{m_u} & 0 & cC_{m_\alpha} & 0 & \frac{1}{2}c^2C_{m_q} & 0 \\ 0 & bC_{n_\beta} & 0 & \frac{1}{2}b^2C_{n_p} & 0 & \frac{1}{2}b^2C_{n_r} \end{bmatrix} \quad (3.39)$$

This allows the generation of the commonly used equations of motion of the single body aircraft [8], in straight and level flight, to be expressed as:

$$\begin{bmatrix} \dot{x} \\ \dot{y} \\ \dot{z} \\ \dot{\phi} \\ \dot{\theta} \\ \dot{\psi} \\ \dot{u} \\ \dot{v} \\ \dot{w} \\ \dot{p} \\ \dot{q} \\ \dot{r} \end{bmatrix} = \begin{bmatrix} 0 & 0 & 0 & 0 & 0 & 0 & 1 & 0 & 0 & 0 & 0 & 0 \\ 0 & 0 & 0 & 0 & 0 & U_0 & 0 & 1 & 0 & 0 & 0 & 0 \\ 0 & 0 & 0 & 0 & -U_0 & 0 & 0 & 0 & 1 & 0 & 0 & 0 \\ 0 & 0 & 0 & 0 & 0 & 0 & 0 & 0 & 0 & 1 & 0 & 0 \\ 0 & 0 & 0 & 0 & 0 & 0 & 0 & 0 & 0 & 0 & 1 & 0 \\ 0 & 0 & 0 & 0 & 0 & 0 & 0 & 0 & 0 & 0 & 0 & 1 \\ 0 & 0 & 0 & 0 & g & 0 & X_u & 0 & X_w & 0 & X_q & 0 \\ 0 & 0 & 0 & -g & 0 & 0 & 0 & Y_v & 0 & Y_p & 0 & Y_r - U_0 \\ 0 & 0 & 0 & 0 & 0 & 0 & Z_u & 0 & Z_w & 0 & Z_q + U_0 & 0 \\ 0 & 0 & 0 & 0 & 0 & 0 & 0 & L_v & 0 & L_p & 0 & L_r \\ 0 & 0 & 0 & 0 & 0 & 0 & M_u & 0 & M_w & 0 & M_q & 0 \\ 0 & 0 & 0 & 0 & 0 & 0 & 0 & N_v & 0 & N_p & 0 & N_r \end{bmatrix} \begin{bmatrix} x \\ y \\ z \\ \phi \\ \theta \\ \psi \\ u \\ v \\ w \\ p \\ q \\ r \end{bmatrix} \quad (3.40)$$

where:

$$\begin{aligned} X_u &= \frac{1}{m} \frac{qS}{U_0} C_{X_u} & X_w &= \frac{1}{m} \frac{qS}{U_0} C_{X_\alpha} & X_q &= \frac{c}{2m} \frac{qS}{U_0} C_{X_q} \\ Y_v &= \frac{1}{m} \frac{qS}{U_0} C_{Y_\beta} & Y_p &= \frac{b}{2m} \frac{qS}{U_0} C_{Y_p} & Y_r &= \frac{b}{2m} \frac{qS}{U_0} C_{Y_r} \\ Z_u &= \frac{1}{m} \frac{qS}{U_0} C_{Z_u} & Z_w &= \frac{1}{m} \frac{qS}{U_0} C_{Z_\alpha} & Z_q &= \frac{c}{2m} \frac{qS}{U_0} C_{Z_q} \end{aligned} \quad (3.41)$$

$$\begin{aligned} L_v &= \frac{b}{I_{xx}} \frac{qS}{U_0} C_{L_\beta} & L_p &= \frac{b^2}{2I_{xx}} \frac{qS}{U_0} C_{L_p} & L_r &= \frac{b^2}{2I_{xx}} \frac{qS}{U_0} C_{L_r} \\ M_u &= \frac{c}{I_{yy}} \frac{qS}{U_0} C_{M_u} & M_w &= \frac{c}{I_{yy}} \frac{qS}{U_0} C_{M_\alpha} & M_q &= \frac{c^2}{2I_{yy}} \frac{qS}{U_0} C_{M_q} \\ N_v &= \frac{b}{I_{zz}} \frac{qS}{U_0} C_{N_\beta} & N_p &= \frac{b^2}{2I_{zz}} \frac{qS}{U_0} C_{N_p} & N_r &= \frac{b^2}{2I_{zz}} \frac{qS}{U_0} C_{N_r} \end{aligned} \quad (3.42)$$

3.2.3 Property estimation

In modern flight dynamics practice, the stability and control derivatives (terms similar to those above that result from changes in the forces due to motion of the control surfaces) are most often calculated numerically. The most common and easiest method is the ‘vortex lattice’ method[8]. The vortex lattice method is a numerical solution of simple lifting surface analysis. It is commonly

used in the initial surface configuration development, because the simplicity and the fast calculation will allow a large number of different configurations to be tested and compared. However, the traditional derivative estimation methods are also very useful to gain some idea into how the wing geometry is affecting the derivatives, and hence the dynamic properties. The reference wing area S , span b , and chord c will be notice below, as well as AR , the aspect ratio ($AR = b^2/S$). The estimation formulas are based on the slope of the lifting curve.

$$C_{\mathcal{L}_\alpha} = \frac{c_{l_\alpha}}{1 + c_{l_\alpha}/(\pi AR)} \alpha \quad (3.43)$$

$$C_{\mathcal{L}_\alpha} = \frac{c_{l_\alpha}}{1 + c_{l_\alpha}/(\pi AR)} \approx \frac{c_{l_\alpha}}{1 + 2/AR} \quad (3.44)$$

The slope c_{l_α} of the lifting curve of the wing surface is based on 2D airfoil experimental data. In this case, a thin flat plate estimate is going to be used in the model. An approximation for the thin airfoil $c_{l_\alpha} \approx 2\pi$ is commonly applied, and the drag coefficient is expressed as:

$$C_D = \frac{C_{\mathcal{L}}^2}{\pi AR} \quad (3.45)$$

$$C_{D_\alpha} = \frac{2C_{\mathcal{L}_0} C_{\mathcal{L}_\alpha}}{\pi AR} \quad (3.46)$$

3.3 Example

In this example , the shimmy problem is repeated with a wing attached at the same place that lateral spring is located. A symmetric thin surface model is generated as the airfoil. The quarter chord point is the reference point of the airfoil and the parameters of the rest model will be all the same. Improvement of the oscillation motion can be expected with attached wing, which behaves as a damper of the system.

The results are shown in the following figures. Results with the wing perform much better in reducing yaw oscillation, as shown in Figures 3.3 and 3.4. Notice that when the centre of mass is placed in a/l range between 0.3 and 0.7, the system without the wing is stable. Since the system stability is strongly depends on the location of center of mass and after the wing is applied, the motion has a greater range of stability, which is between 0.12 and 0.88. The fast eigenvalue in Figure 3.3 is always stable with or without the wing, but it is obvious to see that the real roots of the motion with wing is more negative, meaning more stable. Therefore, a attached wing affects the stability, and can provide a beneficial change in the behaviour.

While the eigenvalue shows the real root as negative, it means the oscillatory motion will approach zero with time. A more negative root will use less time, so it is called the fast eigenvalue,

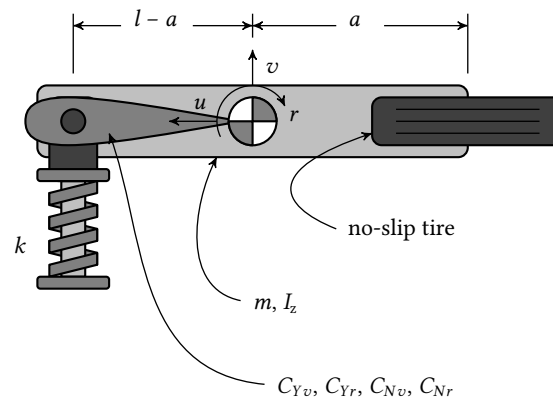


FIGURE 3.2: Swivel wheel example problem, with added aerodynamic effect. The swivel wheel exhibits the shimmy phenomenon, with potential instability, as a function of the location of the mass centre. Figure reproduced from Minaker et al.[20]

meaning it is more stable. The example shown is an example combination of multibody dynamics and aerodynamics. This approach can be applied to more extensive problems in this field, such as ground vehicle models with multiple attached aerodynamic surfaces, or vehicles with flexible wings.

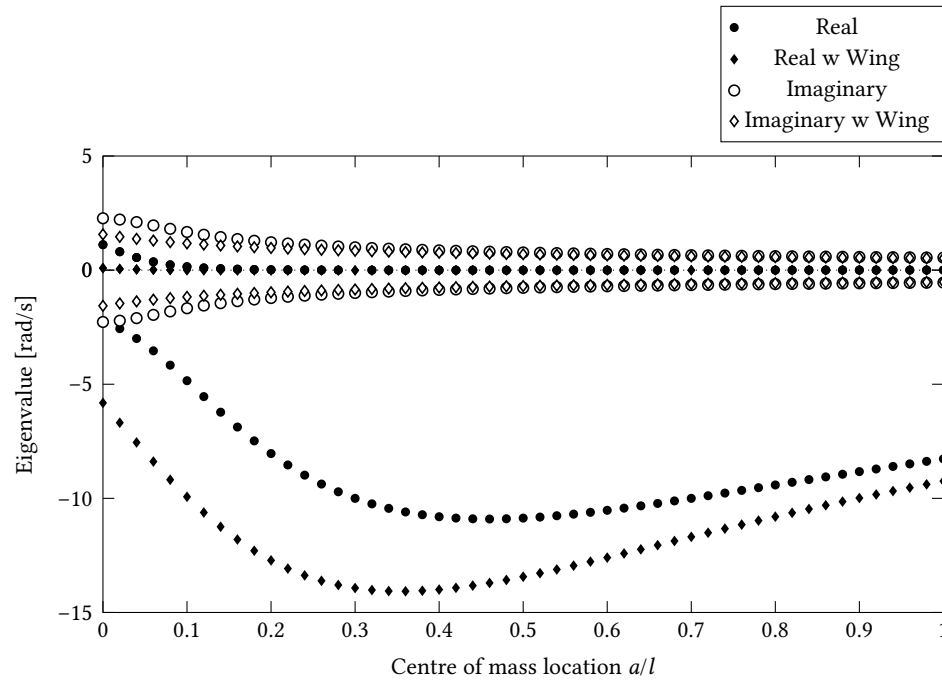


FIGURE 3.3: Eigenvalues vs centre of mass location. The effect of the addition of the wing on the eigenvalues is a significant increase in stability, and decrease in the shimmy frequency in the cases where the centre of mass is shifted rearward. Figure reproduced from Minaker et al.[20]

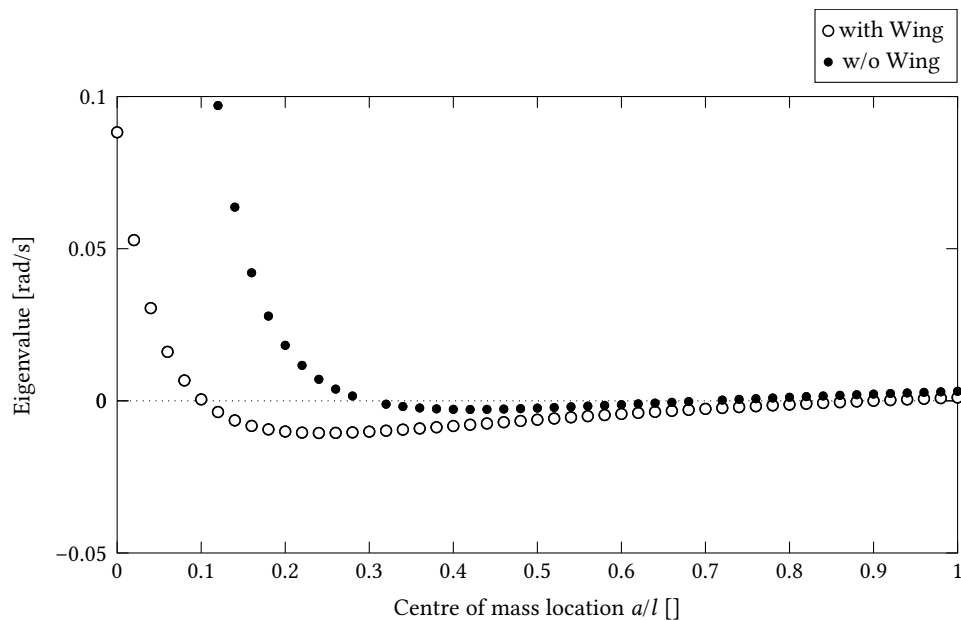


FIGURE 3.4: Slow eigenvalues vs centre of mass location, zoomed. Note that if the centre of mass is located in the range $0.3l < a < 0.7l$ then the system without the wing is stable. When the wing is added the range is expanded. Figure reproduced from Minaker et al.[20]

Chapter 4

Vehicle Model

In this chapter, the half car model, a vehicle model that is used extensively in the literature to study ride quality will be modified to include the the effect of aerodynamic forces. The half car model is quite similar to the bounce and pitch model, but with addition of the suspension and unsprung mass effect, which is more realistic. This chapter will explain the additional aerodynamic effects in detail.

Because the equations of motion are not generated symbolically, but rather numerically, they are quite large and are not presented here, but sample system, input, and output matrices are included in Appendix A.1. The equations of motion of the model are generated by EoM, and the input file in Appendix A.2 contains details of all the components in the model.

This model will be simulated using a random road time history to compare the difference between the model with and without attached wings.

4.1 Model properties

The quarter car model has often been used to determine the natural frequencies of the vehicle motions. The results of the quarter car model show two frequencies of motion, with the lower one normally around 2π rad/s or 1 Hz and the higher one around 20π rad/s or 10 Hz. Due to the big difference between the frequencies, the quarter car model is sometimes replaced by two single degree of freedom models with reasonably accurate results. A ‘wheel hop’ mode is associated with the higher frequency for the system, where the sprung mass is relatively stationary and the unsprung mass is bouncing against the suspension and the tire as both springs’ stiffnesses in parallel. The low frequency expression is very similar to the system without considering unsprung mass, which is the sprung mass bouncing against the suspension and tire as two springs acting in series, in the ‘bounce’ or ‘heave’ mode.

The half car model is actually the combination of two quarter car models, one for the front axle, and one for the rear. This means it has two sets of unsprung mass supporting a common sprung mass. It will have two wheel hop motions and two heave motions in both the front and

the rear; however, instead of using front and rear chassis bounce as coordinates, the centre of mass bounce, and chassis pitch coordinates are used. When the two suspensions are moving in phase, the vehicle will experience mostly bounce motion. However, if the two axles are moving out of phase, a moment will be generated around the center of mass, which gives pitching motion. Mostly, the vehicle motion combines bounce and pitch at the same time, depending on the exact condition occurring.

In the half car model, the chassis is treated as a rigid body, while the unsprung masses are treated as point masses. The parameters are all the same as in the previous models, e.g., a and b are the distances between the center of mass to the front and rear axles. The spring stiffness for the front and rear suspension are k_f and k_r , respectively, while, c_f and c_r represent the damping. The front and rear unsprung mass are m_{uf} and m_{ur} . The tire stiffness is represented by k_t . The deflection of the center of mass z and pitching angle θ , along with z_f and z_r are the coordinates in the model.

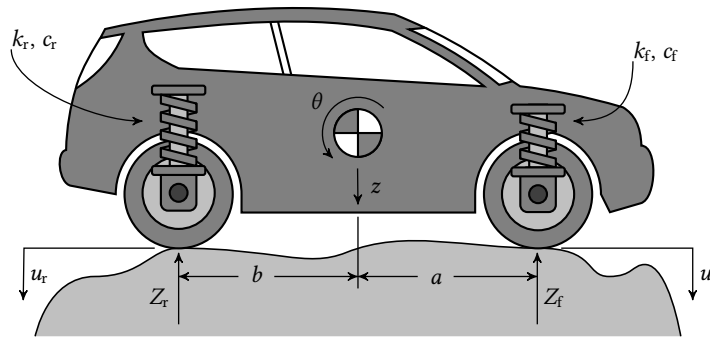


FIGURE 4.1: half car model, used to analysis riding quality. Figure reproduced from Minaker [19]

The half car model is expanded with a combination of aerodynamic effects in this study. A wing is mounted on each of the front and rear of the vehicle, with a mounting that allows rotation along the pitch axis. Each wing system is driven by a mechanical linkage; the configuration is shown in the next section. The angle of attack of the wings is changing with the deflection of the suspension, to generate lifting or downward force acting vertically against the chassis, to oppose the forces from the suspension of the vehicle, to reduce both bounce and pitch motion, to increase ride quality.

4.2 Model geometry

In Figure 4.2, the half car model with the added aerodynamic effects is shown; the wings is designed to be driven by the linkage systems. There are five points in each linkage system, point A is where the mechanism is connected with the suspension, where it transfers the deflection from the suspension to the wing system. Linkage ABC is a massless 'L' beam (or bell-crank) pivoting around point B. Link CD is connecting the L beam with the link contacting with the

wing. Therefore, if a rough road is applied to the model, the deflection of the suspension will affect the system and generate an angular motion on the bell-crank. The angle of attack of the wing will change while the link DE is rotates around point E, pushed by link CD. The front system will work the same way.

This system design follows the idea that the angle of attack of the attached wings can be flexible, to maximize the effect of the wings. For example, when the unsprung mass is bouncing up, compressing the suspension and lifting the vehicle, the wing could have a negative tilting angle to generate a downward force to reduce the amplitude of bouncing. In the next chapter, some numerical experiments are conducted using different configurations of the wing systems.

In Chapter 5, the simulations are conducted using varying model parameters, but the baseline values are given in Table 4.1,

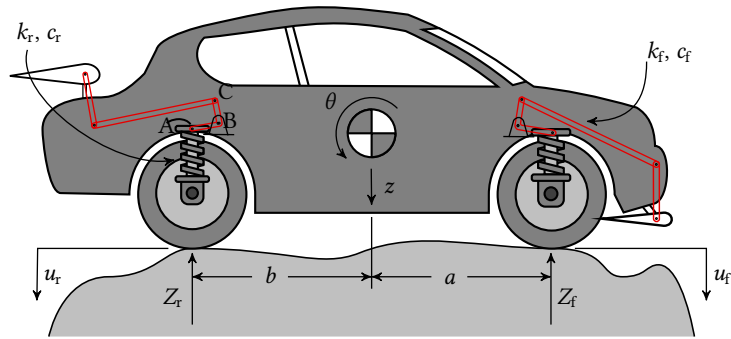


FIGURE 4.2: The half car model with added aerodynamic effects.

TABLE 4.1: Parameters in half car model

Parameter	Notation	Value
Wheelbase dimension	a	1.189 m
Wheelbase dimension	b	1.696 m
Sprung mass	m	1730 kg
Pitch inertia	I_{yy}	3267 kg m ²
Front suspension stiffness	k_f	35000 N/m
Rear suspension stiffness	k_r	38000 N/m
Front suspension damping	c_f	1000 N/m
Rear suspension damping	c_r	1200 N/m
Tire stiffness	k_t	300000 N/m
Forward speed	u	50 m/s
Front unsprung mass	m_{uf}	50 kg
Rear unsprung mass	m_{ur}	50 kg
Linkage dimension	l_{AB}	0.1 m
Linkage dimension	l_{BC}	0.254 m
Linkage dimension	l_{CD}	0.1 m
Linkage dimension	l_{DE}	0.254 m
Wingspan	b_w	2.0 m
Wing chord	c	0.35 m
Front wing location	p_f	$(a + 0.4, 0, 0.2)$
Rear wing location	p_r	$(-b - 0.3, 0, 0.4)$

In addition to the parameters explained in the last chapter, a few more parameters are included in the table since the wing system is applied. The terms m and I are the mass of the vehicle and moment of inertia. The lengths l_{AB} is the horizontal offset of the bell-crank, which is the distance between the point where the bell-crank is joined with the suspension and the location where the bell-crank is hinged on the sprung mass. If l_{AB} is positive, it means the bell-crank hinge is located in between the front and rear axles; if it is negative, means the bell crank is installed on the other side. The length l_{BC} is the vertical offset between the hinge and the horizontal link; this distance controls the sensitivity of the link motion, which in turn affects on the tilting angle of the wing. Similarly, l_{DE} is the length of the rear wing arm.

4.3 Random road

The random road is a road model used in conjunction with the quarter car model or half car model to demonstrate the response from the suspension. According to ISO 8606 [22], there are eight ranges of roughness of the road, from the smooth (A) to roughest (H). Ranges F, G, and H are considered off-road. In this model, a road roughness at the C-D transition (average-poor) will be used. The road deflection is the model input, and the bounce and pitch time history will be the output. The standard of the random road roughness is based on the power spectral density (PSD) plots represented by an unevenness index G_d , which could be expressed as function of two different types of spatial frequencies Ω_0 and n_0 . The corresponding standard index of G_d for different level road roughness is defined while $\Omega_0 = 1.0$ rad/m or $n_0 = 0.1$ cycles/m and are listed in 4.2.

TABLE 4.2: ISO 8608 values of $G_d(n_0)$ and $G_d(\Omega_0)$ [22]

Road class	$G_d(n_0)(10^{-6} m^3)$		$G_d(\Omega_0)(10^{-6} m^3)$	
	Lower limit	Upper limit	Lower limit	Upper limit
A	-	32	-	2
B	32	128	2	8
C	128	512	8	32
D	512	2048	32	128
E	2048	8192	128	512
F	8192	32768	512	2048
G	32768	131072	2048	8192
H	131072	-	8192	-

The index G_d can be expressed as a function of frequency as:

$$G_d(n) = G_d(n_0) \cdot \left(\frac{n}{n_0} \right)^{-2} \quad (4.1)$$

or:

$$G_d(\Omega) = G_d(\Omega_0) \cdot \left(\frac{\Omega}{\Omega_0} \right)^{-2} \quad (4.2)$$

Using the concept of power spectral density, a random road of equivalent roughness can be generated as a sum of a series of sine waves, where the amplitude and frequency vary according to a specific relationship, and the phase angle is random. The relationship between G_d and the amplitude of each wave A_i is:

$$G_d(n_i) = \frac{A_i^2}{2\Delta n} \quad (4.3)$$

Therefore, the amplitude can be expressed as:

$$A_i = \sqrt{2\Delta n \cdot G_d(n_0) \cdot \left(\frac{n}{n_0}\right)^{-2}} \quad (4.4)$$

Since the actual height of the random road h is function of amplitude A and expression is as shown,

$$h(x) = \sum_{i=0}^N A_i \cos(2\pi \cdot i \cdot \Delta n \cdot x + \phi_i) \quad (4.5)$$

and expanded as,

$$h(x) = \sum_{i=0}^N \sqrt{\Delta n} \cdot 2^k \cdot 10^{-3} \cdot \left(\frac{n_0}{i \cdot \Delta n}\right) \cdot \cos(2\pi \cdot i \cdot \Delta n \cdot x + \phi_i) \quad (4.6)$$

where x represents the location along the road from 0 to L , the length. The spatial frequency interval $\Delta n = 1/L$, and the number of frequencies will be expressed as $N = L/B$. The integer value k is the index that shows the level of the road roughness. It ranges from 3 to 9, corresponds to the class A-B transition to class G-H transition, as shown in Table 4.3. The random phase angle ϕ for each frequency is from 0 to 2π . Sample random roads with roughness level 3, 5, and 7 are generated and shown in Figure 4.3. In the half car model, the random road is used to test how effective the attached wing is. Therefore, many simulations are conducted, using this random road input. In the results, the bounce and pitch response of the vehicle with and without wing are compared with respect to the road deflection.

TABLE 4.3: k values for ISO road roughness classification

Road Class		k
Upper limit	Lower limit	
A	B	3
B	C	4
C	D	5
D	E	6
E	F	7
F	G	8
G	H	9

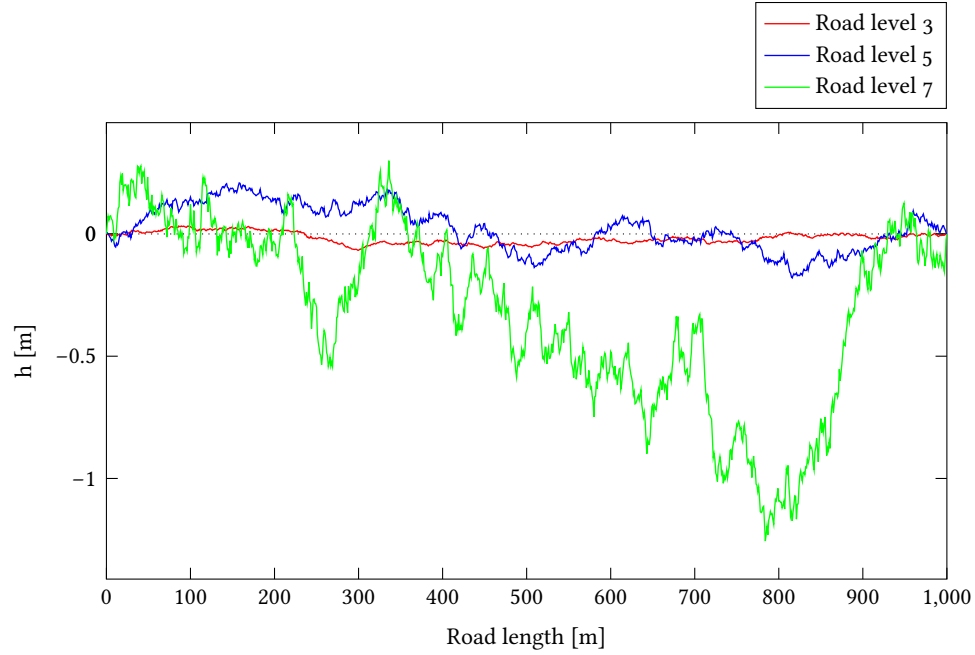


FIGURE 4.3: Random road with different roughness levels. The difference of the three roughness levels are over a meter, which is quiet substantial. Road level 3 is the good condition road, which is highway. Level 5 is a relatively bad condition road and level 7 is offroad.

4.3.1 Wheelbase filter

One of the important effects that should be considered in the results of the bounce pitch model is the concept of ‘wheelbase filtering’. Usually both of the suspensions will experience the same ground motions, with only phase shifted a small amount backward, since the rear wheel will get to the bump with a time lag expressed as:

$$\Delta t = -\frac{a+b}{u} \quad (4.7)$$

which corresponds with a phase lag of:

$$\phi = \omega \Delta t = \frac{-\omega(a+b)}{u} \quad (4.8)$$

The frequency and the phase lag can be written as functions of the road wavelength, the wheelbase and the forward velocity, as:

$$\omega = \frac{2\pi u}{\lambda} \quad (4.9)$$

$$\phi = \frac{-2\pi(a+b)}{\lambda} \quad (4.10)$$

The input can be rewritten as:

$$\mathbf{u} = \begin{Bmatrix} u_f \\ u_r \end{Bmatrix} = \begin{Bmatrix} u_0 e^{i\omega t} \\ u_0 e^{i(\omega t + \phi)} \end{Bmatrix} = \begin{Bmatrix} 1 \\ e^{i\phi} \end{Bmatrix} u_0 e^{i\omega t} \quad (4.11)$$

This implies that the wheelbase filtering effect on the frequency response can be found. Starting with the equations of motion:

$$\dot{\mathbf{x}} = \mathbf{A}\mathbf{x} + \mathbf{B}\mathbf{u} \quad (4.12)$$

$$\mathbf{y} = \mathbf{C}\mathbf{x} \quad (4.13)$$

Now supposing a sinusoidal input and output, i.e., $\mathbf{x} = \mathbf{x}_0 e^{i\omega t}$

$$\dot{\mathbf{x}} = i\omega\mathbf{x} \quad (4.14)$$

$$i\omega\mathbf{x} = \mathbf{A}\mathbf{x} + \mathbf{B}\mathbf{u} \quad (4.15)$$

$$[\mathbf{I}i\omega - \mathbf{A}]\mathbf{x} = \mathbf{B}\mathbf{u} \quad (4.16)$$

With a simple substitution, the first order equation of motion can be rewritten as:

$$\mathbf{x} = [\mathbf{I}i\omega - \mathbf{A}]^{-1}\mathbf{B}\mathbf{u} \quad (4.17)$$

and:

$$\mathbf{y} = \mathbf{C}\mathbf{x} = \mathbf{C}[\mathbf{I}i\omega - \mathbf{A}]^{-1}\mathbf{B}\mathbf{u} \quad (4.18)$$

then:

$$y_0 e^{i\omega t} = \mathbf{C}[\mathbf{I}i\omega - \mathbf{A}]^{-1}\mathbf{B} \begin{bmatrix} 1 \\ e^{i\phi} \end{bmatrix} u_0 e^{i\omega t} \quad (4.19)$$

and output to input ratio will be:

$$\frac{y_0}{u_0} = \mathbf{C}[\mathbf{I}i\omega - \mathbf{A}]^{-1}\mathbf{B} \begin{bmatrix} 1 \\ e^{i\phi} \end{bmatrix} \quad (4.20)$$

The change in wavelength will cause the either the bounce or pitch motions to be excited individually. If the wheelbase is close to the wavelength of the road, or an even multiple of the wavelength, the vehicle will only experience bounce excitation. However, if the wheelbase is one half of the wavelength, or an odd integer multiple of half the wavelength, only pitch will be excited. Some frequency response plots illustrating this effect will be included in Chapter 5.

Chapter 5

Simulation Results

This chapter documents the simulation results, which demonstrates the aerodynamic effects on the half car model. The bounce and pitch response of the vehicle with and without wings is compared under the random road time history response. The change of the angle of attack of both wings are also shown. Different wing system configurations are applied to explore the effect of the tilting direction, and the adjustment of the motion ratio is explored. The unsprung mass effect is also tested. And of course, eigenvalues and frequency response are discussed. The baseline model parameters are listed in Chapter 4; unless varying parameters are highlighted, all the parameters will be the same as in Table 4.1.

5.1 Wing orientation

In the model introduced in Chapter 4, the wing is driven by the linkage system; therefore, different wing configurations will make the vehicle have different bounce pitch response to the same random road time history. First of all, a baseline wing system configuration is sought to ensure the angle of attack of the wings changes in a fashion that is beneficial to the ride quality.

There are two lines of thought on determining the best orientation of the wing. First, if one considers the case where, in response to a disturbance, the vehicle body has moved downward, compressing the suspension, the wing should be oriented in such a way that it generates a lifting force on the body, to help the suspension restore it to its equilibrium position. This would imply that a suspension compression should tilt the leading edge of the wing upward. Alternatively, one might consider the case where the vehicle unsprung mass has been disturbed by a bump or obstacle, lifting it toward the vehicle, compressing the suspension, and generating a lifting force on the vehicle. To oppose this disturbance force, the wing should tilt such that it generates a downward force. While one might be swayed by each of these arguments individually, they are clearly in opposition to each other, and it is unclear which orientation of the wing will prove best. To explore this idea, two simulations were conducted.

The first test set the bell crank hinge of the front wing system behind the front unsprung mass and the rear bell crank hinge in the front of the rear wheel, as shown in Figure 5.1. In the first

condition, for example, if the rear unsprung mass is moving in a negative z direction, then the vehicle body is moving relatively up with respect to the rear unsprung mass. Since the wing bell crank hinge point B is located on the sprung mass, the beam ABC will rotate counter clockwise, pushing beam CD to the back of the vehicle and the wing will rotate in a clockwise direction, to generate downward forces on the vehicle body. The aerodynamic force will push down on the vehicle body in response.

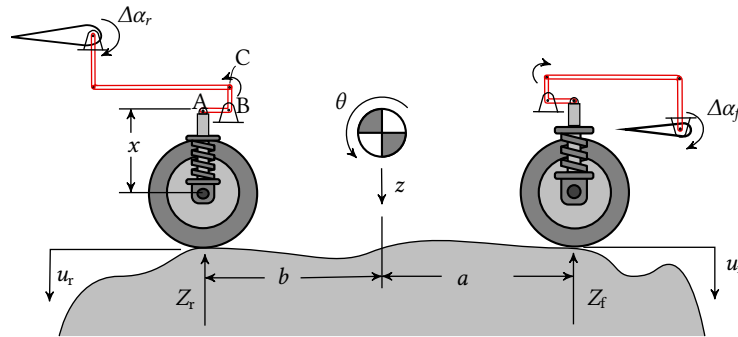


FIGURE 5.1: Half car model with wing effect, with the wing linkage structure shown in red in the figure. The wings tilt clockwise while the suspension moves into rebound. This wing system is referred to as configuration A.

The second test installs the bell crank hinge on the other side of suspension and the geometry is shown in Figure 5.2. The wing system is working in a similar way, but in the opposite direction. Both configurations are tested, and the resulting bounce motion is shown in Figure 5.3 and the pitch motion is shown in Figure 5.4.

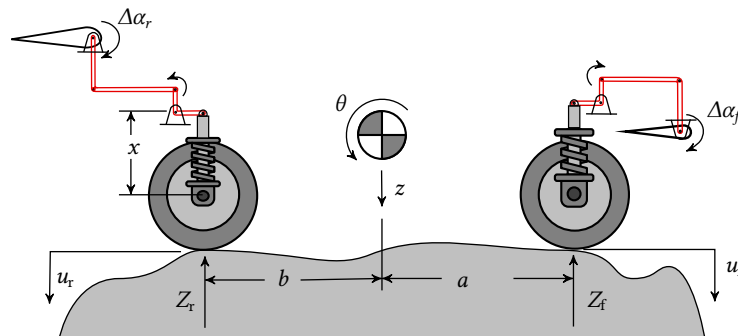


FIGURE 5.2: The opposite wing structure; the wings are tilting clockwise when the suspension moves into compression. This wing system is referred to as configuration B.

5.1.1 Bounce and pitch response

In Figure 5.3, the red line represents the vehicle bounce response from the random road without wings. It is hard to see any improvement in the first model, shown in blue. In fact, in a few points the response has clearly higher amplitude than the original model. The testing result fits the expectation, while the unsprung mass is pulling the vehicle body down, with the wing also

generating a downward force, the vehicle will have more bounce or pitch motion. In comparison, the second test, with the front bell-crank hinge installed in the front of the wheel and the rear bell-crank hinge located behind the wheel, has a significant improvement. Both the bounce and pitch motions from the vehicle are reduced by the wing system. By inspection, configuration A displays approximately 0.08 m decrease in peak amplitude when compared against the motion of the system without wings. While the vehicle body moves up relative to the unsprung mass, the wing should be tilting down to generate a larger downward force, in order to reduce the bounce motion of the vehicle body. If each wing is reducing the displacement of the body at each end, then the cooperation of both wing systems should reduce the pitching angle at the same time. Therefore, the wing system configuration in Figure 5.2 is working in the correct orientation.

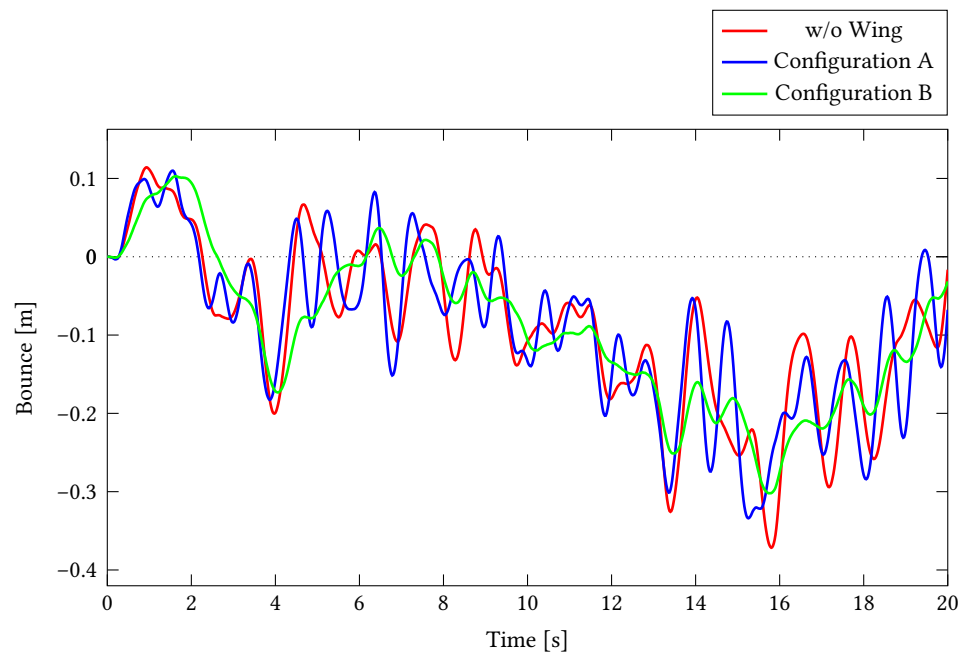


FIGURE 5.3: Comparison between the vehicle bounce response of the half car model on a random road with wings in varying configurations. Configuration A is shown in Figure 5.1 and Configuration B is shown in Figure 5.2. The response suggests that Configuration B results in a decrease in bounce motion on the random road.

Figure 5.4 shows the pitch angle time history of the vehicle during 20 seconds of random road with a road roughness of level 5. Wing system B appears to offer an improvement; the amplitude of the pitch angle remains within the range of ± 0.05 rad ($\pm 2.86^\circ$), where the baseline configuration shows . It is expected that this smaller pitch angle should provide a relatively better ride quality. In comparison, Configuration A is not as functional as system B; the blue line shows an increased pitching angle from the original model, which is definitely not desired. Configuration B has reduced the amplitude of the pitch angle by about 0.02 rad, or almost 30%.

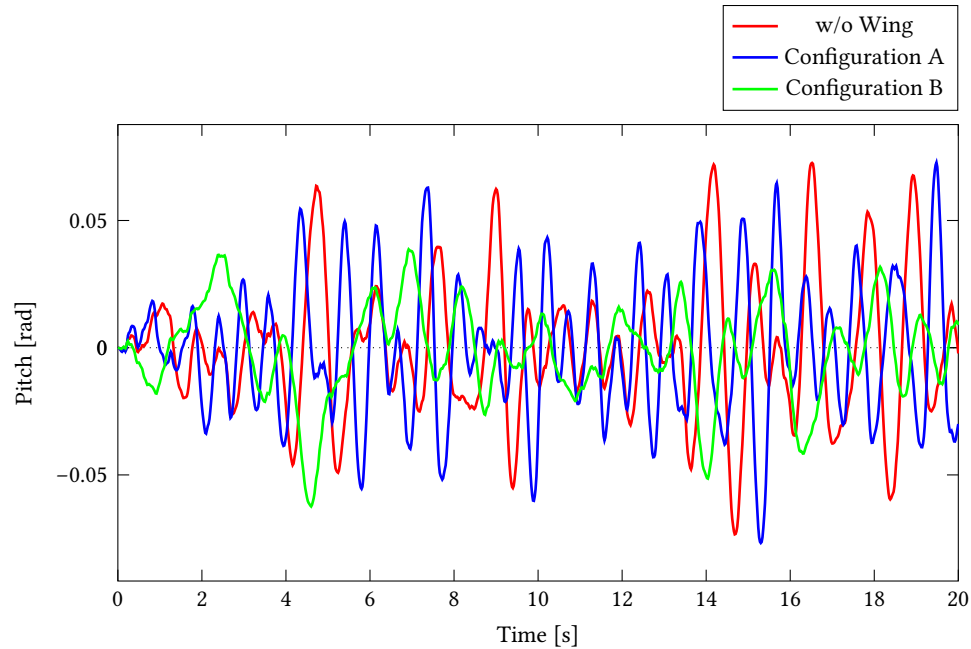


FIGURE 5.4: Comparison between the vehicle pitch response of the half car model on random road with wings in varying configurations. Configuration A represents the wing configuration shown in Figure 5.1 and Configuration B is showing the bounce response of the structure in Figure 5.2. The response suggests that Configuration B results in a decrease in pitch motion on the random road.

5.2 Wing sensitivity

After the correct orientation of the angle of attack is determined, the ratio of the bell-crank ABC should be defined in order to find a suitable range or sensitivity of the tilting angle of the wings. The rear wing system in Figure 5.6 is taken as example to show the relationship between the input/output ratio and the length of beams. If the length ratio of l_{AB}/l_{BC} is changed, the ratio of output α to the input δx will also change. Therefore, the length of l_{AB} is chosen to be constant, at 0.1 m and the vertical offset will be added on l_{BC} . Changes in l_{BC} also move the vertical position of the link AB , since AB should be always perpendicular to the BC . The same holds true for the front wing system. If the ratio is too large, it may lead to an unstable result; if the ratio is too small, it may not have a significant effect on the time history response. Therefore, different lengths of the bell-crank are tested to make sure the system has the optimal ratio of output wing angle to input suspension travel.

Taking the rear wing system as an example, the ratio is calculated using the following three equations. Assuming small rotation angles of the bell-crank, and taking Δy as the displacement of the horizontal link, Δx as the suspension travel, and $\Delta \alpha$ as the change in the tilt angle of the wing:

$$\Delta y = \frac{l_{BC}}{l_{AB}} \Delta x \quad (5.1)$$

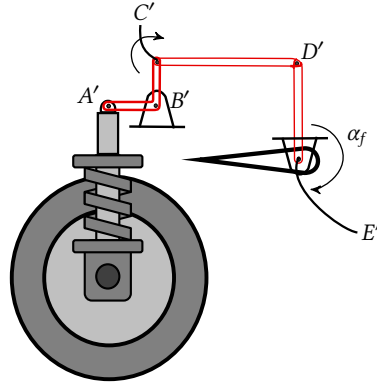


FIGURE 5.5: The front wing system, where the values $l_{A'B'}$, $l_{B'C'}$, $l_{C'D'}$, and $l_{D'E'}$ are the lengths of the wing system mechanism components.

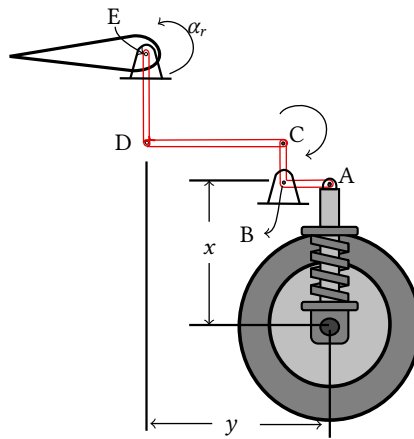


FIGURE 5.6: The rear wing system, where x is the distance between the center of wheel and point A. The horizontal displacement of the beam CD is Δy . The values l_{AB} , l_{BC} , l_{CD} , and l_{DE} are the lengths of the wing system mechanism components. The wing sensitivity, or the ratio of $\Delta\alpha$ to Δx depends on these lengths.

$$\Delta\alpha = \frac{\Delta y}{l_{DE}} \quad (5.2)$$

$$\Delta\alpha = \frac{l_{BC}}{l_{AB}l_{DE}} \Delta x \quad (5.3)$$

There is a ratio between the input Δx and the output $\Delta\alpha$, (here the angle α is measured in radians). After a few preliminary tests, it was found that a $\Delta\alpha/\Delta x$ ratio of approximately 4.6 rad/m, (0.26°/mm) for both front and rear wing systems, gave noticeable changes to the time history, but was close to the stability threshold. However, in order to optimize the aerodynamic effect, a quadrant is made, where the x-axis represents the vertical offset for front wing system, and the y-axis represents vertical offset for the rear. In the previous tests, the result shows the output and input ratio should not be more than 4.6 rad/m, since a higher ratio will cause a larger range of

angle of attack changing during the simulation, which will lead to an unstable response for random road time history. Therefore, the testing area of the quadrant is shrunk, with only positive side for both axes, as shown in Figure 5.7. In the quadrant, there are 49 points tested in the process. Most of the results did not produce positive effects. However, some of the sets do show better performance; these points are indicated by red circles, with the bounce pitch response shown as following figures in bounce pitch response. The results suggest that the front wing system is more sensitive than the rear, since most of the stable points are close to y axis.

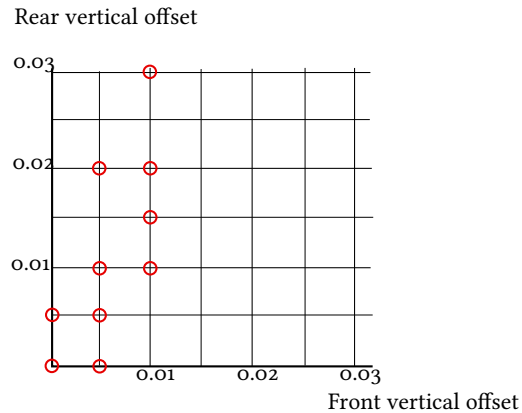


FIGURE 5.7: This quadrant map is the stable range of the entire testing map. All the points circled in red are the points that have relatively better performance.

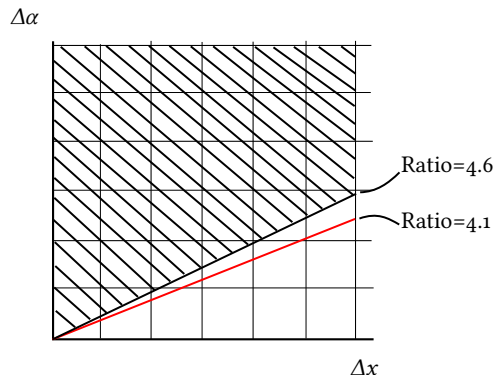


FIGURE 5.8: The ratio higher than 4.6 rad/m will lead an unstable response, which is represented by the shadowed area. The best output to input ratio for the front wing system will be 4.6 rad/m and the best performance for the rear is 4.1 rad/m.

5.2.1 Bounce pitch response

In the bounce pitch response, four sets of the test points are taken into this section for comparison. The specific parameters of the wing systems are shown in Table 5.1. The lengths for the bell-crank vary, causing the output to input ratio to change.

From inspection of the response, Configuration C has the best performance. Very few points go beyond the original bouncing response from the system without the wing. However, from the bouncing response plots, Configuration C is smoother than the others. This system has a front

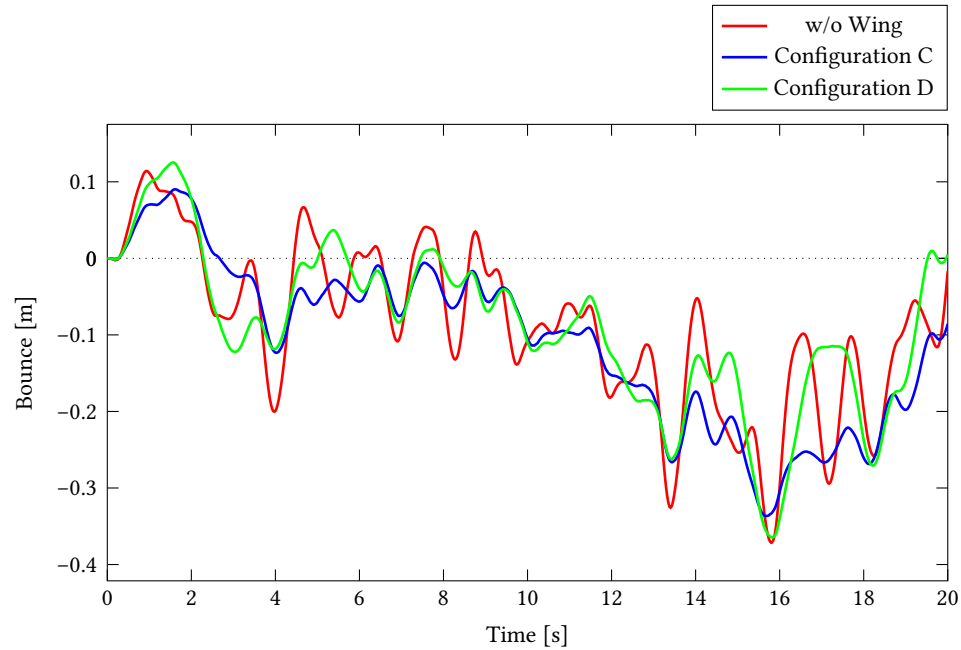


FIGURE 5.9: Bounce response for wing Configurations C and D, represented by the blue and green lines, respectively. The amplitudes of both Configuration C and Configuration D are smaller when compared to the system without wings. Configuration D does not perform as well as Configuration C.

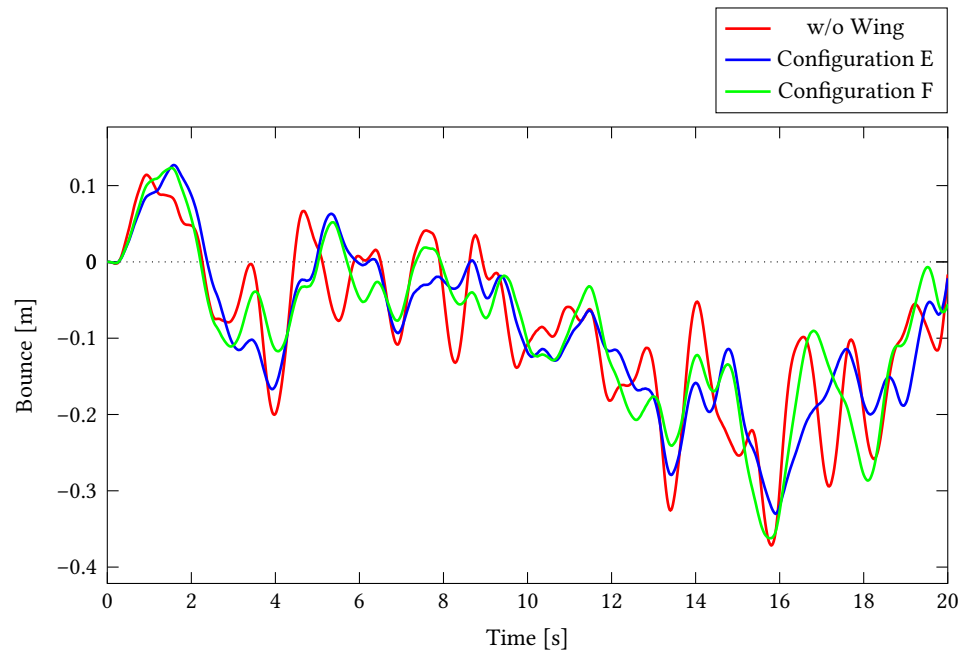


FIGURE 5.10: Bounce response for Configurations E and F, represented by the blue and green lines, respectively. The result shows that both wing designs have a similar range of bounce motion. The systems with reduced wing sensitivity do not appear to offer as much improvement.

TABLE 5.1: Wing system parameters in half car model

Configuration C	Arm length
l_{BC}	0.046 m
$l_{B'C'}$	0.041 m
Configuration D	Arm Length
l_{BC}	0.036 m
$l_{B'C'}$	0.036 m
Configuration E	Arm length
l_{BC}	0.036 m
$l_{B'C'}$	0.026 m
Configuration F	Arm length
l_{BC}	0.041 m
$l_{B'C'}$	0.016 m

wing system sensitivity ratio of 4.1 rad/m, and a rear wing system ratio remaining at 4.6 rad/m has the best performance in this case. In Figure 5.9, Configuration C has reduced peak amplitudes from the baseline bounce response by about 0.12 m, which is substantial for a normal vehicle motion. When comparing all four configurations, the improvement of Configurations D, E, and F have no significant difference, and are around 0.08 m to 0.1 m.

The pitch response is shown in Figures 5.11 and 5.12. All of the configurations have a narrower pitch angle range when compared to the system without wings. Considering the points at the peaks, Configuration C reduces the maximum pitch angle by about 0.03 rad, ($\pm 1.72^\circ$), which is a significant improvement when compared to the system without wings.

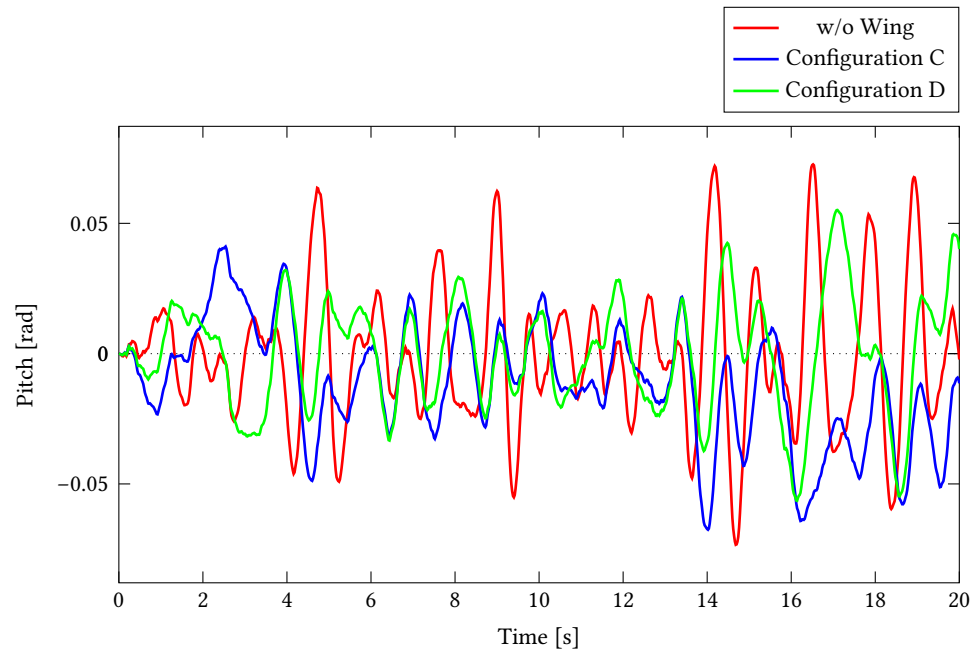


FIGURE 5.11: Pitch response for Configurations C and D, represented by the blue and green lines, respectively. The overall range of pitch angle for Configuration C is less than both Configuration D and system without wings. Configuration C appears to offer the most improvement.

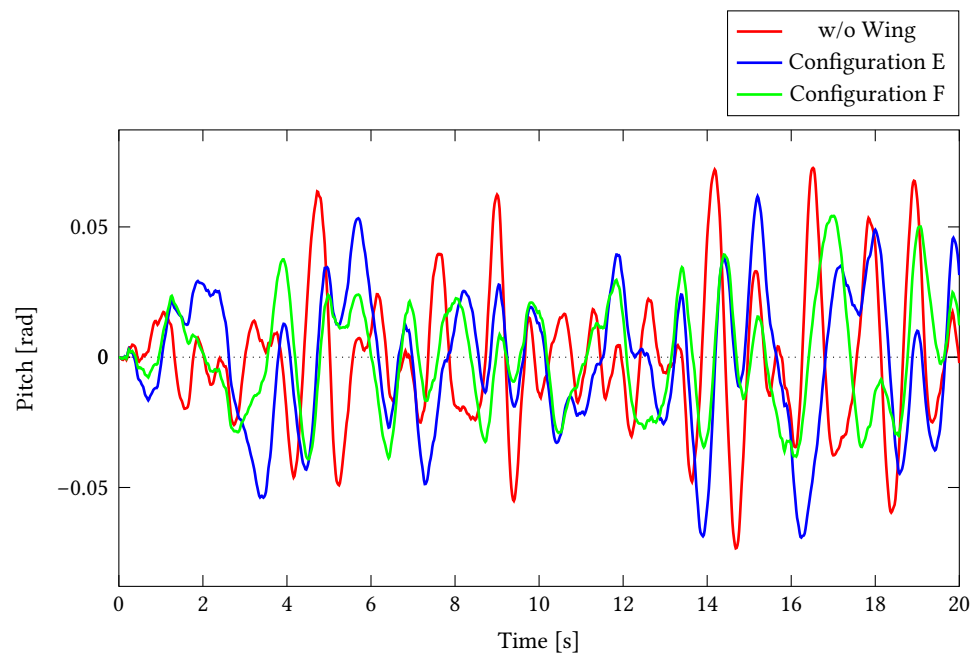


FIGURE 5.12: Pitch response for Configurations E and F, represented by the blue and green lines, respectively. Configuration F appears to offer some improvement over Configuration E and the baseline system, but not as much as Configuration C.

5.2.2 Frequency response

In addition to the time history solutions, frequency response plots were also generated. In the frequency plot, the y axis represents the vehicle response to road disturbance ratio, which are output and input, respectively. Because the plot uses units of [dB], the zero line shows that the output to input ratio is one to one; if the line falls below zero, this means less vehicle response will be generated from the same road roughness. When the transfer function reaches -20 dB, it means that only 10% of the disturbance will be transferred to vehicle. A value of -40 dB implies only 1% of the input reaches the output. Therefore, it is generally not worthwhile to consider the result below -40 dB.

In Figure 5.13, the system with wings shows a slight increase in the very low frequency range (below 0.1 Hz). Generally, this is below the range of relevant frequencies for passenger comfort. The system with wings has reduced the transfer functions for bounce by about 5 dB in the low frequency range (between 0.1 Hz and 1 Hz), and increased the pitch by about the same amount. In the more important working frequency range, from 1 Hz to 10 Hz, both the bounce and pitch response for Configuration C moves about 5 dB lower than the baseline. The sensitivity to disturbance will be approximately halved when the transfer function decreases by 5 dB, which shows that the aerodynamic element is improving the system substantially. The region above 10 Hz shows no significant change.

Figure 5.13 shows a generally better performance with wings since the response of the system with aerodynamic effect is almost entirely much lower than the system without wings at a forward speed of 50 m/s. During the low frequency range, the bounce is lower, while the pitch is larger. While the vehicle is moving along a road with high wavelength around more than 100 m, the slope is so small that the response becomes almost entirely flat, i.e., bounce without pitch. The system with wings has a similar behaviour, except the transition to flat ride occurs at a much lower frequency.

In the mid range of frequencies, the road disturbance will usually be absorbed by suspension motion. During the frequency range from 1 Hz to 10 Hz, the system with wing performs better than the system without wings, except for a short interval near 1 Hz. The wing system also shows only one distinct resonant peak, unlike the baseline system with two peaks.

When the input frequency exceeds 10 Hz, the two systems converge toward the same response. This is reasonable, as the quarter model shows that above the wheel hop frequency, most of the disturbance from the road is absorbed by tire compression rather than suspension travel or body motion.

5.2.3 Wing performance

It is also valuable to review the change of the tilting angle of the front and rear wing during the entire random road time history, as shown in Figures 5.14 and 5.15, respectively. The front

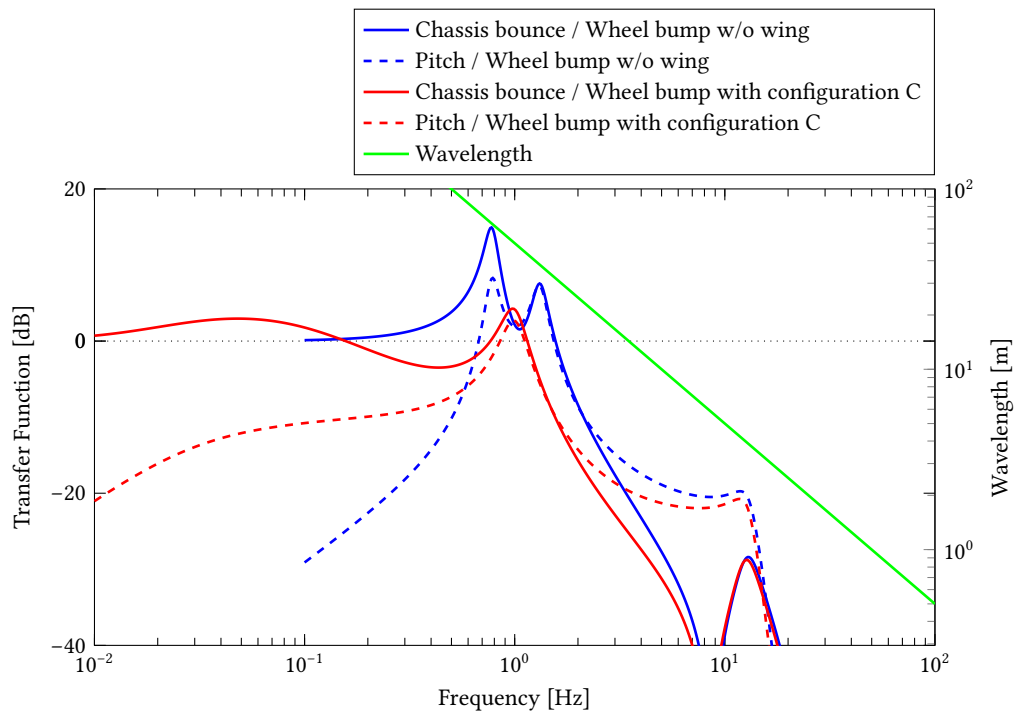


FIGURE 5.13: Frequency response: Wheel bump. System with wings has a lower transfer function means lower output to input ratio. The natural frequencies of the system become lower.

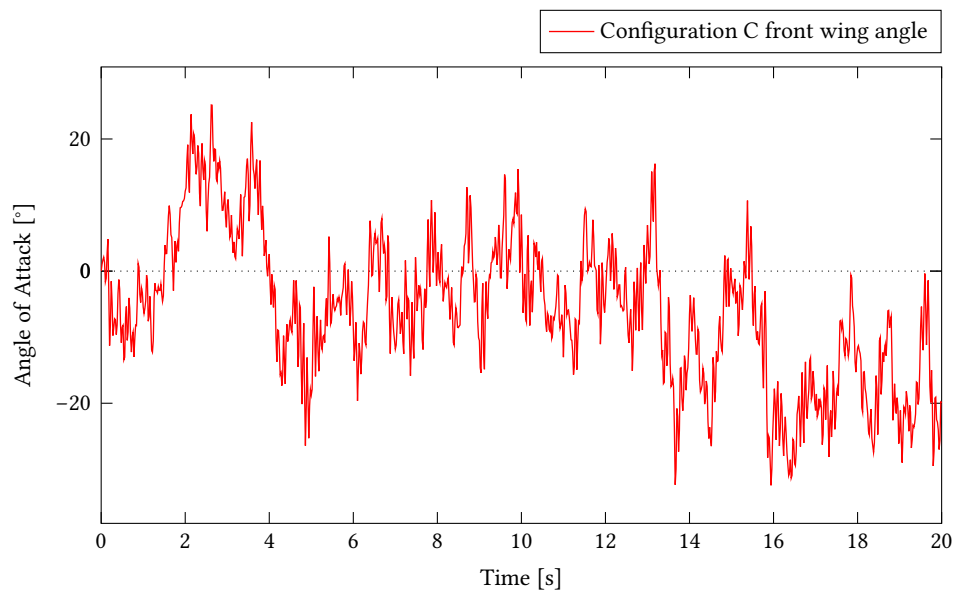


FIGURE 5.14: Tilt angle of the front wing is varying between 20 to negative 20 degrees, which is a reasonable range for airfoils to generate lifting force.

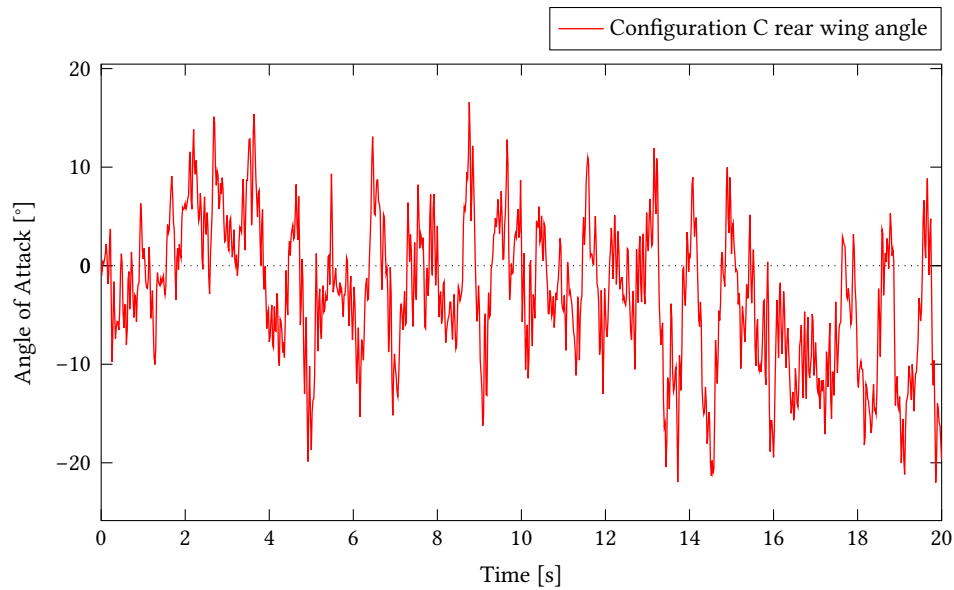


FIGURE 5.15: Tilt angle of the rear wing is varying between 15° to -20° , which is a reasonable range for airfoils to generate lifting force.

wing angle is mainly varying in between $\pm 20^\circ$, and the rear wing system is a little less, from $\pm 15^\circ$. When the vehicle has a large amplitude drop, it causes a relatively larger stretch motion in the suspension, and the wing has touched an angle of attack,

In practice, this would likely exceed the stall angle of the wing, where the behaviour changes dramatically, and the linear force vs angle assumption would not be valid. However, in the plot, the large angle exists only for a short period of time, so the overall results are likely not significantly affected.

This is also the reason for the places that the pitching angle of the vehicle gets lower than -0.05 in the figure 5.11.

It should be noted that the level 5 random road is the ISO transition between average and poor. Of course, the wing angle is also affected by the random road roughness. In reality, travelling at 50 m/s on such a road would be unlikely. If the vehicle is tested on a smoother road, the range of angles would reduce. A better road condition is tested for comparison, and is shown in Figures 5.16 and 5.17. The range of tilt angles falls inside a range reasonable for linear treatment.

It is important to note that this tilt angle is not exactly equivalent to the angle of attack. The wing tilt angle plus the angle of attack of the vehicle is the angle of attack of the wing. However, the angle of attack of the vehicle can be shown to be very small compared with the tilting angle of wings, so in effect the tilt angle can be treated as the angle of attack.

It is also noteworthy that the tilt angle contains some significant high frequency content because the high frequency wheel hop motions. In a real wing application, this high frequency would not be captured in the resulting aerodynamic force, as there is a time lag required before the wing

will generate forces. (The time lag is based on the time it takes for a air particle to travel the distance of the wing chord.) This time delay is not considered in this model, and so is a source of error. However, the vehicle body motion itself is relatively low frequency and it is reasonable to expect that if the high frequency content was filtered from the applied aerodynamic forces, the resulting vehicle motion would not be significantly changed.

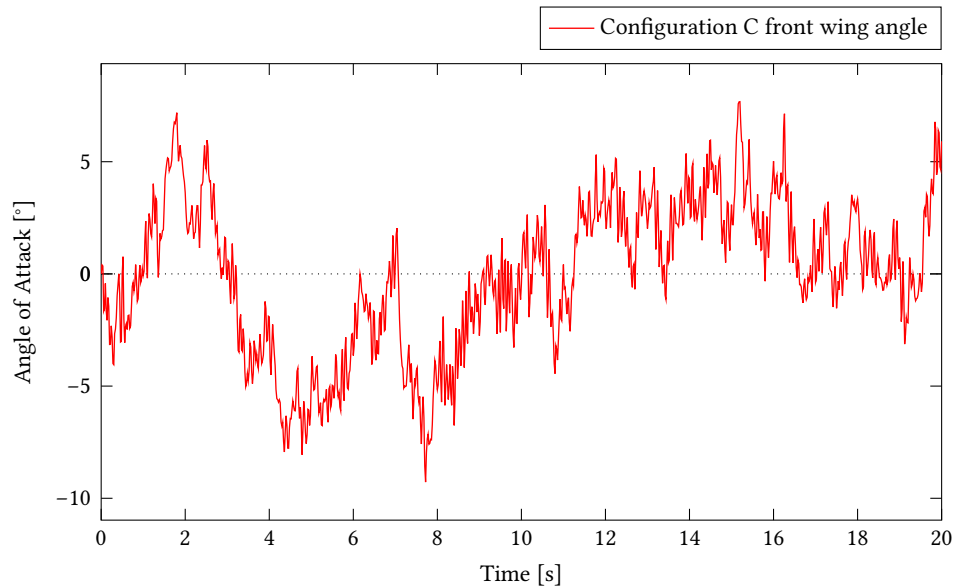


FIGURE 5.16: Front wing angle while operating on the road level 3. The range of the tilting angle become narrow within $\pm 7^\circ$ while the road disturbance decreases.

5.3 Unsprung mass effects

Because the motion of the wings is driver by suspension travel, it was anticipated that the value of the unsprung mass may have some influence on the overall motion.

Different unsprung mass distribution was also considered in the study. The various values of unsprung mass considered are given in Table 5.2. All other parameters and the configurations of wings are all the same as the baseline. The time history plots are shown in Figures 5.18 and 5.20. Clearly, the changes in the bounce and pitch response are insignificant. It is difficult to see any difference at all, without zooming in on the figures to a very small scale.

Considering the natural frequencies of the system, this is a reasonable result. The natural frequency of the body motion, which is around 1 Hz, is hardly affected by the unsprung mass change, but the wheel hop frequency changes from 10 Hz to as high as 16 Hz, depending on the values. At these high frequencies, the response is largely absorbed by tire compression, so if the low frequency behaviour is similar, it should be anticipated that the ride quality will be similar.

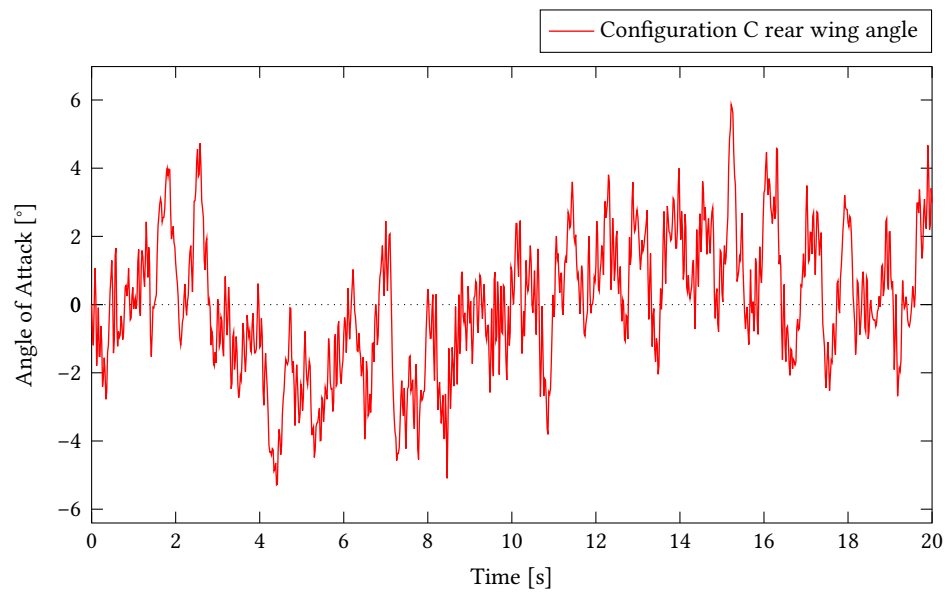


FIGURE 5.17: Rear wing angle at road level 3. The range of the tilting angle become narrow within $\pm 5^\circ$ while the road disturbance decreases.

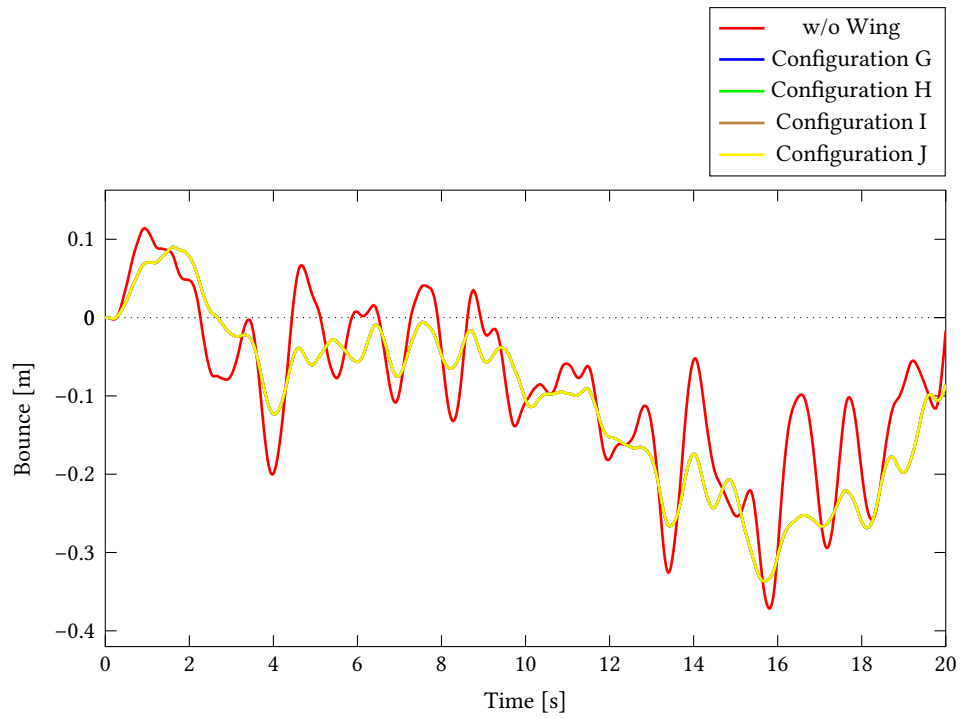


FIGURE 5.18: Road bounce response for different unsprung mass distribution, all the responses are overlapped with each other.

TABLE 5.2: Different unsprung mass distribution

Configuration G	Unsprung mass
m_{uf}	70 kg
m_{ur}	70 kg
Configuration H	Unsprung mass
m_{uf}	30 kg
m_{ur}	70 kg
Configuration I	Unsprung mass
m_{uf}	70 kg
m_{ur}	30 kg
Configuration J	Unsprung mass
m_{uf}	40 kg
m_{ur}	60 kg

5.3.1 Bounce pitch response

5.4 Velocity effects

The previous experiments have the vehicle with a forward speed of 50 m/s. However, since the lifting force is a function of the square of velocity, it is treated as a variable in this section. The test is taking the velocity from 30 m/s and increasing it up to 70 m/s. The assumption is made that if the velocity is reduced, the effect of the wing system will also be reduced. Similarly, if the vehicle moves much faster, the aerodynamic effect will become more significant. However, there will be a limit of speed that will cause the system become unstable.

5.4.1 Bounce pitch response

In Figures 5.20 and 5.22, the random road time history response with different velocities are shown. With a speed of 30 m/s, the wing system is affecting the bouncing response of the vehicle, but it is not as significant as the one shown in Figure 5.22, which is driven at 40 m/s. The system with 30 m/s has an overall bounce reduction of 0.03 m and the improvement is expanded to 0.06 m while increasing the speed up to 40 m/s. If both sets of responses are compared with the previous result at 50 m/s, which is presented in Figure 5.24 shows the aerodynamic wing system has reduced an average bounce motion of 0.1 m, the faster the forward speed is, the smoother the path the wing system will display. In Figure 5.28 the system is operating with a forward speed of only 10 m/s; it offers barely have any improvement over the baseline vehicle, which again is reasonable, since the lifting force is function of velocity squared, and is significantly reduced.

In the vehicle pitch motion, the effectiveness of the wing system is also affected by the increasing speed. From an inspection of the overall pitch response with a forward speed of 30 m/s in Figure 5.21, the pitch angle has been reduced about 0.1 rad. While raising the forward speed up to 40 m/s and inspecting the entire pitch response in Figure 5.23, the pitch angle of the model has been

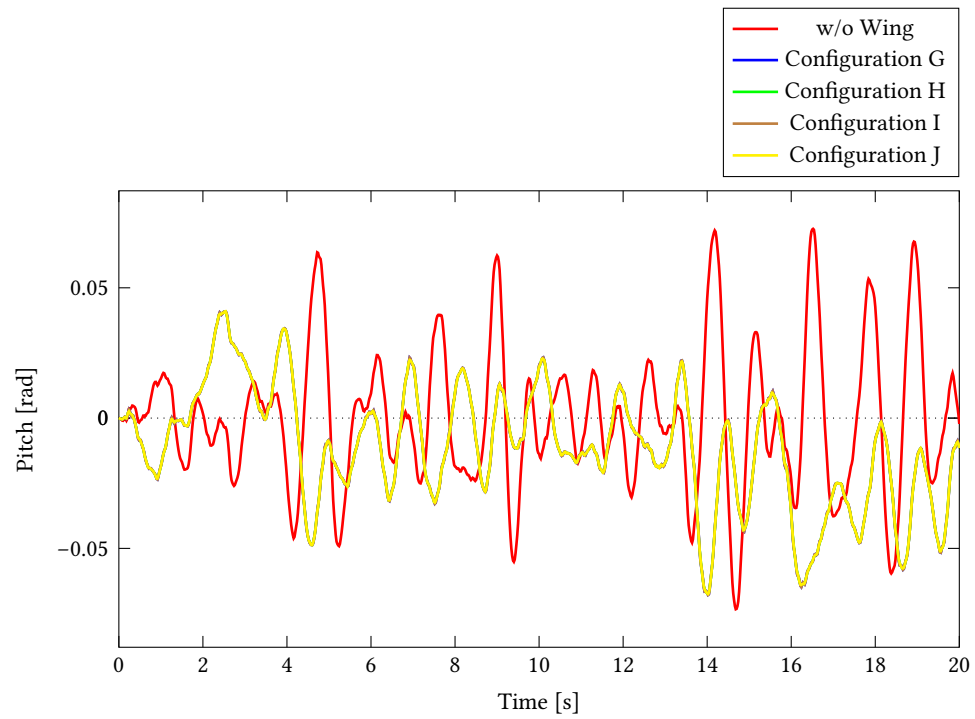


FIGURE 5.19: Road pitch response for different unsprung mass distribution, all the responses are overlapped with each other.

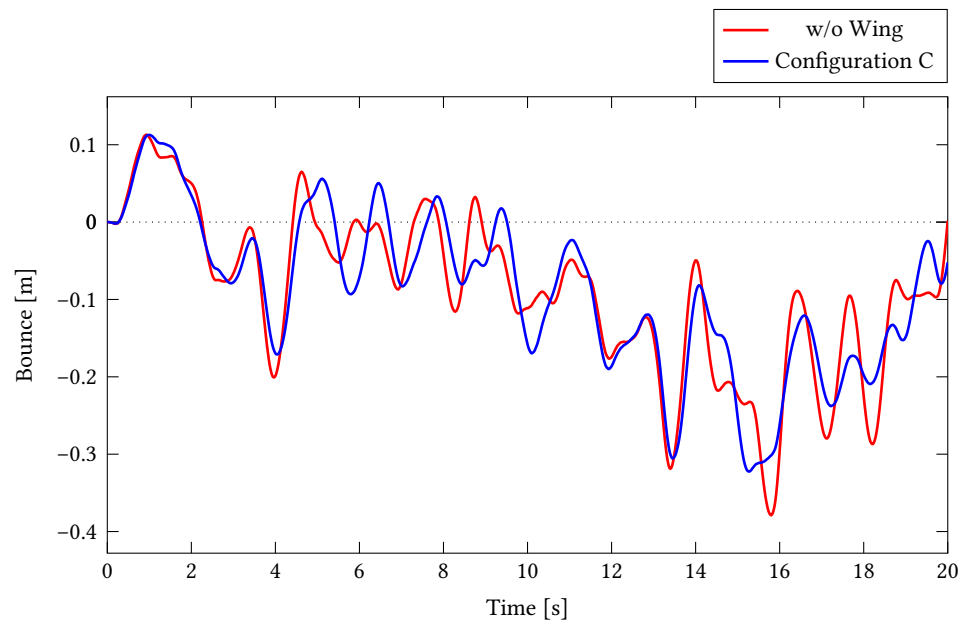


FIGURE 5.20: Road bouncing response with a forward speed of 30 m/s.

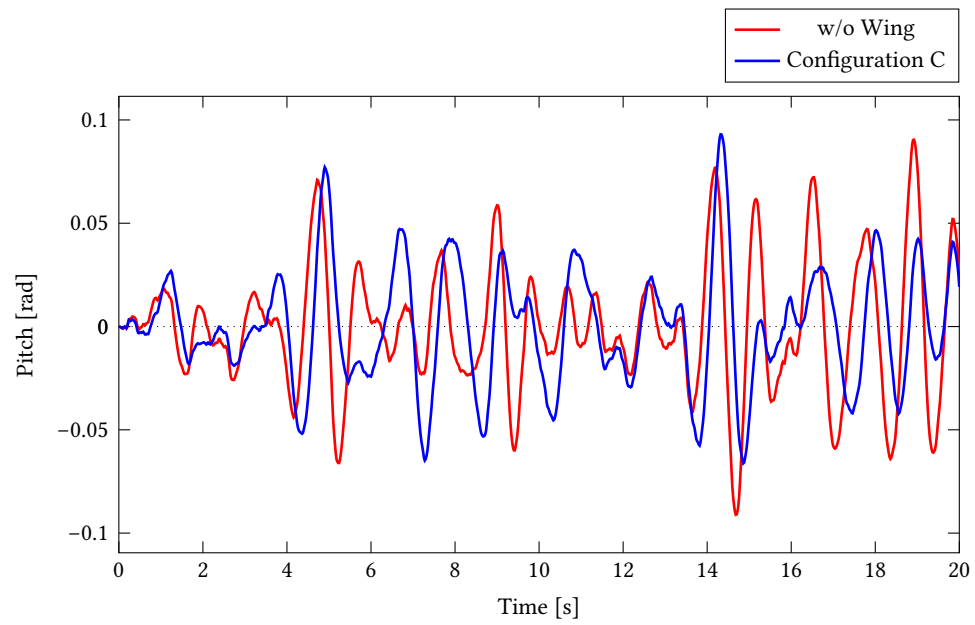


FIGURE 5.21: Road pitch response with a forward speed of 30 m/s.

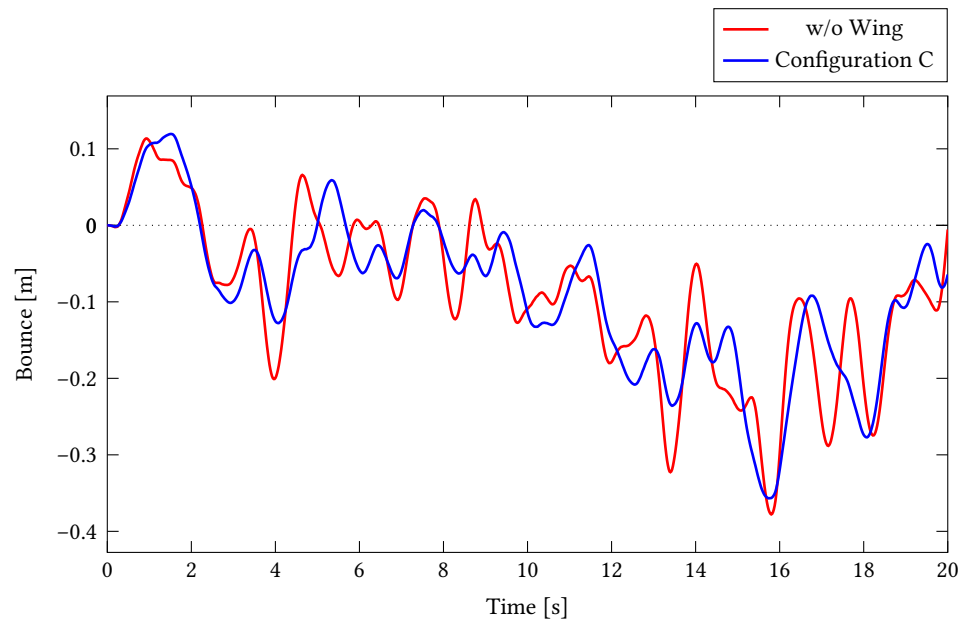


FIGURE 5.22: Road bouncing response with a forward speed of 40 m/s.

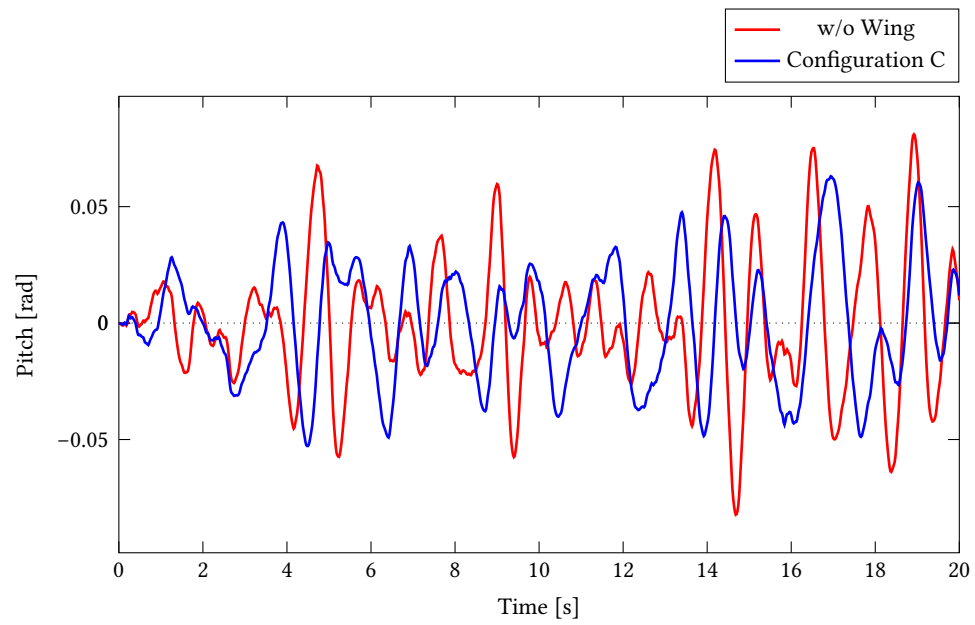


FIGURE 5.23: Road pitch response with a forward speed of 40 m/s.

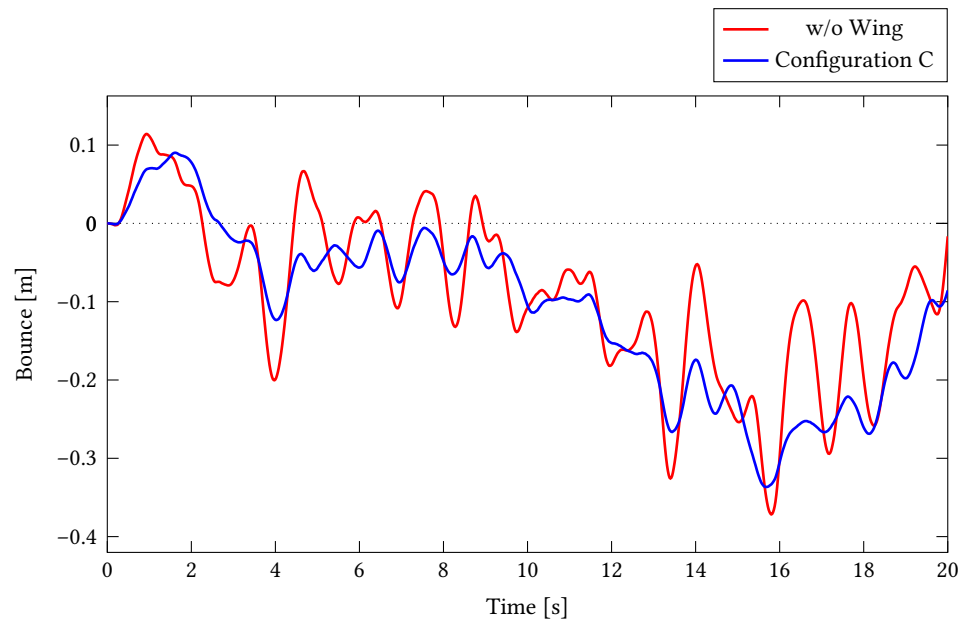


FIGURE 5.24: Road bouncing response with a forward speed of 50 m/s.

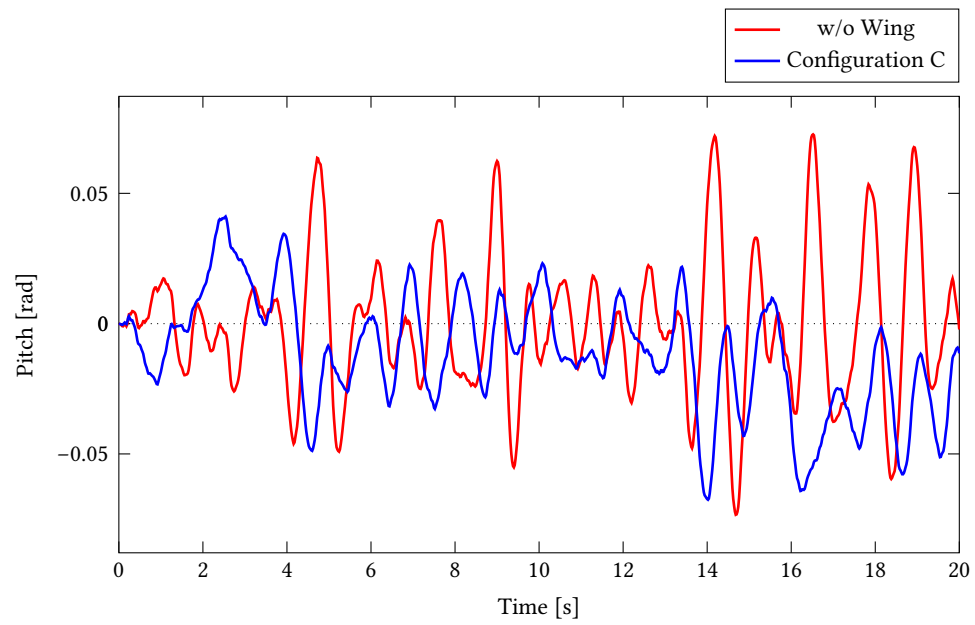


FIGURE 5.25: Road pitch response with a forward speed of 50 m/s.

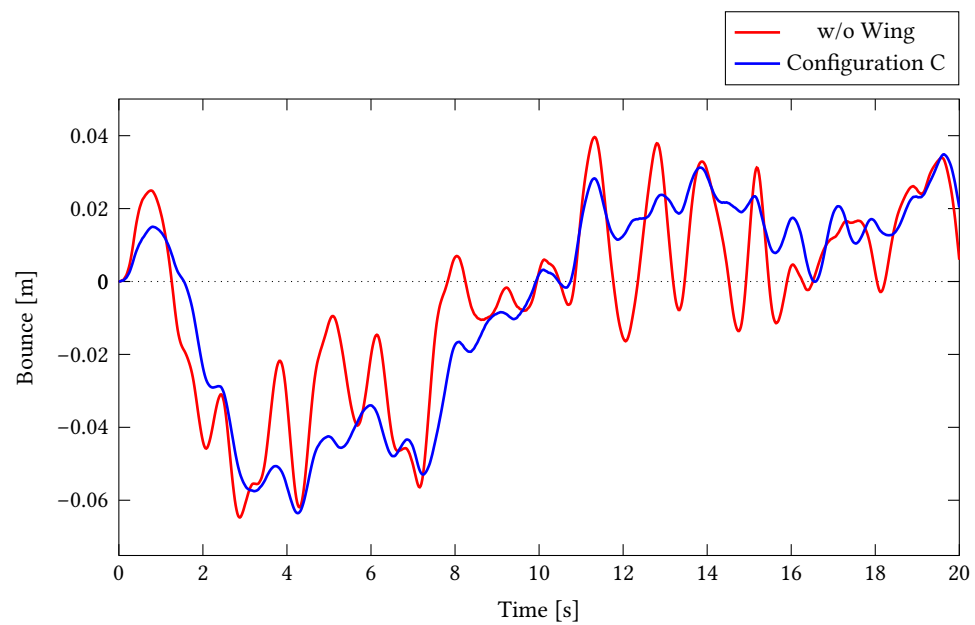


FIGURE 5.26: Road bouncing response with a forward speed of 50 m/s at road level 3.

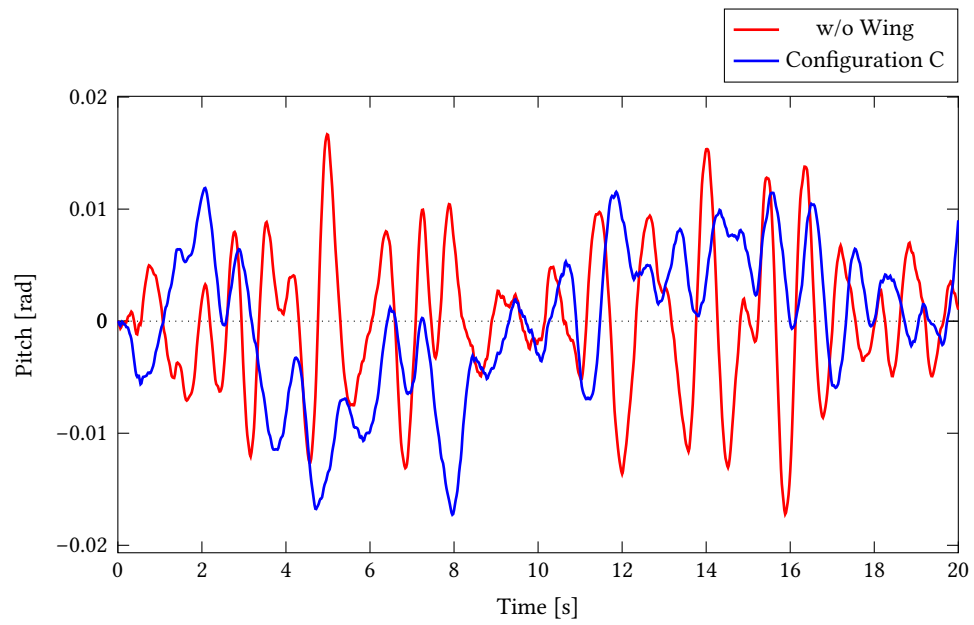


FIGURE 5.27: Road pitch response with a forward speed of 50 m/s at road level 3.

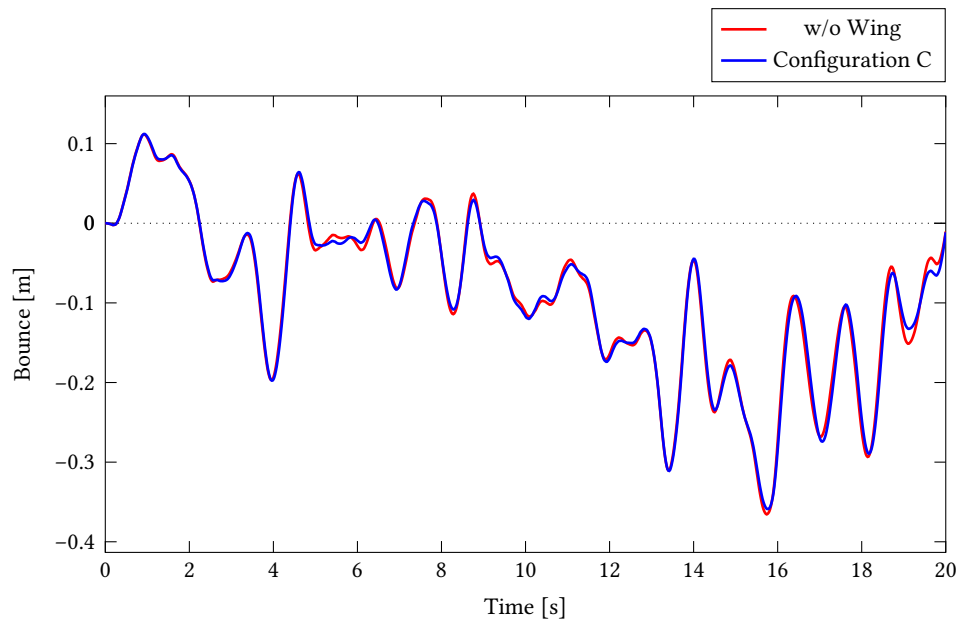


FIGURE 5.28: Road bouncing response with a forward speed of 10 m/s.

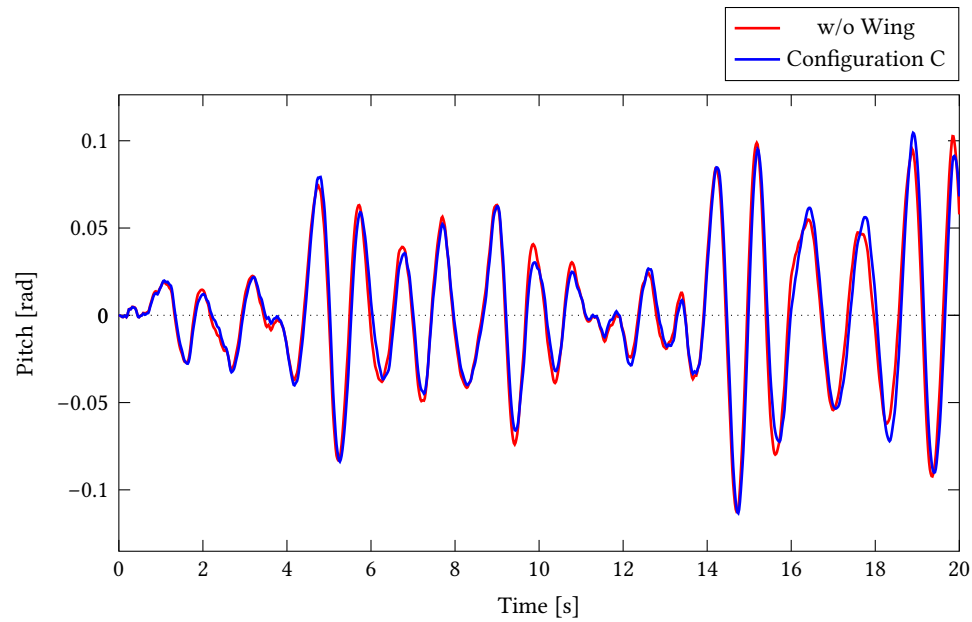


FIGURE 5.29: Road pitch response with a forward speed of 10 m/s.

narrowed within the range between ± 0.05 rad with an average improvement around 0.02 rad. The system with a forward speed of 50 m/s in Figure 5.25 fits the expectation that the overall range of the pitch angle becomes smaller, between ± 0.03 rad, and it decreases the pitch angle over 0.03 rad.

Not all of the results with speed higher than 50 m/s are shown in the chapter, since they all show an unstable response with speeds that high. The eigenvalues of the system with a speed of 51 m/s are listed in Table 5.3, and it has a positive real root, which explains the unstable result. Modes 7 and 8 have no natural frequency, and mode 8 has a negative time constant τ , a measure of the time needed to return to the equilibrium state. A negative time constant with no natural frequency represents a non-oscillatory unstable result. While the system has a negative time constant, the exponential function will approach to infinity with time. One set of unstable road bounce and pitch responses are shown in Figures 5.30 and 5.31 with a forward speed at 51 m/s.

In addition, the result is also affected by different random road roughness. The system is evaluated at 50 m/s on a smooth road with level 3. The linearity of the model predicts that the output will scale with the input, so as the level 3 road is composed of sine waves that are $1/4$ the amplitude of the level 5 road, the resulting bounce, pitch, and wing tilt should also scale by $1/4$. The results are shown in Figures 5.26 and 5.27. As expected, both front and rear wing angles have also become much smaller with the decrease in the road roughness, as shown in Figures 5.16 and 5.17.

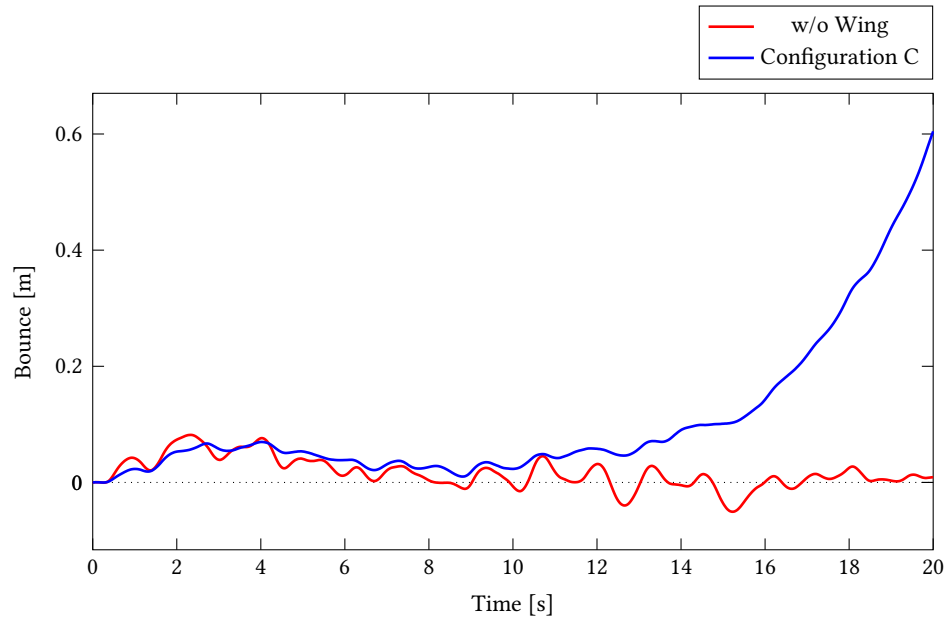


FIGURE 5.30: Road bouncing response with a forward speed of 51 m/s.

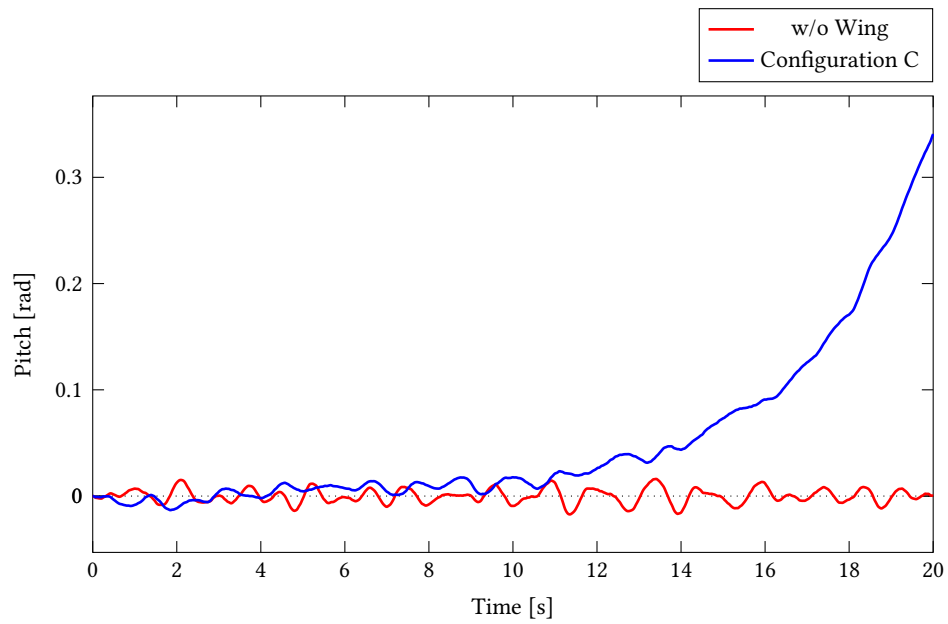


FIGURE 5.31: Road pitch response with a forward speed of 51 m/s.

TABLE 5.3: Eigenvalues at forward speed 51 m/s

Mode	Real [rad/s]	Imag [rad/s]	ω_n [Hz]	τ [s]
1	-11.74	79.82	12.84	0.0852
2	-11.74	-79.82	12.84	0.0852
3	-9.59	79.49	12.74	0.104
4	-9.59	79.49	12.74	0.104
5	-0.885	6.18	0.994	1.13
6	-0.885	-6.18	0.994	1.13
7	-0.160	0.0	NaN	0.862
8	0.329	0.0	NaN	-3.04

5.4.2 Frequency Response

To complement the time history solution of the equations of motion, the frequency responses were also computed. Usually the front and rear suspensions are experiencing the same ground motion. It is not meaningful to analyse two exact same transfer functions for both front and rear. A wheelbase filter is applied to combine two transfer functions into one. It shows the frequency change respect to the relationship between the wheelbase and wavelength. The frequency response for system with a forward speed of 10 m/s is shown in Figure 5.32. As expected, the wing system is not affecting the motion very much at this low speed.

However, at low speed, the wheelbase filtering effect becomes more significant as it shifts into the lower frequency range. The bounce and pitch response have alternating peaks and zeros that align. For example, when the frequency is at 5 Hz, bounce motion falls back to zero with only pitch motion left, since when the wheelbase is close to an odd integer multiple of half the wavelength, only pitch will be excited. Similarly, if the wheelbase is close to the wavelength of the road, or an even multiple, the vehicle will experience only bounce, as seen when the frequency is at 7 Hz.

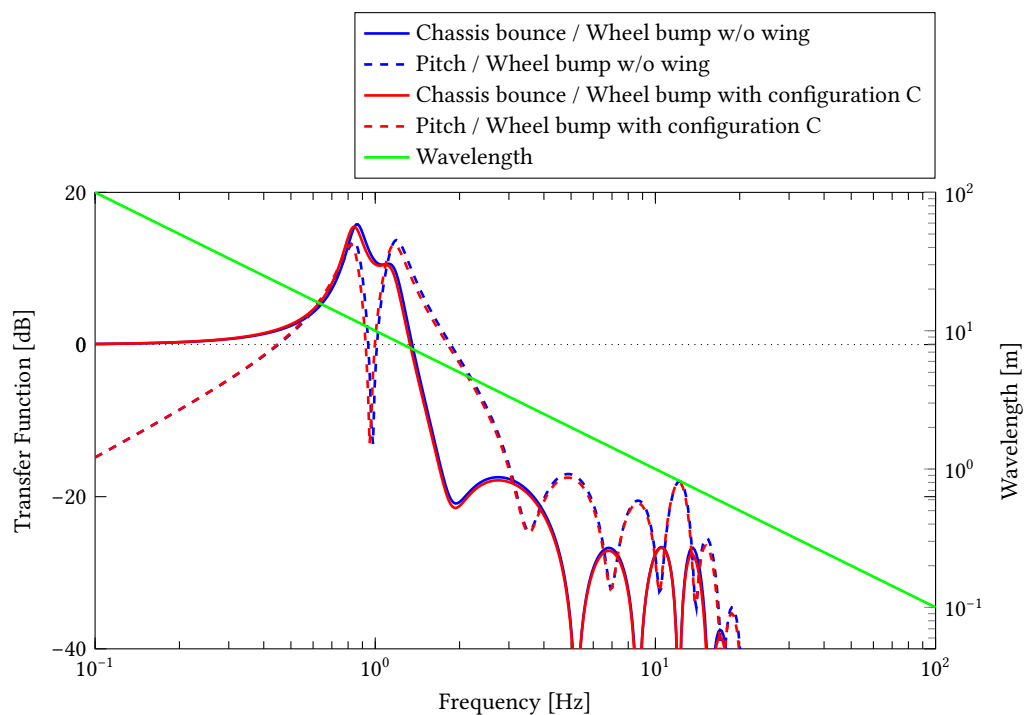


FIGURE 5.32: Frequency response: Wheel bump at 10 m/s forward speed

The frequency plots for both speeds of 30 m/s and 40 m/s show improvement of the output to input ratio, since the system with wings displays a lower output than the system without wings. The only difference is that the system with higher speed has the frequency response shifted slightly toward the negative direction in both axes, which is making sense that wing effect is function of the velocity and it grows proportionally with respect to square of velocity. The system is becoming more effective as the speed increases.

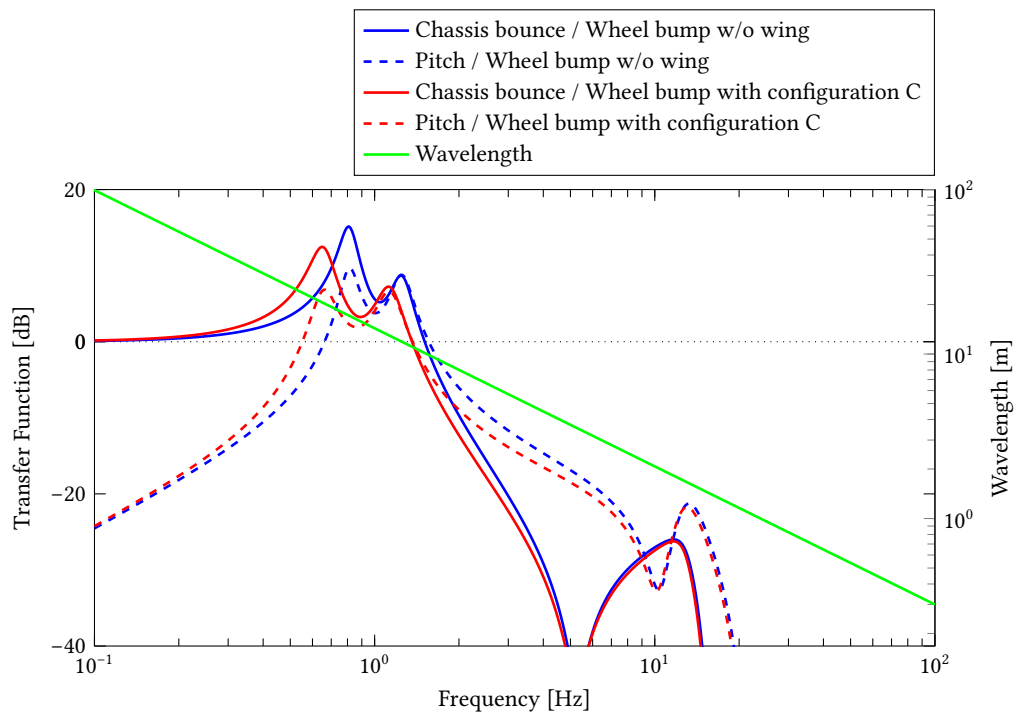


FIGURE 5.33: Frequency response: Wheel bump at 30 m/s forward speed.

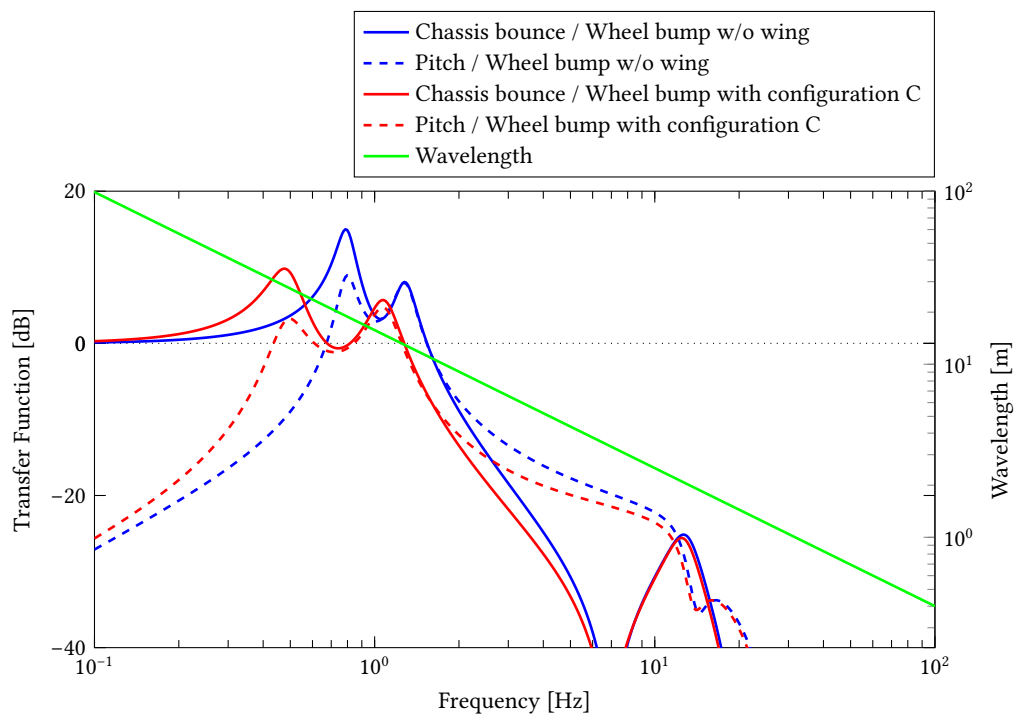


FIGURE 5.34: Frequency response: Wheel bump at 40 m/s forward speed.

Chapter 6

Conclusions and Recommendations

6.1 Conclusions

In this thesis, the author's emphasis has been on the study of aerodynamics effects in multibody vehicle dynamics using a half car model with an attached wing system. All objectives of this research, as defined in Chapter 1, have been accomplished. The multibody dynamics approach has been shown to be an effective tool for making predictions. The vehicle model has been constructed and tested; furthermore, the simulation results suggest the enhancement of the vehicle ride quality performance as expected.

The simulation is constructed to determine the orientation angle of the wing systems from the relative displacement between the sprung mass and the unsprung mass. With the same degree of displacement, two sets of hinge systems were applied to both the front and rear axles of the vehicle model. The location of the bell-crank hinges influences the direction of the tilt angle of the wings. The simulations have determined the proper configuration such that the direction of the generated forces will act to minimize the effects from the road disturbance.

The change of the vertical offset of the bell-crank is intended to determine the best choice for the output-to-input ratio that can be achieved by adjusting the sensitivity of the wing tilting angles under the same displacement of suspension. The front wing system shows higher sensitivity compared to the rear wing system; the graph indicates a trend in which the most stable points have a lower ratio for the rear wing. The front and rear wing systems with output to input ratios of 4.6 rad/m and 4.1 rad/m, respectively, which can be referred to as 'Configuration C', appears to be the best combination that can be obtained, based on the bounce and pitch responses shown. From comparison between Configuration C and the system without wings, with respect to the bounce and pitch response on a random road with level 5 roughness, the wing system generally reduces the peak amplitude of the bounce motion by about 0.12 m and decreases pitch angle about 0.03 rad. The range of angles of attack are controlled within $\pm 20^\circ$, which is a reasonable range for linear analysis of the wing operation. If the wing tilt is used to the maximum linear range, it is expected to be very effective in influencing motion, if the speed is sufficient. Most of the airfoils have stall angles at 15° to 20° ; exceeding the stall angle will cause the wing stop producing lifting

force, so the wing system will not be working as effectively as expected. Care may need to be taken when operating on poor quality roads to avoid stall of the wings. Smooth roads are expected to allow a very reasonable range of tilt angles.

The unsprung mass effect on the vehicle has been explored on Configuration C. It was discovered that no significant changes in either both bounce and pitch responses resulted from changes in the unsprung mass. The result is confirmed in frequency data analysis, which shows the vehicle body bounce has only minor effects, which can be neglected in this investigation. The wheel hop mode was at high frequency that varied over a range of 10 Hz to 16 Hz. As the high frequency disturbance is usually absorbed by the tire compression, rather than body motion, the changes to wheel hop had only a small influence.

It is important to note that in general, the aerodynamic effect is proportional to the square of velocity. The effect of velocity changes were evaluated in this research. The testing range of the velocity has been set from 30 m/s to 70 m/s with a 10 m/s interval. The effects on the vehicle is as expected; at low speed, the system has very little influence, while at very high speed, it may cause instabilities to appear.

The quality of the ride and vehicle performance may be greatly affected by the aerodynamic characteristics of the vehicle body. The application of the wing system has actively enhanced the vehicle comfort of the ride under various road surface conditions. The wing design is able to modify the air motion surrounding the vehicle, directing it in such a way that it enhances the vehicle performance and the ride quality. An important result was that for any choice of wing sensitivity, a maximum safe speed existed. As wing sensitivity increased, the maximum safe speed decreased. In a practical application, care would have to be taken to avoid instabilities. It was also noted that in order for the wing system to have a significant effect on the motion, that some type of wing tilting system would be required. The angle of attack of vehicle itself is insufficient to make the fixed configuration effective.

6.2 Recommendations

Following the full scope of this thesis, more work can be expected to extend the results of this particular research topic. This innovative subject has much more potential to be explored. This chapter will offer proposals for future work. Based on a wide range of literature reviews, several potential developments of the research topic can be expanded.

6.2.1 Improved quantification of ride quality

In this work, no objective metric of ride quality was calculated to determine the range of improvement. Rather, the results were based primarily on visual inspection of the time histories and frequency response data. While in most cases, the results were sufficiently distinct to allow

confident visual inspection, there are existing metrics for ride quality that could potentially allow less subjective interpretation of the results, including those that consider human response to vibration (e.g., Olley's famous 'flat ride' principle suggests that bounce should be preferred over pitch). These metrics can be included, to measure the vertical acceleration or pitch acceleration, to demonstrate a quantitative improvement of ride quality. Root mean square and state calculation analysis are candidates in the future study. In the frequency response plots, it is hard to tell if the ride comfort is improved while natural frequency becomes lower, as passengers feel most comfort in a certain range of natural frequencies. By manipulating the spring stiffness for front and rear suspensions, a more desirable natural frequency might be reached.

6.2.2 Optimum control

Numerical control of vehicle systems can potentially provide modification of the entire tendency of the vehicle. With the application of a controller instead of the mechanically driven wings, the angle of tilt can be more fully utilized within the reasonable range with reduced likelihood of reaching the stall angle. With force and moment actuators applied, there could be a still further significant improvement of the overall performance.

6.2.3 Wing design

Testing on varying wing types is critical; multiple experiments should be conducted with the design to ensure that maximum performance is reached. The simulations conducted utilized only a flat plate approximation of the airfoil, while many other options may be available. The effect of asymmetric profiles might be worth exploring. Even concepts such as modular wing design where various elements of the wing can be altered (opened or closed) could be explored. Further, models that include the time varying nature of the aerodynamic force generation could be explored. The effect of the high frequency content in the wing tilt angle should be explored.

6.2.4 Future experiments or simulations

In order to fully appreciate the results of analysis, physical experiments are suggested. For example, there are existing facilities where road test simulators (RTS), colloquially known as four-post-shakers, are located inside a wind tunnel. This would allow road disturbance and aerodynamic loads to be applied simultaneously. Such a facility could provide very interesting opportunity to compare experimental and simulation results. However, it is noted that if a small-scale vehicle has to be used for the experiments, the scaling ratio for vehicle's different parameters has to be selected with care. A non-dimensional analysis may be required.

Additionally, a computational fluid dynamics (CFD) approach could be taken to the simulation. Measurements of downforce and drag with respect to the changing speed and various angles of attack can be obtained. This idea is inspired by an experiment described by Kajiwara[14], which shows the importance of considering the effects of vibrations on the wings. Adding a damper

to the attached wing design to resist unwanted vibration of the wing is one potential avenue to explore.

Beside the ride quality assessment, the multibody simulation approach can be expanded using different vehicle models, e.g., the yaw plane model, the truck trailer model, or a full car model to analyze the aerodynamic effects on different types of vehicle motions. The application of aerodynamic elements can help improve the handling of the vehicle during cornering maneuvers; a significant reduction in the delay of the response of the lateral acceleration and yaw rate can be expected. Utilizing the wing system in the truck and trailer model to modify the wind flow could also assist the reduction of drag forces, stabilize the trailer, and help avoid jackknifing or fishtailing motions, which can cause accidents. Since the stability of the trailer is influenced by parameters such as the tire cornering stiffness, a vertical wing stabilizer has potential to improve the trailer stability and controllability.

A full car model can demonstrate a wider range of desirable motion analysis, provide more comprehensive testing results, and better reflect the reality of vehicle responses with the aerodynamic effects to various road conditions. The current study is only focusing on the linear and linearized analysis, but a model can be simulated in other multibody dynamics software tools, e.g. Altair MotionView, for the entire system, which allows both linear and nonlinear analysis. MotionView allows more detailed assessment, including factors such as nonlinear deformation and large displacements. The results will be more precisely represented, without linearization.

6.3 Summary of contributions

This section will highlight three primary contributions of the work.

First, the existing state of knowledge in the field of combined aerodynamic effects in multibody dynamics is very limited. This thesis provides a timely example of the utility of the combination of these two fields. Not only can the two topics overlap, there is excellent potential for exploring the behaviour of complex fluid-mechanism interaction, and predicting the vibration of such a system, and this thesis highlights that fact.

Secondly, this thesis demonstrates the implementation of a novel variable tilt wing system at both front and rear suspensions of a road vehicle. To the best knowledge of the author, this analysis is the first in the literature to explore the behaviour of a half car model using a combined multibody dynamics and aerodynamics approach on such a system.

Finally, the work has shown the effectiveness of the system described above for improvement of vehicle ride quality. The results suggest that such a system could be quite capable, but that there is good reason to have concerns over the stability. When operated at the high speeds where such a system would be effective, the presence of any instability could be very dangerous. Any

practical implementation would need to include some means of limiting the aerodynamic forces in the event that unintended conditions occurred.

References

- [1] Wolf-Heinrich Hucho. *Aerodynamics of Road Vehicles*. Aerodynamics Of Road Vehicles. 1993. ISBN: 9780262526449.
- [2] Joseph Katz. “Aerodynamics Of Race Cars”. In: 2006.
- [3] Peter Gullberg, Lennart Löfdahl, and Zhiling Qiu. “Influence of Aerodynamics on the Fatal Crash in Le Mans 1955”. In: *European Automotive Simulation Conference*. 2009.
- [4] Hans J Witten. *Aerodynamic side panels for a tractor-trailer truck*. US Patent 4,518,188. 1985.
- [5] M. Olley. “Road manners of the modern car”. In: *Proceedings of the Institution of Automobile Engineers* 41.1 (1946), pp. 523–551.
- [6] Michael Blundell and Damian Harty. *Multibody systems approach to vehicle dynamics*. Elsevier, 2004.
- [7] Krzysztof Kurec et al. “Advanced Modeling and Simulation of Vehicle Active Aerodynamic Safety”. In: *Journal of Advanced Transportation* 2019 (2019).
- [8] M. Drela. *Flight Vehicle Aerodynamics*. Flight Vehicle Aerodynamics. MIT Press, 2014. ISBN: 9780262526449.
- [9] Arvin R. Savkooor and C.T. Chou. “Application of Aerodynamic Actuators to Improve Vehicle Handling”. In: *Vehicle System Dynamics* 32.4-5 (1999), pp. 345–374. DOI: 10.1076/vesd.32.4.345.2081.
- [10] Carlo Doniselli, Giampiero Mastinu, and Massimiliano Gobbi. “Aerodynamic Effects on Ride Comfort and Road Holding of Automobiles”. In: *Vehicle System Dynamics* 25.sup1 (1996), pp. 99–125. DOI: 10.1080/00423119608969190.
- [11] Fereydoon Diba, Ahmad Barari, and Ebrahim Esmailzadeh. “Active Aerodynamic System to Improve the Safety and Handling of Race Cars in Lane Change and Wet Road Maneuvers”. In: *ASME 2012 International Design Engineering Technical Conferences and Computers and Information in Engineering Conference*. American Society of Mechanical Engineers. 2012, pp. 417–423.
- [12] Giulio Reina and Mario Foglia. “Modelling and handling dynamics of a wind-driven vehicle”. In: *Vehicle System Dynamics* 57.5 (2019), pp. 697–720. DOI: 10.1080/00423114.2018.1479529.
- [13] Matteo Corno et al. “Improving high speed road-holding using actively controlled aerodynamic surfaces”. In: *2013 European Control Conference (ECC)*. IEEE. 2013, pp. 1493–1498.
- [14] Shinji Kajiwara. “Passive variable rear-wing aerodynamics of an open-wheel racing car”. In: *Automotive and Engine Technology* 2.1-4 (2017), pp. 107–117.

- [15] JP Meijaard, AR Savkoor, and G Lodewijks. “Potential for vehicle ride improvement using both suspension and aerodynamic actuators”. In: *Proceedings of the IEEE International Symposium on Industrial Electronics, 2005. ISIE 2005*. Vol. 1. IEEE. 2005, pp. 385–390.
- [16] Arash Hosseinian Ahangarnejad and Stefano Melzi. “Numerical analysis of the influence of an actively controlled spoiler on the handling of a sports car”. In: *Journal of Vibration and Control* 24.22 (2018), pp. 5437–5448. DOI: 10.1177/1077546318754683.
- [17] J.P. Den Hartog. *Mechanical Vibrations, fourth edition*. McGraw Hill, New York, 1956.
- [18] Arend Schwab and J.P. Meijaard. “Dynamics of Flexible Multibody Systems with Non-Holonomic Constraints: A Finite Element Approach”. In: *Multibody System Dynamics* 10 (Jan. 2003), pp. 107–123. DOI: 10.1023/A:1024575707338.
- [19] Bruce Minaker. “The tangent stiffness matrix in rigid multibody vehicle dynamics”. In: *Mathematical and Computer Modelling of Dynamical Systems* 21.3 (2015), pp. 288–310. DOI: 10.1080/13873954.2014.953549.
- [20] Bruce Minaker, Mingyu Sun, and Jeff Defoe. “Inclusion Of Aerodynamic Effects In Multibody Dynamics”. In: May 2018. DOI: 10.25071/10315/35261.
- [21] D.K. Schmidt. *Modern Flight Dynamics*. McGraw-Hill Higher Education, 2011. ISBN: 9780071316460. URL: <https://books.google.ca/books?id=PHC7YgEACAAJ>.
- [22] Peter Múčka. “Simulated road profiles according to ISO 8608 in vibration analysis”. In: *Journal of Testing and Evaluation* 46.1 (2017), pp. 405–418.

Appendix A

Model Details

A.1 Equations of motion

This section presents the first order equations of motion of the vehicle model with wings attached (Configuration C). The equations are in the form:

$$\begin{Bmatrix} \dot{x} \\ y \end{Bmatrix} = \begin{bmatrix} \mathbf{A} & \mathbf{B} \\ \mathbf{C} & \mathbf{D} \end{bmatrix} \begin{Bmatrix} x \\ u \end{Bmatrix}$$

where:

$$\mathbf{A} = \begin{bmatrix} -8.5903e+0 & -1.6543e+1 & -3.9639e+0 & -1.6906e+2 & 5.0117e-1 & 2.6618e-1 & -6.1099e-2 & -5.6488e-1 \\ 2.5475e+1 & 7.7035e+0 & -2.1149e+1 & 1.8103e+2 & -1.6893e-1 & 7.6369e-1 & 1.1871e+0 & -2.4598e+0 \\ 1.9312e+1 & 2.0095e+0 & -1.6495e+1 & -3.2034e+3 & 7.4876e-1 & 5.9856e+0 & -7.0756e+0 & 1.6871e-1 \\ 1.1531e-1 & -9.1491e-2 & 1.8609e+0 & 1.0970e-10 & 2.3372e-3 & 1.1002e-2 & 2.5350e-3 & 1.2849e-1 \\ 1.5300e+3 & -3.2953e+2 & -1.8930e+3 & -1.1025e+0 & -2.2139e+1 & 9.3466e+1 & 8.5504e+1 & -1.8029e+2 \\ -1.0945e+2 & 2.1305e+1 & 1.3156e+2 & 2.8395e+3 & -3.6963e+1 & -6.0054e+0 & 3.1206e-1 & 4.3342e+1 \\ 5.1783e+1 & -1.0859e+1 & -6.4037e+1 & 6.8979e+2 & -3.3278e+1 & 8.1476e-1 & 2.6101e+0 & -4.4422e+1 \\ -2.1318e+2 & 5.2944e-1 & 2.0129e+2 & 3.3494e+4 & -4.3798e+0 & -6.3758e+1 & 7.3492e+1 & -2.3317e+0 \end{bmatrix}$$

$$\mathbf{B} = \begin{bmatrix} -1.3491e+0 & -5.5565e-1 \\ -1.0500e+0 & 3.0897e+0 \\ -1.7993e+1 & -1.8100e+1 \\ -5.2674e-13 & 1.7533e-12 \\ -1.8972e+2 & 1.8970e+2 \\ 2.7661e+1 & 4.3309e+0 \\ -2.8834e+0 & 1.0655e+1 \\ 1.8970e+2 & 1.8768e+2 \end{bmatrix}$$

$$C = \begin{bmatrix} 4.7315e-1 & -1.5449e-1 & -7.0821e-1 & -8.8755e+1 & -5.8068e-3 & -5.8376e-2 & 6.7000e-2 & -6.0942e-2 \\ 7.5482e+0 & -1.7301e+0 & -1.0082e+1 & 9.8885e-14 & -6.6189e-3 & -3.1249e-2 & 2.7909e-3 & -9.1426e-1 \\ -1.2878e+2 & -2.9756e+1 & 5.1572e+0 & -1.9879e-10 & -6.5983e+0 & -1.1260e+2 & 8.9539e+0 & 9.3653e+0 \\ 2.4323e+2 & 6.7782e+1 & -9.0040e+0 & 7.8864e-13 & -1.0560e+0 & 2.1879e+0 & -3.3644e-1 & -2.2076e-1 \\ 1.9463e+1 & -2.7344e+1 & -2.5783e+0 & 6.5333e-11 & -2.9017e+0 & 7.9861e+0 & 1.0187e+2 & -2.7756e+0 \\ 7.9072e+1 & -1.5643e+2 & -1.3011e+1 & -1.0168e-12 & 1.4200e+0 & -3.7463e-1 & 1.1808e+0 & -2.4802e-2 \end{bmatrix}$$

$$D = 0$$

A.2 Code

This section presents the source code used to generate the vehicle model equations.

A.2.1 Input file for half car model with wing

```
function input_half_car_wings(;u=0,a=1.189,b=2.885-1.189,kf=35000,kr=38000,cf=1000,
cr=1200,m=16975/9.81,I=3267,kt=300000,muf=50,mur=50,mbc=0,hoff=0.1,voff_f=0.02,
voff_r=0.02)
```

```
the_system=mbd_system("Half Car Wings Model")
```

```
item=body("chassis")
item.mass=m
item.moments_of_inertia=[0,I,0] ## Only the Iy term matters here
item.products_of_inertia=[0,0,0]
item.location=[0,0,0.25]
item.velocity=[u,0,0]
push!(the_system.item,item)
push!(the_system.item,weight(item))
```

```
item=body("front unsprung")
item.mass=muf
item.location=[a,0,0.1]
item.velocity=[u,0,0]
push!(the_system.item,item)
push!(the_system.item,weight(item))
```

```
item=body("rear unsprung")
item.mass=muf
item.location=[-b,0,0.1]
item.velocity=[u,0,0]
push!(the_system.item,item)
push!(the_system.item,weight(item))
```



```
item=body("front wing body")
item.mass=5
item.moments_of_inertia=[0,0.1,0] ## Only the Iy term matters here
item.products_of_inertia=[0,0,0]
item.location=[a+0.4,0,0.2]
item.velocity=[u,0,0]
push!(the_system.item,item)

item=body("rear wing body")
item.mass=5
item.moments_of_inertia=[0,0.1,0] ## Only the Iy term matters here
item.products_of_inertia=[0,0,0]
item.location=[-b-0.3,0,0.4]
item.velocity=[u,0,0]
push!(the_system.item,item)

item=rigid_point("front wing hinge")
item.body[1]="chassis"
item.body[2]="front wing body"
item.location=[a+0.4,0,0.2]
item.forces=3
item.moments=2
item.axis=[0,1,0]
push!(the_system.item,item)

item=rigid_point("rear wing hinge")
item.body[1]="chassis"
item.body[2]="rear wing body"
item.location=[-b-0.3,0,0.4]
item.forces=3
item.moments=2
item.axis=[0,1,0]
push!(the_system.item,item)

item=body("front wing bell crank")
item.mass=mbc
item.location=[a+hoff,0,0.254+voff_f]
item.velocity=[u,0,0]
push!(the_system.item,item)

item=body("rear wing bell crank")
item.mass=mbc
item.location=[-b-hoff,0,0.254+voff_r]
item.velocity=[u,0,0]
push!(the_system.item,item)
```

```
item=rigid_point("front bell crank hinge")
item.body[1]="chassis"
item.body[2]="front wing bell crank"
item.location=[a+hoff,0,0.254+voff_f]
item.forces=3
item.moments=2
item.axis=[0,1,0]
push!(the_system.item,item)
```

```
item=rigid_point("rear bell crank hinge")
item.body[1]="chassis"
item.body[2]="rear wing bell crank"
item.location=[-b-hoff,0,0.254+voff_r]
item.forces=3
item.moments=2
item.axis=[0,1,0]
push!(the_system.item,item)
```

```
item=link("front wing linkage")
item.body[1]="front unsprung"
item.body[2]="front wing bell crank"
item.location[1]=[a,0,0.1]
item.location[2]=[a,0,0.254+voff_f]
push!(the_system.item,item)
```

```
item=link("rear wing linkage")
item.body[1]="rear unsprung"
item.body[2]="rear wing bell crank"
item.location[1]=[-b,0,0.1]
item.location[2]=[-b,0,0.254+voff_r]
push!(the_system.item,item)
```

```
item=link("front wing linkage")
item.body[1]="front wing body"
item.body[2]="front wing bell crank"
item.location[1]=[a+0.4,0,0.3]
item.location[2]=[a+hoff,0,0.3]
push!(the_system.item,item)
```

```
item=link("rear wing linkage")
item.body[1]="rear wing body"
item.body[2]="rear wing bell crank"
item.location[1]=[-b-0.3,0,0.3]
item.location[2]=[-b-hoff,0,0.3]
push!(the_system.item,item)
```

```
cla=2pi
a0=-5*pi/180

span=2
chord=0.35
AR=span/chord

CLa=cla/(1+cla/(pi*AR))
CL0=CLa*a0
CDa=(2*CL0*CLa)/(pi*AR)
CD0=CL0^2/(pi*AR)

# Horizontal wing coefficients

wing1=wing("test wing 1")
wing1.CXu=-2*CD0
wing1.CXw=-CDa+CL0
wing1.CZu=2*CL0
wing1.CZw=-CLa-CD0
wing1.span=span
wing1.chord=chord

wing2=wing("test wing 2")
wing2.CXu=-2*CD0
wing2.CXw=-CDa+CL0
wing2.CZu=2*CL0
wing2.CZw=-CLa-CD0
wing2.span=span
wing2.chord=chord

mtx,vec=aero_damping(wing1,velocity=u)

item=flex_point("front wing")
item.body[1]="front wing body"
item.body[2]="ground"
item.location=[a+0.4,0,0.2]
item.d_mtx=mtx
item.forces=3
item.moments=3
push!(the_system.item,item)

mtx,vec=aero_damping(wing2,velocity=u)
```

```
item=flex_point("rear wing")
item.body[1]="rear wing body"
item.body[2]="ground"
item.location=[-b-0.3,0,0.4]
item.d_mtx=mtx
item.forces=3
item.moments=3
push!(the_system.item,item)

## Add a spring, to connect our chassis to the front suspension
item=flex_point("front susp")
item.body[1]="chassis"
item.body[2]="front unsprung"
item.location=[a,0,0.25] ## Front axle "a" m ahead of cg
item.forces=1
item.moments=0
item.axis=[0,0,1] ## Spring acts in z direction
item.stiffness=[kf,0]
item.damping=[cf,0]
push!(the_system.item,item)

## Rear suspension
item=flex_point("rear susp")
item.body[1]="chassis"
item.body[2]="rear unsprung"
item.location=[-b,0,0.25] ## Front axle "a" m ahead of cg
item.forces=1
item.moments=0
item.axis=[0,0,1] ## Spring acts in z direction
item.stiffness=[kr,0]
item.damping=[cr,0]
push!(the_system.item,item)

item=flex_point("tire")
item.body[1]="front unsprung"
item.body[2]="ground"
item.stiffness=[kt,0]
item.damping=[0,0]
item.location=[a,0,0]
item.forces=1
item.moments=0
item.axis=[0,0,1]
push!(the_system.item,item)
```

```
item=flex_point("tire")
item.body[1]="rear unsprung"
item.body[2]="ground"
item.stiffness=[kt,0]
item.damping=[0,0]
item.location=[-b,0,0]
item.forces=1
item.moments=0
item.axis=[0,0,1]
push!(the_system.item,item)
```

```
item=rigid_point("slider front")
item.body[1]="front unsprung"
item.body[2]="ground"
item.location=[a,0,0.1]
item.forces=2
item.moments=3
item.axis=[0,0,1]
push!(the_system.item,item)
```

```
item=rigid_point("slider rear")
item.body[1]="rear unsprung"
item.body[2]="ground"
item.location=[-b,0,0.1]
item.forces=2
item.moments=3
item.axis=[0,0,1]
push!(the_system.item,item)
```

```
## Constrain to linear motion in z direction (bounce)
```

```
item=rigid_point("road frc")
item.body[1]="chassis"
item.body[2]="ground"
item.location=[0,0,0.25]
item.forces=2
item.moments=0
item.axis=[0,0,1]
push!(the_system.item,item)
```

```
item=rigid_point("road mmt")
item.body[1]="chassis"
item.body[2]="ground"
item.location=[0,0,0.25]
item.forces=0 ## Constrain to rotational motion around y axis (pitch)
item.moments=2 ## Reset forces, moments axis, all other properties are the same
```

```
item.axis=[0,1,0]
push!(the_system.item,item)

## Force the bounce and pitch
item=actuator("front bump")
item.body[1]="front unsprung"
item.body[2]="ground"
item.location[1]=[a,0,0.25]
item.location[2]=[a,0,0]
item.gain=kt
push!(the_system.item,item)

## Force the bounce and pitch
item=actuator("rear bump")
item.body[1]="rear unsprung"
item.body[2]="ground"
item.location[1]=[-b,0,0.25]
item.location[2]=[-b,0,0]
item.gain=kt
push!(the_system.item,item)

## Measure the bounce and pitch
item=sensor("\$z_\\text{G}\\$")
item.body[1]="chassis"
item.body[2]="ground"
item.location[1]=[0,0,0.25]
item.location[2]=[0,0,0]
push!(the_system.item,item)

item=sensor("\$(a+b)\\theta\\$")
item.body[1]="chassis"
item.body[2]="ground"
item.location[1]=[0,0,0.25]
item.location[2]=[0,0.1,0.25]
item.twist=1
item.gain=a+b
push!(the_system.item,item)

item=sensor("front wing angle")
item.body[1]="front wing body"
item.body[2]="chassis"
item.twist=1
item.gain=180/pi
item.location[1]=[a+0.4,0,0.2]
item.location[2]=[a+0.4,0.1,0.2]
```

```
push!(the_system.item, item)

item=sensor("front angle of attack")
item.body[1]="chassis"
item.body[2]="ground"
item.gain=180/pi/u
item.order=2
item.frame=0
item.location[1]=[a+0.4,0,0.2]
item.location[2]=[a+0.4,0,0.3]
push!(the_system.item, item)

item=sensor("rear wing angle")
item.body[1]="rear wing body"
item.body[2]="chassis"
item.twist=1
item.gain=180/pi
item.location[1]=[-b-0.3,0,0.4]
item.location[2]=[-b-0.3,0.1,0.4]
push!(the_system.item, item)

item=sensor("rear angle of attack")
item.body[1]="chassis"
item.body[2]="ground"
item.gain=180/pi/u
item.order=2
item.frame=0
item.location[1]=[-b-0.3,0,0.4]
item.location[2]=[-b-0.3,0,0.5]
push!(the_system.item, item)

the_system

end
```

A.2.2 Run file

```
include("wheelbase_filter.jl")
using EoM
using EoM_X3D
using EoM_TeX

a=1.189
b=2.885-1.189
kf=35000
```

```

kr=38000
cf=1000
cr=1200
m=16975/9.81
Iyy=3267
kt=300000

muf=50
mur=50

muf1=70
mur1=70

muf2=30
mur2=30

muf3=40
mur3=40

muf4=60
mur4=60

u=50
#u=1:1:70
#####
include("input_half_car.jl")
temp(x)=input_half_car(u=x,m=m,I=Iyy,a=a,b=b,kf=kf,kr=kr,cf=cf,cr=cr,muf=muf,
mur=mur,kt=kt)

my_sys,my_eqns=run_eom(temp,vpts=u,verbose=true)
my_result=analyze(my_eqns)
folder=write_output(my_sys,my_eqns,my_result,dir_time="folder")
wheelbase_filter(folder,my_sys,my_result,a+b)
#animate_modes(folder,my_sys[1],my_result[1])
write_report(folder,my_sys,verbose=true,build=false) ## Build LaTeX report

#####

include("aero_damping.jl")
include("input_half_car_wings.jl")

temp(x)=input_half_car_wings(u=x,m=m,I=Iyy,a=a,b=b,kf=kf,kr=kr,cf=cf,cr=cr,
muf=muf,mur=mur,kt=kt,mbc=5,hoff=0.1,voff_f=0.0,voff_r=0.0)

```



```

my_sys, my_eqns=run_eom(temp, vpts=u, verbose=true)
my_result_1=analyze(my_eqns)
folder_1=write_output(my_sys, my_eqns, my_result_1, dir_time="folder_1")
wheelbase_filter(folder_1, my_sys, my_result_1, a+b)
animate_modes(folder_1, my_sys[1], my_result_1[1])
write_report(folder_1, my_sys, verbose=true, build=false) ## Build LaTeX report

temp(x)=input_half_car_wings(u=x, m=m, I=Iyy, a=a, b=b, kf=kf, kr=kr, cf=cf, cr=cr,
muf=muf, mur=mur, kt=kt, mbc=5, hoff=-0.1, voff_f=0.0, voff_r=0.0)

my_sys, my_eqns=run_eom(temp, vpts=u, verbose=true)
my_result_2=analyze(my_eqns)
folder_2=write_output(my_sys, my_eqns, my_result_2, dir_time="folder_2")
wbf_2=wheelbase_filter(folder_2, my_sys, my_result_2, a+b)
animate_modes(folder_2, my_sys[1], my_result_2[1])
write_report(folder_2, my_sys, verbose=true, build=false) ## Build LaTeX report

#####

temp(x)=input_half_car_wings(u=x, m=m, I=Iyy, a=a, b=b, kf=kf, kr=kr, cf=cf, cr=cr,
muf=muf, mur=mur, kt=kt, mbc=5, hoff=0.1, voff_f=0.0, voff_r=0.005)

my_sys, my_eqns=run_eom(temp, vpts=u, verbose=true)
my_result_3=analyze(my_eqns)
folder_3=write_output(my_sys, my_eqns, my_result_3, dir_time="folder_3")
wbf_3=wheelbase_filter(folder_3, my_sys, my_result_3, a+b)
animate_modes(folder_3, my_sys[1], my_result_3[1])
write_report(folder_3, my_sys, verbose=true, build=false) ## Build LaTeX report

temp(x)=input_half_car_wings(u=x, m=m, I=Iyy, a=a, b=b, kf=kf, kr=kr, cf=cf, cr=cr,
muf=muf, mur=mur, kt=kt, mbc=5, hoff=0.1, voff_f=0.01, voff_r=0.01)

my_sys, my_eqns=run_eom(temp, vpts=u, verbose=true)
my_result_4=analyze(my_eqns)
folder_4=write_output(my_sys, my_eqns, my_result_4, dir_time="folder_4")
wbf_4=wheelbase_filter(folder_4, my_sys, my_result_4, a+b)
animate_modes(folder_4, my_sys[1], my_result_4[1])
write_report(folder_4, my_sys, verbose=true, build=false) ## Build LaTeX report
#

temp(x)=input_half_car_wings(u=x, m=m, I=Iyy, a=a, b=b, kf=kf, kr=kr, cf=cf, cr=cr,
muf=muf, mur=mur, kt=kt, mbc=5, hoff=0.1, voff_f=0.01, voff_r=0.02)

```

```

my_sys, my_eqns=run_eom(temp, vpts=u, verbose=true)
my_result_5=analyze(my_eqns)
folder_5=write_output(my_sys, my_eqns, my_result_5, dir_time="folder_5")
wbf_5=wheelbase_filter(folder_5, my_sys, my_result_5, a+b)
animate_modes(folder_5, my_sys[1], my_result_5[1])
write_report(folder_5, my_sys, verbose=true, build=false) ## Build LaTeX report
#

temp(x)=input_half_car_wings(u=x, m=m, I=Iyy, a=a, b=b, kf=kf, kr=kr, cf=cf, cr=cr,
muf=muf, mur=mur, kt=kt, mbc=5, hoff=0.1, voff_f=0.015, voff_r=0.015)

my_sys, my_eqns=run_eom(temp, vpts=u, verbose=true)
my_result_6=analyze(my_eqns)
folder_6=write_output(my_sys, my_eqns, my_result_6, dir_time="folder_6")
wbf_6=wheelbase_filter(folder_6, my_sys, my_result_6, a+b)
animate_modes(folder_6, my_sys[1], my_result_6[1])
write_report(folder_6, my_sys, verbose=true, build=false) ## Build LaTeX report
#
#####

temp(x)=input_half_car_wings(u=x, m=m, I=Iyy, a=a, b=b, kf=kf, kr=kr, cf=cf, cr=cr,
muf=muf1, mur=mur1, kt=kt, mbc=5, hoff=0.1, voff_f=0.0, voff_r=0.005)

my_sys, my_eqns=run_eom(temp, vpts=u, verbose=true)
my_result_7=analyze(my_eqns)
folder_7=write_output(my_sys, my_eqns, my_result_7, dir_time="folder_7")
wbf_7=wheelbase_filter(folder_7, my_sys, my_result_7, a+b)
animate_modes(folder_7, my_sys[1], my_result_7[1])
write_report(folder_7, my_sys, verbose=true, build=false) ## Build LaTeX report
#

temp(x)=input_half_car_wings(u=x, m=m, I=Iyy, a=a, b=b, kf=kf, kr=kr, cf=cf, cr=cr,
muf=muf2, mur=mur1, kt=kt, mbc=5, hoff=0.1, voff_f=0.0, voff_r=0.005)

my_sys, my_eqns=run_eom(temp, vpts=u, verbose=true)
my_result_8=analyze(my_eqns)
folder_8=write_output(my_sys, my_eqns, my_result_8, dir_time="folder_8")
wbf_8=wheelbase_filter(folder_8, my_sys, my_result_8, a+b)
animate_modes(folder_8, my_sys[1], my_result_8[1])
write_report(folder_8, my_sys, verbose=true, build=false) ## Build LaTeX report
#

temp(x)=input_half_car_wings(u=x, m=m, I=Iyy, a=a, b=b, kf=kf, kr=kr, cf=cf, cr=cr,
muf=muf1, mur=mur2, kt=kt, mbc=5, hoff=0.1, voff_f=0.0, voff_r=0.005)

```

```

my_sys, my_eqns=run_eom(temp, vpts=u, verbose=true)
my_result_9=analyze(my_eqns)
folder_9=write_output(my_sys, my_eqns, my_result_9, dir_time="folder_9")
wbf_9=wheelbase_filter(folder_9, my_sys, my_result_9, a+b)
animate_modes(folder_9, my_sys[1], my_result_9[1])
write_report(folder_9, my_sys, verbose=true, build=false)  ## Build LaTeX report

temp(x)=input_half_car_wings(u=x, m=m, I=Iyy, a=a, b=b, kf=kf, kr=kr, cf=cf, cr=cr,
muf=muf3, mur=mur4, kt=kt, mbc=5, hoff=0.1, voff_f=0.0, voff_r=0.005)

my_sys, my_eqns=run_eom(temp, vpts=u, verbose=true)
my_result_10=analyze(my_eqns)
folder_10=write_output(my_sys, my_eqns, my_result_10, dir_time="folder_10")
wbf_10=wheelbase_filter(folder_10, my_sys, my_result_10, a+b)
animate_modes(folder_10, my_sys[1], my_result_10[1])
write_report(folder_10, my_sys, verbose=true, build=false)  ## Build LaTeX report

#####

temp(x)=input_half_car(u=x, m=m, I=Iyy, a=a, b=b, kf=kf, kr=kr, cf=cf, cr=cr, muf=muf,
mur=mur, kt=kt)

my_sys, my_eqns=run_eom(temp, vpts=30, verbose=true)
my_result_11=analyze(my_eqns)
folder_11=write_output(my_sys, my_eqns, my_result_11, dir_time="folder_11")
wbf_11=wheelbase_filter(folder_11, my_sys, my_result_11, a+b)
animate_modes(folder_11, my_sys[1], my_result_11[1])
write_report(folder_11, my_sys, verbose=true, build=false)  ## Build LaTeX report

temp(x)=input_half_car_wings(u=x, m=m, I=Iyy, a=a, b=b, kf=kf, kr=kr, cf=cf, cr=cr,
muf=muf, mur=mur, kt=kt, mbc=5, hoff=0.1, voff_f=0.0, voff_r=0.005)

my_sys, my_eqns=run_eom(temp, vpts=30, verbose=true)
my_result_12=analyze(my_eqns)
folder_12=write_output(my_sys, my_eqns, my_result_12, dir_time="folder_12")
wbf_12=wheelbase_filter(folder_12, my_sys, my_result_12, a+b)
animate_modes(folder_12, my_sys[1], my_result_12[1])
write_report(folder_12, my_sys, verbose=true, build=false)  ## Build LaTeX report

temp(x)=input_half_car(u=x, m=m, I=Iyy, a=a, b=b, kf=kf, kr=kr, cf=cf, cr=cr, muf=muf,
mur=mur, kt=kt)

my_sys, my_eqns=run_eom(temp, vpts=40, verbose=true)
my_result_13=analyze(my_eqns)
folder_13=write_output(my_sys, my_eqns, my_result_13, dir_time="folder_13")

```

```

wbf_13=wheelbase_filter(folder_13,my_sys,my_result_13,a+b)
animate_modes(folder_13,my_sys[1],my_result_13[1])
write_report(folder_13,my_sys,verbose=true,build=false) ## Build LaTeX report

temp(x)=input_half_car_wings(u=x,m=m,I=Iyy,a=a,b=b,kf=kf,kr=kr,cf=cf,cr=cr,
muf=muf,mur=mur,kt=kt,mbc=5,hoff=0.1,voff_f=0.0,voff_r=0.005)

my_sys,my_eqns=run_eom(temp,vpts=40,verbose=true)
my_result_14=analyze(my_eqns)
folder_14=write_output(my_sys,my_eqns,my_result_14,dir_time="folder_14")
wbf_14=wheelbase_filter(folder_14,my_sys,my_result_14,a+b)
animate_modes(folder_14,my_sys[1],my_result_14[1])
write_report(folder_14,my_sys,verbose=true,build=false) ## Build LaTeX report

temp(x)=input_half_car(u=x,m=m,I=Iyy,a=a,b=b,kf=kf,kr=kr,cf=cf,cr=cr,muf=muf,
mur=mur,kt=kt)

my_sys,my_eqns=run_eom(temp,vpts=51,verbose=true)
my_result_15=analyze(my_eqns)
folder_15=write_output(my_sys,my_eqns,my_result_15,dir_time="folder_15")
wbf_15=wheelbase_filter(folder_15,my_sys,my_result_15,a+b)
animate_modes(folder_15,my_sys[1],my_result_15[1])
write_report(folder_15,my_sys,verbose=true,build=false) ## Build LaTeX report

temp(x)=input_half_car_wings(u=x,m=m,I=Iyy,a=a,b=b,kf=kf,kr=kr,cf=cf,cr=cr,
muf=muf,mur=mur,kt=kt,mbc=5,hoff=0.1,voff_f=0.0,voff_r=0.005)

my_sys,my_eqns=run_eom(temp,vpts=51,verbose=true)
my_result_16=analyze(my_eqns)
folder_16=write_output(my_sys,my_eqns,my_result_16,dir_time="folder_16")
wbf_16=wheelbase_filter(folder_16,my_sys,my_result_16,a+b)
animate_modes(folder_16,my_sys[1],my_result_16[1])
write_report(folder_16,my_sys,verbose=true,build=false) ## Build LaTeX report

temp(x)=input_half_car(u=x,m=m,I=Iyy,a=a,b=b,kf=kf,kr=kr,cf=cf,cr=cr,muf=muf,
mur=mur,kt=kt)

my_sys,my_eqns=run_eom(temp,vpts=10,verbose=true)
my_result_17=analyze(my_eqns)
folder_17=write_output(my_sys,my_eqns,my_result_17,dir_time="folder_17")
wbf_17=wheelbase_filter(folder_17,my_sys,my_result_17,a+b)
animate_modes(folder_17,my_sys[1],my_result_17[1])
write_report(folder_17,my_sys,verbose=true,build=false) ## Build LaTeX report

temp(x)=input_half_car_wings(u=x,m=m,I=Iyy,a=a,b=b,kf=kf,kr=kr,cf=cf,cr=cr,
muf=muf,mur=mur,kt=kt,mbc=5,hoff=0.1,voff_f=0.0,voff_r=0.005)

```

```

my_sys, my_eqns=run_eom(temp, vpts=10, verbose=true)
my_result_18=analyze(my_eqns)
folder_18=write_output(my_sys, my_eqns, my_result_18, dir_time="folder_18")
wbf_18=wheelbase_filter(folder_18, my_sys, my_result_18, a+b)
animate_modes(folder_18, my_sys[1], my_result_18[1])
write_report(folder_18, my_sys, verbose=true, build=false) ## Build LaTeX report

#####

include("random_road_c.jl")
zi, n, phi, z0=random_road_c(class=3, L=1000)

## convert to time index, x=ut
z(t)=zi'*cos.(n*2pi*u*t+phi)-z0

zz(t)=z(t-(a+b)/u)
road(t)=[z(t), zz(t)]

tend=(1/n[1])/u

tspan=0.0:0.002:tend
include("lsim_d.jl")
@time y=lsim_d(my_result[1].ss_eqns, road.(tspan), tspan, verbose=true)
@time y1=lsim_d(my_result_1[1].ss_eqns, road.(tspan), tspan, verbose=true)
@time y2=lsim_d(my_result_2[1].ss_eqns, road.(tspan), tspan, verbose=true)
@time y3=lsim_d(my_result_3[1].ss_eqns, road.(tspan), tspan, verbose=true)
@time y4=lsim_d(my_result_4[1].ss_eqns, road.(tspan), tspan, verbose=true)
@time y5=lsim_d(my_result_5[1].ss_eqns, road.(tspan), tspan, verbose=true)
@time y6=lsim_d(my_result_6[1].ss_eqns, road.(tspan), tspan, verbose=true)
@time y7=lsim_d(my_result_7[1].ss_eqns, road.(tspan), tspan, verbose=true)
@time y8=lsim_d(my_result_8[1].ss_eqns, road.(tspan), tspan, verbose=true)
@time y9=lsim_d(my_result_9[1].ss_eqns, road.(tspan), tspan, verbose=true)
@time y10=lsim_d(my_result_10[1].ss_eqns, road.(tspan), tspan, verbose=true)
@time y11=lsim_d(my_result_11[1].ss_eqns, road.(tspan), tspan, verbose=true)
@time y12=lsim_d(my_result_12[1].ss_eqns, road.(tspan), tspan, verbose=true)
@time y13=lsim_d(my_result_13[1].ss_eqns, road.(tspan), tspan, verbose=true)
@time y14=lsim_d(my_result_14[1].ss_eqns, road.(tspan), tspan, verbose=true)
@time y15=lsim_d(my_result_15[1].ss_eqns, road.(tspan), tspan, verbose=true)
@time y16=lsim_d(my_result_16[1].ss_eqns, road.(tspan), tspan, verbose=true)
@time y17=lsim_d(my_result_17[1].ss_eqns, road.(tspan), tspan, verbose=true)
@time y18=lsim_d(my_result_18[1].ss_eqns, road.(tspan), tspan, verbose=true)

```

```

## write solution to file
println("Writing...")
using DelimitedFiles

res=[tspan y' hcat(road.(tspan)...)]
writedlm(joinpath(folder,"bounce_pitch_tilting_wings.txt"),res)

res1=[tspan y' y1' y2' hcat(road.(tspan)...)]
writedlm(joinpath(folder_1,"bounce_pitch_tilting_wings.txt"),res1)

res2=[tspan y' y3' y4' hcat(road.(tspan)...)]
writedlm(joinpath(folder_3,"bounce_pitch_tilting_wings.txt"),res2)

res3=[tspan y' y5' y6' hcat(road.(tspan)...)]
writedlm(joinpath(folder_5,"bounce_pitch_tilting_wings.txt"),res3)

res4=[tspan y' y7' y8' y9' y10' hcat(road.(tspan)...)]
writedlm(joinpath(folder_7,"bounce_pitch_tilting_wings.txt"),res4)

res5=[tspan y11' y12' hcat(road.(tspan)...)]
writedlm(joinpath(folder_11,"bounce_pitch_tilting_wings.txt"),res5)

res6=[tspan y13' y14' hcat(road.(tspan)...)]
writedlm(joinpath(folder_13,"bounce_pitch_tilting_wings.txt"),res6)

res7=[tspan y15' y16' hcat(road.(tspan)...)]
writedlm(joinpath(folder_15,"bounce_pitch_tilting_wings.txt"),res7)

res8=[tspan y17' y18' hcat(road.(tspan)...)]
writedlm(joinpath(folder_17,"bounce_pitch_tilting_wings.txt"),res8)

println("Plotting...")
using Plots
plotly()

display(plot(tspan,[y[1,:],y1[1,:],y2[1,:],y3[1,:],y4[1,:],y5[1,:],y6[1,:],
y7[1,:],y8[1,:],y9[1,:],y10[1,:],y11[1,:],y12[1,:],y13[1,:],y14[1,:],y15[1,:],
y16[1,:],y17[1,:],y18[1,:]],size=(1200,800),label=["Bounce" "Bounce w wing"
"Bounce w rev wing"]))

display(plot(tspan,[y[2,:],y1[2,:],y2[2,:],y3[2,:],y4[2,:],y5[2,:],y6[2,:],
y7[2,:],y8[2,:],y9[2,:],y10[2,:],y11[2,:],y12[2,:],y13[2,:],y14[2,:],
y15[2,:],y16[2,:],y17[2,:],y18[2,:]],size=(1200,800),
label=["Pitch" "Pitch w wing" "Pitch w rev wing"]))

```

```

l1=0:1:1000

zi_1,n_1,phi_1,z0_1=random_road_c(class=3,L=1000)
z1(x)=zi_1'*cos.(n_1*2pi*x+phi_1)-z0_1

zi_2,n_2,phi_2,z0_2=random_road_c(class=5,L=1000)
z2(x)=zi_2'*cos.(n_2*2pi*x+phi_2)-z0_2

zi_3,n_3,phi_3,z0_3=random_road_c(class=7,L=1000)
z3(x)=zi_3'*cos.(n_3*2pi*x+phi_3)-z0_3

road_2(x)=[z1(x),z2(x),z3(x)]

res=[tspan hcat(road_2.(l1)...)]
writedlm(joinpath(folder,"road.txt"),res)

println("Done.")

```

A.2.3 Random road

```

function random_road(;class::Int=3,L=100.,B=0.05)

# class is an integer from 3 - 9, where class=3 is an A-B road (smooth),
class=9 is G-H road (rough)
# L is max wavelength [m], also equals road length
# B shortest wavelength, approx [m]

if(class<3)
    class=3
    println("Warning: class out of range, resetting to minimum value (3)")
end

if(class>9)
    class=9
    println("Warning: class out of range, resetting to maximum value (9)")
end

deltan=1/L # spatial frequency interval
N=Int(round(L/B)) # number of frequencies

n=deltan:deltan:N*deltan # frequency span

```

```
phi=rand(1,N)*2*pi # N random phase lag, 1 for each frequency, from 0-2pi

a=sqrt(deltan)*(2^class)*1e-4./n # amplitude of each frequency, based on psd content

x=0:L/N/10:L # road coordinate, resolution fine enough to give 10 point even
shortes wavelength
z=zeros(size(x)) # road vertical
for i=1:length(n) # sum for each frequency included
    z.+=a[i]*cos.(2*pi*n[i]*x.+phi[i])
end

z.-=z[1] # set start to 0
x,z # return road path

end ## Leave
```


Appendix B

Eigenvalue Results

B.1 Eigenvalue tables

This section presents the eigenvalues computed as the solution to the equations of motion.

B.1.1 Eigenvalue and eigenvalue analysis table(baseline)

TABLE B.1: Eigenvalues for baseline model

num	speed	real	imag	realhz	imaghz
1	50	-12.24	81.17	-1.95	12.92
2	50	-12.24	-81.17	-1.95	-12.92
3	50	-10.08	81.14	-1.6	12.91
4	50	-10.08	-81.14	-1.6	-12.91
5	50	-0.71	8.25	-0.11	1.31
6	50	-0.71	-8.25	-0.11	-1.31
7	50	-0.36	4.89	-5.68×10^{-2}	0.78
8	50	-0.36	-4.89	-5.68×10^{-2}	-0.78

Note: oscillatory roots appear as complex conjugates.

TABLE B.2: Eigenvalue Analysis for baseline model

num	speed	nfreq	zeta	tau	lambda
1	50	13.06	0.15	8.17×10^{-2}	7.74×10^{-2}
2	50	13.06	0.15	8.17×10^{-2}	7.74×10^{-2}
3	50	13.01	0.12	9.93×10^{-2}	7.74×10^{-2}
4	50	13.01	0.12	9.93×10^{-2}	7.74×10^{-2}
5	50	1.32	8.6×10^{-2}	1.4	0.76
6	50	1.32	8.6×10^{-2}	1.4	0.76
7	50	0.78	7.29×10^{-2}	2.8	1.29
8	50	0.78	7.29×10^{-2}	2.8	1.29

Notes: a) oscillatory roots are listed twice,

b) negative time constants denote unstable roots.

B.1.2 Eigenvalue and eigenvalue analysis table (premium)

TABLE B.3: Eigenvalues for premium model

num	speed	real	imag	realhz	imaghz
1	50	-9.59	79.49	-1.53	12.65
2	50	-9.59	-79.49	-1.53	-12.65
3	50	-11.74	79.82	-1.87	12.7
4	50	-11.74	-79.82	-1.87	-12.7
5	50	-0.88	6.22	-0.14	0.99
6	50	-0.88	-6.22	-0.14	-0.99
7	50	-0.19	0	-3.05×10^{-2}	0
8	50	-0.64	0	-0.1	0

Note: oscillatory roots appear as complex conjugates.

TABLE B.4: Eigenvalue Analysis for premium model

num	speed	nfreq	zeta	tau	lambda
1	50	12.74	0.12	0.1	7.9×10^{-2}
2	50	12.74	0.12	0.1	7.9×10^{-2}
3	50	12.84	0.15	8.52×10^{-2}	7.87×10^{-2}
4	50	12.84	0.15	8.52×10^{-2}	7.87×10^{-2}
5	50	1	0.14	1.13	1.01
6	50	1	0.14	1.13	1.01
7	50	NaN	NaN	5.23	NaN
8	50	NaN	NaN	1.56	NaN

Notes: a) oscillatory roots are listed twice,

b) negative time constants denote unstable roots.

Vita Auctoris

Mingyu Sun was born in 1994 in Shijiazhuang, Hebei, China. He graduated from Dalian Maple Leaf International high school in 2012. From there he pursued his undergraduate study in B.S.c in Mechanical Engineering with automobile option at University of Windsor. He obtained his degree with distinction and decided to pushed forward his education to a higher level. He is presently a candidate for the Master's degree in Machinal Engineering at University of Windsor and is expected to graduate in September, 2019.

Education– Master of Mechanical Engineering student at University of Windsor, September 2017- present. Thesis title: “ Inclusion of Aerodynamic Effects in Multibody Vehicle Dynamics.”. Bachelor of Science (August 2017) in Mechanical Engineering, University of Windsor, Ontario, Canada.

Academic Employment– Graduate Teaching Assistant, Department of Engineering, University of Windsor, 2017-2018. Responsibilities include: assisting professors with undergraduate courses, grading examinations or papers and tutoring.

Academic Awards– Graduate with Distinction, Department of Engineering, University of Windsor, August 2017.